

UNIVERSITÀ DEGLI STUDI DI PADOVA
Dipartimento di Ingegneria Industriale

Corso di Laurea Magistrale in
INGEGNERIA DELL'ENERGIA ELETTRICA



Tesi di Laurea Magistrale

TRANSIENT OVERVOLTAGES IN GAS INSULATED SYSTEMS

RELATORE: *Prof. Roberto Turri*
Dipartimento di Ingegneria Industriale

CORRELATORE: *Prof. Manu Haddad*
School of Engineering, Cardiff University

Laureando: Giulia Corellas
Matricola: 1080668

Anno Accademico 2015/2016

Abstract

Le linee miste, composte per esempio da una linea aerea e un GIL (gas insulated transmission line) potrebbero costituire un interessante compromesso per quanto riguarda costi, efficienza e impatto ambientale. Diverse questioni sono state sollevate riguardo il comportamento di questo tipo di sistema in entrambi i casi di regime stazionario e transitorio. Lo scopo di questo lavoro é di investigare il comportamento di una linea di trasmissione a $400[kV]$ considerando diversi scenari, utilizzando il software EMTP, e tenendo conto della presenza di una sottostazione in SF_6 . In particolare sono state studiate sovratensioni di origine interna ed esterna, ponendo particolare attenzione al comportamento del GIL. Infatti operazioni tramite interruttori portano ad un Very Fast Transient Overvoltage e ad un Very Fast Transient Overcurrent all'interno del GIL, i quali possono andare a stressare l'isolamento, l'equipaggiamento secondario e l'adiacente equipaggiamento in alta tensione. In questo lavoro sono stati presi in considerazione i seguenti casi di studio: l'effetto Ferranti a fine linea, prima considerando un semplice confronto fra la linea aerea e il GIL e successivamente considerando la linea mista con diverse lunghezze. L'energizzazione e la ri-energizzazione della linea di trasmissione é stata studiata considerando un'analisi di tipo statico tenendo conto di diversi valori di carica rimasta immagazzinata lungo la linea. Al fine di studiare le operazioni di apertura é stato poi necessario costruire un modello dell'arco che si crea fra i contatti dell'interruttore. Infine sono state studiate le fulminazioni, considerando entrambi i casi di fulminazione su fine di guardia e fulminazione diretta su conduttore. Poiché il valore delle sovratensioni eccedeva il valor limite é stato necessario introdurre gli scaricatori. É stato così fatto un confronto fra gli scaricatori esterni e quelli interni, ed infine é stato condotto un interessante studio riguardo le onde viaggianti lungo il GIL, in caso di fulminazione su fine di guardia, per differenti valori di carico.

Introduzione

Le linee aeree sono largamente impiegate nei sistemi di trasmissione di alta tensione. D'altra parte attualmente diverse questioni sono apparse a riguarda, come per esempio l'impatto ambientale. Per queste ragioni e grazie alla diffusione dei GIS (Gas Insulated Switchgear), le line miste, composte da linee aeree e GIL potrebbero essere una buona soluzione. Al fine di avere una buona coordinazione degli isolamenti e un'alta efficienza e affidabilita é necesario studiare il comportamento delle linee miste, in entrambi i casi di regime permanente e transitorio. Infatti in una GIS un certo numero di archi si stabilizzando fra i contatti dell'interruttore durante le operazione di apertura e chiusura. Questo accade per via del lento movimento del contatto mobile. Per questa ragione un Very Fast Transient Overvoltage VFTO si presenta lungo la linea di trasmissione GIL, il che significa che si ha la presenza di sovratensioni con un certo tempo di salita, dell'ordine di alcuni $[ns]$, seguito da delle componenti in alta frequenza. Solitamente l'ampiezza della sovratensione non é pericolosa per l'isolamento, ma potrebbe andare a stressare la linea aerea a monte. Inoltre le sovratensioni di origine atmosferica associate a fulminazioni della linea aerea potrebbero risultare pericolose per GIS e GIL. Al fine di non eccedere il valore limite per l'isolamento potrebbe essere necessario aggiungere degli scaricatori. Isolatori esterni sono la soluzione piu commune, ma potrebbero portare ad una situazione eccessivamente stressante per il GIL. D'altro lato gli scaricatori integrati sono piu costosi. Diversi software sono stati create al fine di studiare il transitorio. The Electro Magnetic Transient Program EMTP e uno dei piu prestanti. E necessario cotruire un opportune modello di rete, questa e uno dei piu importanti compiti dell'ingegneria moderna.

Abstract

In this work a 400[kV] mixed lines composed by Overhead Transmission Lines and Gas Insulated Transmission Lines (GIL) has been investigated because it represents an interesting compromise between costs, efficiency, and environment. There are several issues regarding the behaviour of the mixed lines in both steady state and transient conditions. The model of the transmission line has been built using the software EMTP: it involves a source, an overhead line, the terminal tower and the gantry, the bushings, a simplified model of a Gas Insulated Switchgear (GIS) considering the Circuit Breaker and the Disconnecter as an ideal switch, and finally the GIL. In particular Internal and External Overvoltages has been investigated, with particular attention of the voltage along the GIL. In fact during switching operations Very Fast Transient Overvoltages VFTO occurs in the GIS and it could be stressful for the insulation, the secondary equipment and the adjacent HV equipment. In this work the following scenarios have been investigated: the Ferranti Effect at the open end of the line, considering first a comparison between GIL and OHL, and finally considering the mixed line with different lengths. The Energization and Re-Energization of the transmission line have been investigated by a statistical analysis considering different values of trapped charge. In order to investigate the opening operations in GIS the arc model between the contacts of the circuit breaker has been built. Finally the lightning events have been investigated, considering both cases of Stroke on Tower Peak and Shielding Failure. Because the overvoltages reached the limit value it was necessary to introduce the surge arresters. Comparison between integrated and external surge arresters has been done, and a study about the travelling wave along the GIL in case of stroke on tower peak for different values of load has been done, in particular for $R_{load} < Z_{GIL}$, $R_{load} = Z_{GIL}$ and $R_{load} > Z_{GIL}$.

Introduction

Overhead transmission lines in High Voltage Power Systems are widely used. On the other hand nowadays some problems about this kind of lines have been appeared, for example the impact on environment. For these reasons, and due the diffusion of the GIS, the mixed lines, composed by the OHL and GIL represent a smart solution. In order to have a good insulation coordination and high efficiency and reliability it is necessary to study the behaviour of the composed line, in both steady state and transient conditions. In fact in GIS a large number of restrike occur across the switching contacts during opening or closing operations. This occurs due to the slow speed of the moving contacts. For this reason a Very Fast Transient Overvoltage VFTO occurs along the GIL, it means that there is the presence of overvoltage with a certain rise time in the range of few [ns] followed by high frequency oscillations. The magnitude of the overvoltages usually is lower than the BIL of the system, but could be stressful for the overhead line attached at the GIS and for the insulation due to the high frequency components. Hence there is a need to estimate the magnitudes of VFTO generated during switching operations, it depends on the closing time, on the pole-span delay and on the location of the switching point. Another important factor is the presence of trapped charge at the end of the network. Moreover, atmospheric overvoltages associated with lightning strikes to the OHL may result dangerous for the GIS and for the GIL. Hence there is a need to estimate the magnitude of the voltage at any point along the Gas Insulated Transmission Line. In order to don't exceed the limit value for the insulation coordination, $1425[kV]$ in case of $V_n = 400[kV]$, it should be necessary to add the surge arresters. External surge arresters are the most common solutions, but otherwise should be stressful for the GIL. On the other hand Integrated surge arresters are a more expensive solutions. Many softwares have been developed in order to study the transient analysis. The Electro Magnetic Transient Program EMTP is one of the most appreciate. It is necessary to build an appropriate network model, this is one of the most important tasks in the modern engineering.

Contents

1	Transmission Lines	21
1.1	Introduction	21
1.2	Gas Insulated Systems	22
1.2.1	Design	22
1.2.2	Advantages of GIL	29
1.2.3	OverHead line connection	30
1.2.4	Economic Aspects	30
1.3	Composed Lines	30
2	Transient Analysis	33
2.1	Introduction	33
2.1.1	Transient Analysis with non linear conditions	33
2.2	Transmission Lines Transient Analysis	34
2.2.1	Theory of Travelling Wave	35
2.2.2	Trawelling Wave in Hybrid System	40
2.3	Capacitive Load Switching	42
2.4	Very Fast Transient Overvoltage on Gas Insulated Systems	45
2.4.1	Internal VFT	49
2.4.2	External VFT	50
2.4.3	Representation of the GIL components	51
2.5	Electro Magnetic Transient Program	55
2.5.1	The History of the Transient Analysis in Power System	55
2.5.2	The Classification of frequency ranges	57
2.5.3	The Time Step	58
2.5.4	The accuracy	58
2.5.5	The statistical analysis	59
2.5.6	The aim of the EMTP	59
3	Components Design	61
3.1	Overhead Line Design	61
3.2	GIL Model	65
3.3	Source Design	70

4	Internal Overvoltages	73
4.1	Introduction	73
4.2	Temporary Overvoltages: The Ferranti Effect	73
4.3	Transient Overvoltages: No-Load Energization	78
4.3.1	No-Load Energization of Overhead Line	78
4.3.2	No-Load Energization of the GIS	81
4.4	Opening Operations	92
4.4.1	Opening Operations on OHL	92
4.4.2	Opening Operations on GIL	96
5	External Overvoltages: Lightning	101
5.1	Introduction	101
5.2	Model on EMTP	104
5.3	Shielding Failure	104
5.4	Stroke on Tower Peak	107
5.5	Accurate Tower Model by Akiro Ametani	107
5.5.1	Shielding Failure	110
5.5.2	Stroke on Tower Peak	110
5.6	The Surge Arresters	114
5.6.1	The model of Surge Arrester on EMTP	117
5.6.2	Integrated Surge Arrester	119
5.6.3	Effect of Tower Model	120
5.6.4	Comparison with the External Surge Arrester	121
5.7	The load effect	123
5.7.1	Travelling Wave along the GIL for different values of R_{load}	126
6	Conclusion	131

List of Figures

1.1	242 kV GIL being installed in the PSEG Hudson generating station. New Jersey. 1972. View looking back from the SF6-Air bushings.	22
1.2	Schluchsee Hydro Pump Storage Plant.	23
1.3	Conductor pipe	24
1.4	conical insulators with slinding contact	24
1.5	Typical configuration by Simens	25
1.6	Relationship between Enclosure and Conductor Diameters [HK08]	25
1.7	BIL performance for various conductor diameters for 115[kV] – 800[kV] applications [HK08]	25
1.8	60Hz breakdown results for a 145kV Coaxial Geometry with Enclosure/Conductor Dimensions of 241.3/88.9mm [HK08]	26
1.9	Gas-insulated Switchgear ELK-04 by ABB	26
1.10	Gas-insulated Switchgear ELK-04 by ABB	27
1.11	Gas-insulated Switchgear ELK-04 by ABB	27
1.12	Circuit Breaker by ABB	28
1.13	Disconnecter by ABB	28
1.14	Overhead Line-bushing connection [Koc12]	30
1.15	Terminal Tower and Gantry, picture by David Neale on Flickr	31
1.16	Costs of GIL [Koc12]	31
2.1	Approximation of non-linear characteristic	35
2.2	Electric and magnetic field around a line segment Δx of a transmission line	36
2.3	Voltage and Current Wave	37
2.4	Superposition of Waves	38
2.5	Overhead Transmission line terminated by a underground cable	38
2.6	Hybrid transmission line: OHL and GIL with external surge arresters [GW15]	40
2.7	Example of voltage at cable end [THUB05]	41
2.8	Example of voltage at the position where the maximum voltage occurs simultaneously [THUB05]	41
2.9	Reflected voltage wave and arrester voltage as a function of incoming voltage wave [THUB05]	42

2.10	Reflected wave as function of incoming wave fro different values of instanteneous value v_0 of power frequency voltage [THUB05]	43
2.11	Reflected and incident voltage wave at the remote end of the cable $l = 9km$ [THUB05]	43
2.12	Reflected and incident voltage wave at the remote end of the cable $l = 500m$ [THUB05]	44
2.13	Voltage waves at the remote and and at $x = l - \Delta x$ considering $l = 9km$ at the left and $l = 500m$ at the right [THUB05]	44
2.14	Circuit Capacitive Load Switching [DR15]	45
2.15	Voltage Trend during the Capacitive Load Switching [DR15]	45
2.16	3D simplified representation of the 1100kV GIS type ELK-5 and details of its disconnector	46
2.17	Disconnector operations	47
2.18	Voltage Difference Between the Contacts	47
2.19	3D simulation model of the 1100kV GIS type ELK-5	47
2.20	Results of the 3D time-domain full-Maxwell simulations of the 1100kV GIS type ELK-5	48
2.21	Very Fast Transient Classification	49
2.22	Steep Voltage Transient	49
2.23	Oscillation of the GIS with some MHz	50
2.24	Propagation of travelling waves caused by a disconnector operation	50
2.25	Equivalent Circuit	51
2.26	Equivalent Circuit	51
2.27	Equivalent circuits for GIS components for representation of VFT (1)	52
2.28	Equivalent circuits for GIS components for representation of VFT (2)	52
2.29	Equivalent circuits for GIS components for representation of VFT (3)	53
2.30	The equivalent circuit model of bus duct	54
2.31	The equivalent circuit model of disconnector	55
2.32	The basin-insulator diagram	56
2.33	The electric field distribution of basin-insulator	56
2.34	The equivalent circuit model of basin-insulator	56
2.35	The equivalent circuit models of other main GIS components	56
2.36		58
3.1	L-6 Tower 400 kV	62
3.2	Tower Geometry	62
3.3	ElectroMagnetic Transient Program	63
3.4	ElectroMagnetic Transient Program	63
3.5	Overhead Line Model [LB11]	65
3.6	GIL Design on EMTP	68
3.7	GIL Design on EMTP	69
3.8	GIL Design on EMTP	69
3.9	Line Model Frequency Scan Results	69

3.10 Source Design	70
4.1 Equivalent Circuit [LB11]	74
4.2 Ferranti Effect in case of 100 km line length (considering the phase A)	75
4.3 Ferranti Effect in case of 300 km line length (considering the phase A)	75
4.4 Model of the Composed Line on EMTP: Source-OHL- terminal tower and a gantry-GIL-open end	76
4.5 Ferranti Effect in case of Weak Network in a Composed Line, phase A	77
4.6 Ferranti Effect in case of Weak Network in a Composed Line, phase B	77
4.7 Ferranti Effect in case of Weak Network in a Composed Line, phase C	77
4.8 Ferranti Effect: Voltage at the source side (red) and at the receiving end (green)	77
4.9 Composed Line Model on EMTP considering the energization of the first circuit in the L-6 tower	78
4.10 Composed Line Model on EMTP considering the energization of both circuits at the same time	79
4.11 Voltage trend downstream the Switch compared with the voltage trend of the source	79
4.12 Voltage trend downstream the Switch	79
4.13 Voltage trend upstream the Switch	79
4.14 Trend of the Voltage at the Sending End (red) and at the Receiving End (green)	80
4.15 Value of $U_{2\%}$ by international standard IEC 60071-2	81
4.16 Probability Function in case of OHL 30km no-load energization	81
4.17 Voltage Trend at the Bushing side, phase A (red), phase B (green) and phase C (blue)	82
4.18 Zoom of picture 4.17: Voltage Trend at the Bushing side phase A - high frequency components -	82
4.19 Rise Time at the bushing side - 1[ns]	83
4.20 Voltage Trend Downstream the Disconnecter: phase A (red), phase B (green) and phase C (blue)	83
4.21 Zoom of picture 4.20 : Voltage Trend Downstream the Disconnecter phase A - high frequency components -	83
4.22 Rise Time Downstream the Disconnecter - 1[ns] -	83
4.23 Voltage Trend at the Receiving End: phase A (red), phase B (green) and phase C (blue)	84
4.24 Zoom of picture fig:receivingend1: Voltage Trend at the Receiving End phase A - no high frequency components -	84
4.25 Voltage trend at $l = 0[km]$ (brown), $l = 10[km]$ (blue), $l = 20[km]$ (green), $l = 30[km]$ (red).	85
4.26 Voltage trend at the end of the OHL	86

4.27	Zoom of the picture 4.26: Voltage trend at the end of the OHL .	86
4.28	Voltage trend at the end of OHL $l = 30[km]$ (blue) and at $l = 20[km]$ (red)	86
4.29	Current at the bushing side	86
4.30	Current downstream the DS	87
4.31	Current at $l = 20[km]$ (blue) and $l = 40[km]$ (brown) along the GIL	87
4.32	Comparison between the trend of the voltage at the receiving end (blue) and at the source side (red) and sending end downstream the DS (green))	87
4.33	Model Line on EMTP in case of Statistical Analysis During GIL Energization	88
4.34	Probability Fuction	88
4.35	Line Model on EMP with Trapped Charge	88
4.36	Voltage Trend at the sending end (left) and at the receiving end (right) with Trapped Charge	89
4.37	Probability Function at the Bushing	89
4.38	Probability Function Downstream the DS	90
4.39	Probability Function at the Receiving End	90
4.40	More Accurate Model on EMTP For the Trapped Charge as suggested by [MA15]	90
4.41	AC-Source to model the trapped charge on EMTP, as suggested by [MA15]	91
4.42	Probability Function at the bushing Side considering AC-Source to model the trapped charge	91
4.43	Probability Function Downstream the DS considering AC-Source to model the trapped charge	91
4.44	Probability Function at the Receiving End of the GIL considering AC-Source to model the trapped charge	92
4.45	Circuit on EMTP for the Opening Operations on the OHL	93
4.46	Voltage Trend Across the contacts of the CB	93
4.47	Current Across the contacts of the CB	93
4.48	Voltage Trend at the source side (red) and downstream the Switch (green)	93
4.49	Zoom of the voltage jump at the source side	94
4.50	Voltage Trend at the Bushing	94
4.51	Voltage Trend at the source side (red), downstream the switch (green) and at the bushing side (blue)	94
4.52	Voltage trend at the source side, 3-phases, compared with the voltage trend downstream the Switch	94
4.53	Voltage trend at the busghing side (red), at $l = 30[km]$ (green) and $l = 60[km]$ (blue)	95
4.54	Voltage trend at the busghing side (red) and at $l = 30[km]$ (green)	95
4.55	Trend of the current at the bushing side (blue) and downstream the CB (green)	95
4.56	Non-Linear Resistance on EMTP	96

4.57	Voltage trend of the source (blue), at the bushing side (red) and at the load side (green)	97
4.58	Zoom of picture 4.57	97
4.59	Line Model on EMTP	97
4.60	Arc Model on EMTP	98
4.61	Voltage Trend at the Source Side (blue), at the bushing side (red) and downstream the CB (green), considering $t_{opening} = 20[ms]$	99
4.62	Probability Function at the Bushing side	99
4.63	Probability Function Downstream the DS	100
4.64	Probability Function at the Open End of the GIL	100
5.1	Lightning Current [Coo10]	102
5.2	Characterist Parameters of Lightning Current [Coo10]	102
5.3	$I(t)$ for different steepness factor	103
5.4	Variation of R_t as a function of I, E_0, ρ	103
5.5	HEIDLER component on EMTP	104
5.6	model on EMTP for shield failure	104
5.7	Trend of the voltage at the sending end of the GIL (red), at the receiving end (green) in case of Shielding Failure	105
5.8	Zoom of the picture 5.7	105
5.9	Lightning Voltage in case of Shielding Failure	105
5.10	Trend of the Voltage at the sending end of the GIL (red), at the receiving end (green) and lightning voltage (blue) in case of Shielding Failure	106
5.11	Lightning Current	106
5.12	Value of Voltage as a function of GIL length	106
5.13	trend of the voltage at the sending end of the GIL (red) and the receiving end of the GIL (green) without taking into account the lightning-path impedance in case of Shielding Failure	107
5.14	Model on EMTP in case of Stroke on Tower Peak	108
5.15	trend of the voltage at the sending end of the GIL (red) and at the receiving end of the GIL (green) in case of Stroke on Tower Peak	108
5.16	Tower Model Recommended in Japan [Ame14]	109
5.17	Model on EMTP	110
5.18	Trend of the voltage at the sending end of the GIL, accurate tower model, Shielding Failure	110
5.19	Trend of the voltage at the receiving end of the GIL, accurate tower model, Shielding Failure	111
5.20	Accurate Tower Model on EMTP in case of Stroke on Tower Peak	112
5.21	Voltage at the sending end (red) and at the receiving end (green) in case of Stroke on Tower Peak	112
5.22	Model on EMTP using a MODELS flash and controlled switch	113
5.23	Trend of the voltage at the sending end (red) and at the receiving end (green) in case of Stroke on Tower Peak using a MODELS flash and controlled switch	113

5.24	Trend of the voltage across the insulator (blue) and the voltage in the OHL (red)	114
5.25	Model on EMTP 3-phase flashover,	114
5.26	Trend voltage at the sending end of the GIL (red) and at the receiving end of the GIL (green) in case of 3-phase flashover,	115
5.27	Trend voltage at the sending end of the GIL (red) and at the receiving end of the GIL (green) considering that the flashover between the insulator and conductor occurs for the phase A in both circuits	115
5.28	trend voltage at the sending end of the GIL (red) and at the receiving end of the GIL (green) for the 3-phase flashover case in both circuits	115
5.29	Protection Characteristic of Surge Arrester for 550kV applications [KS03]	116
5.30	Thermal Stability Characteristic of Surge Arrester for 550kV applications [KS03]	117
5.31	Surge Arrester Design for Overhead Transmission Line HV [KS03]	117
5.32	Hybrid transmission line: OHL and GIL [GW15]	117
5.33	Surge Arrester simplified model by [PG99]	118
5.34	Non-linear resistances characteristic [PG99]	118
5.35	Model on EMTP: External SA (right) and Internal SA (left)	119
5.36	Voltage trend at the sending end of the GIL (red) and at the receiving end (green), without SA (left) and with Integrated SA (right) in case of shielding failure	120
5.37	Voltage trend at the sending end of the GIL (red) and at the receiving end (green), without SA (left) and with Integrated SA (right) in case of Stroke on Tower peak	120
5.38	Voltage trend at the sending end of the GIL as a function of the foot resistance considering $I_{peak} = 200[kA]$	121
5.39	Voltage trend at the receiving end of the GIL as a function of the foot resistance considering $I_{peak} = 200[kA]$	121
5.40	Voltage trend at the sending end of the GIL as a function of the foot resistance considering $I_{peak} = 150[kA]$	122
5.41	Voltage trend at the receiving end of the GIL as a function of the foot resistance considering $I_{peak} = 150[kA]$	122
5.42	Voltage trend at the sending end of the GIL as a function of the foot resistance considering $I_{peak} = 200[kA]$	123
5.43	Voltage trend at the receiving end of the GIL as a function of the foot resistance considering $I_{peak} = 200[kA]$	123
5.44	Voltage trend at the sending end of the GIL as a function of the foot resistance considering $I_{peak} = 150[kA]$	124
5.45	Voltage trend at the receiving end of the GIL as a function of the foot resistance considering $I_{peak} = 150[kA]$	124
5.46	Voltage Impulses for different value of load resistance, in case of Shielding failure, $I_{peak} = 10[kA]$, without Surge Arresters, considering the Accurate Tower Model	125

5.47	Voltage Impulses for different value of load resistance, in case of Stroke on Tower Peak, $I_{peak} = 200[kA]$, without Surge Arresters, considering the Accurate Tower Model	125
5.48	Voltage Impulses for different value of load resistance, in case of Stroke on Tower Peak, $I_{peak} = 150[kA]$, with Integrated Surge Arresters, considering the Accurate Tower Model	126
5.49	Travelling wave at the end the GIL in case of Stroke on Tower Peak considering $R_{load} = 20[Ohm]$	127
5.50	Travelling wave at the end the GIL in case of Stroke on Tower Peak considering $R_{load} = 70[Ohm]$	127
5.51	Travelling wave at the end the GIL in case of Stroke on Tower Peak considering $R_{load} = 300[Ohm]$	128
5.52	Travelling wave at the end the GIL in case of Stroke on Tower Peak considering $R_{load} = 500[Ohm]$	128
5.53	Travelling wave at the end the GIL in case of Stroke on Tower Peak considering $R_{load} = 20[Ohm]$	128
5.54	Travelling wave at the end the GIL in case of Stroke on Tower Peak considering $R_{load} = 70[Ohm]$	129
5.55	Travelling wave at the end the GIL in case of Stroke on Tower Peak considering $R_{load} = 300[Ohm]$	129
5.56	Travelling wave at the end the GIL in case of Stroke on Tower Peak considering $R_{load} = 500[Ohm]$	129

List of Tables

2.1	Classification of frequency ranges [UR11]	58
3.1	Tower Geometry	61
3.2	Resistance at 20	62
3.3	Electrical Components	64
3.4	Data Evaluated	65
3.5	Distance Between the conductors	66
3.6	Comparison of the Electrical Parameters of the Overhead Line evaluated by the analytical formulas and by the software	66
3.7	GIL 400 kV	66
3.8	GIL Electrical Parameters evaluated	67
3.9	GIL Electrical Parameters evaluated	67
3.10	GIL Electrical Parameters	68
3.11	GIL Electrical Parameters	70
3.12	Network	70
3.13	Value of the Voltage L-L	71
3.14	Value of the Voltage G-L	71
4.1	Limit Value of the Overvoltage [AH04]	73
4.2	Overvoltages Phase A	80
4.3	Overvoltages During the GIL Energization	87
4.4	Overvoltages During the GIL Energization with a trapped charge by a grounded capacitance	89
4.5	Overvoltages During the GIL Opening Operations in case of weak network	98
4.6	Overvoltages During the GIL Opening Operations in case of strong network	98
5.1	Maximum Value of Voltage as a function of GIL length	106
5.2	Comparison between the results obtained by the simplify tower model and the accurate tower model in case of shielding failure	111
5.3	Non-linear resistance A_0 and A_1 for Suge Arrester model on EMTP	118
5.4	Overvoltages at the Receiving End of the GIL considering $I_{peak} =$ 200[kA]	122

5.5	Overvoltages at the Receiving End of the GIL considering $I_{peak} =$ 150[kA]	122
-----	--	-----

Chapter 1

Transmission Lines

1.1 Introduction

Overhead transmission lines in High Voltage Power Systems are widely used. On the other hand nowadays some problems about this kind of lines have been appeared, for example the impact on environment. For these reasons, and due the diffusion of the GIS, the mixed lines, composed by the OHL and GIL represent a smart solution. In order to have a good insulation coordination and high efficiency and reliability it is necessary to study the behaviour of the composed line, in both steady state and transient conditions. In fact in GIS a large number of restrike occur across the switching contacts during opening or closing operations. This occurs due to the slow speed of the moving contacts. For this reason a Very Fast Transient Overvoltage VFTO occurs along the GIL, it means that there is the presence of overvoltage with a certain rise time in the range of few [ns] followed by high frequency oscillations. The magnitude of the overvoltages usually is lower than the BIL of the system, but could be stressful for the overhead line attached at the GIS and for the insulation due to the high frequency components. Hence there is a need to estimate the magnitudes of VFTO generated during switching operations, it depends on the closing time, on the pole-span delay and on the location of the switching point. Another important factor is the presence of trapped charge at the end of the network. Moreover, atmospheric overvoltages associated with lightning strikes to the OHL may result dangerous for the GIS and for the GIL. Hence there is a need to estimate the magnitude of the voltage at any point along the Gas Insulated Transmission Line. In order to don't exceed the limit value for the insulation coordination, $1425[kV]$ in case of $V_n = 400[kV]$, it should be necessary to add the surge arresters. External surge arresters are the most common solutions, but otherwise should be stressful for the GIL. On the other hand Integrated surge arresters are a more expensive solutions. Many softwares have been developed in order to study the transient analysis. The Electro Magnetic Transient Program EMTP is one of the most appreciate. It is necessary to build an appropriate network



Figure 1.1: 242 kV GIL being installed in the PSEG Hudson generating station. New Jersey. 1972. View looking back from the SF₆-Air bushings.

model, this is one of the most important tasks in the modern engineering.

1.2 Gas Insulated Systems

The first Gas Insulated Transmission Line was installed at the PSEG Hudson Generating Station in New Jersey in 1972, shown in Picture 1.1 . The 242 kV, 1600 Amp system is rated 900kV BIL. This installation is still energized and in use today. The first Gas Insulated Transmission Line installed in Europe was in 1974 to connect the electrical generator of a hydro pump storage plant in Schluchsee, Germany. Picture 1.2 shows a view onto the tunnel in the Black Forest Mountain with two systems of 420kV to be connected to the overhead line on top on mountain. With 700 meters of system length running through a tunnel in the mountain, this is the longest application at this voltage level in the world. [HK08]

1.2.1 Design

The insulating mechanism in a GIL is, therefore, similar to an overhead line where the air around the line acts as gas insulation. A GIL is like an overhead line inside an enclosure. The conductor needs to be held in the centre of the enclosure so that the electric field distributes equally in the concentric pipe system. Insulators are typically made of epoxy resin with filler material. The conductor pipe is an extruded pipe made of electrical aluminium with high electric conductivity. Also the outer enclosure pipe is made by aluminium. Picture 1.3 shows conductor pipe in the enclosure pipe. Picture 1.4 shows a conical insulators with sliding contact. Picture 1.5 shows a typical configuration by Siemens. [Koc12]

The Dielectric Dimensioning

The dielectric design of a GIL is based on a formula 1.1 for the electric field in coaxial geometry.



Figure 1.2: Schluchsee Hydro Pump Storage Plant.

$$E = U \frac{1}{r_2 \ln \frac{r_2}{r_1}} \quad (1.1)$$

E is the electrical field strength which is identified through voltage tests, typical field strength is about $20kV/mm$ [Eln14]. U is the applied voltage (usually the high frequency lightning impulse voltage test) , and r_2 and r_1 are the enclosure and conductor radii respectively. The most economical use of materials occurs when the conductor stress is minimized. This occurs when $\ln(r_2/r_1) = 1$. Most GIL designs in use today are based on log ratios close to unit. The allowable voltage stress depends on the insulating gas used and the gas density. The usual choice consist in a mixture of SF_6 and Nitrogen (Second Generation of GIL) instead a pure SF_6 (First Generation GIL) [Eln14] , but nowadays many studies are developed in order to find solutions for better environmental conditions. SF_6 (Solphur hexafluoride) is an artificial gas which is non-toxic, non-flammable, non-corrosive, inert and stable over the long term. [Eln14] Picture 1.6 show the relationship between enclosure and conductor diameters for $\ln(r_2/r_1) = 1$. But first it is necessary to select the conductor diameter, which depends on the BIL, the negative impulse voltage. Picture 1.7 shows BIL performance for various conductor diameters, for the range from 115kV trough 800kV.



pipe.png

Figure 1.3: Conductor pipe

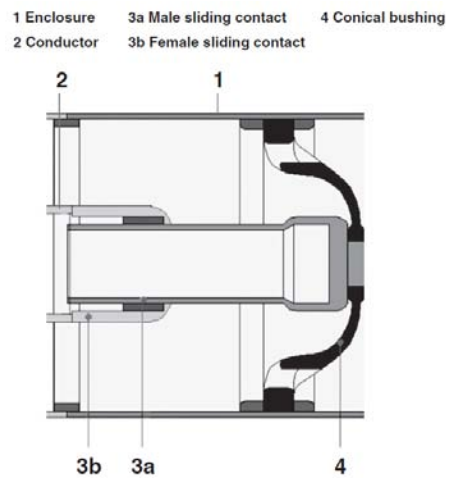


Figure 1.4: conical insulators with sliding contact



Figure 1.5: Typical configuration by Siemens

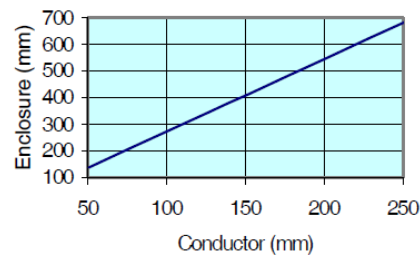


Figure 1.6: Relationship between Enclosure and Conductor Diameters [HK08]

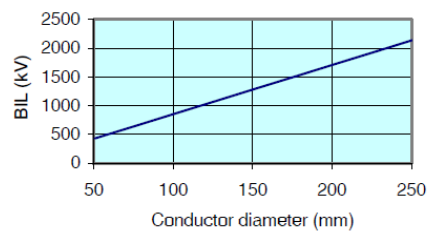


Figure 1.7: BIL performance for various conductor diameters for 115[kV] – 800[kV] applications [HK08]

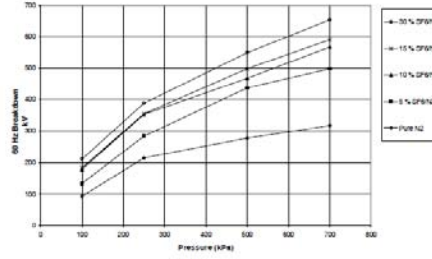


Figure 1.8: 60Hz breakdown results for a 145kV Coaxial Geometry with Enclosure/Conductor Dimensions of 241.3/88.9mm [HK08]

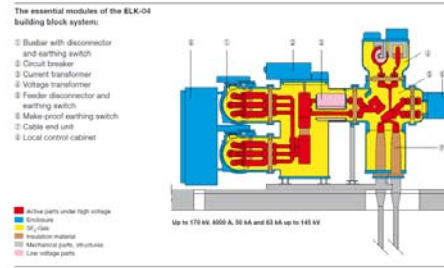


Figure 1.9: Gas-insulated Switchgear ELK-04 by ABB

Thermal Dimensioning [Eln14]

For the Thermal Design it is necessary to find a compromise between the current rating, which is responsible for the heat generated from the GIL conductor, and the costs. The current depends on r_1 and r_2 and on the thickness. A conductor with a large diameter means more current can be transmitted, for this reason a larger enclosure pipe diameter is required, in order to offer enough surface area to transfer the heat to the ambient air. This has a great impact on the total cost. The IEC 62271-1 affirm that the typical temperature of the insulators is 105–120C and for the enclosure 50C for directly buried and 60–70C for tunnel laid GIL.

Gas Dimensioning

In matter of the choice of insulating gas, for long circuit lengths, SF_6/N_2 mixtures offer an environmentally friendly and economical approach. Moreover small amounts of SF_6 in a nitrogen base have very beneficial effects on the dielectric performance. Picture 1.8 shows how, at the same pressure, a modest 15% SF_6 contents will double the breakdown voltage compared with a pure Nitrogen. [HK08]. The gas pressure ranges is from 0.4MPa to 0.8MPa, depends on the mixture of gas. [Eln14]



Figure 1.10: Gas-insulated Switchgear ELK-04 by ABB

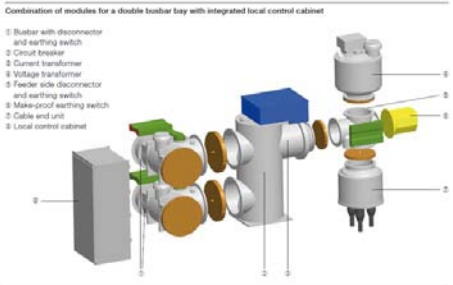


Figure 1.11: Gas-insulated Switchgear ELK-04 by ABB

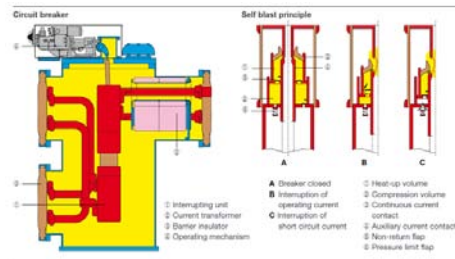


Figure 1.12: Circuit Breaker by ABB

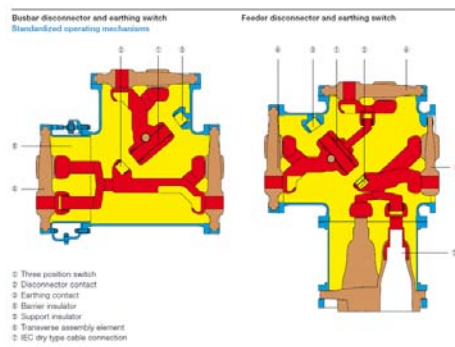


Figure 1.13: Disconnecter by ABB

The Switchgear

The picture 1.9 shows a Gas-insulated Switchgear ELK-04 by ABB. [ABB09]. The outstanding arc interruption performance of SF_6 increased the switching efficiency of circuit breakers and led to the development of a very successful high voltage switchgear with high capability and reliability. [Eln14] The Circuit Breaker CB are the most important modules of the switchgear. The picture 1.12 shows an innovative design by ABB. This is a self blast interrupting unit, equipped with a two-stage blast volume. The partial volumes are separated from each other by means of a freely movable non-return flap (5). In the compression volume(2), the SF_6 -gas is compressed during the switch off movement. The gas suppresses switching arcs in the range of the operating currents in the same manner as known from the conventional puffer interrupting unit: there is a presence of a fixed piston and a moving cylinder, fixed and moving contact. When the CB open and the arc occurs the SF_6 is compressed to extinguish the arc. In matter of disconnecter and earthing switch the busbar module contains the busbar conductors and a transversal arranged three position switch (1). This guarantees that the circuit breaker can safely be disconnected and earthed. As shown in picture 1.13

1.2.2 Advantages of GIL

The GIL has the advantage of having electrical behaviour similar to an overhead line, as explained before. GIL capacitance is lower than cable capacitance, as shown by the formula 1.2, typically $C_{GIL} = 55\mu F/km$, for this reason it is possible build long lines without compensation.[RB10] [LB11] Furthermore, the dielectric gases are non-aging so that there is almost no limitation to lifetime, no electric aging and no thermal aging. The GIL has the lowest electrical losses of all available transmission systems due its large cross-section of the conductor and enclosure pipes. In fact it is possible to affirm that the GIL power losses are around 1/3 compared with the Overhead Lines, and 1/2 compared with cables. [DL15]

$$C_{cable} = (4 \div 7)C_{GIL} \quad (1.2)$$

$$C_{GIL} = 4C_{OHL} \quad (1.3)$$

$$C_{cable} = (20 \div 60)C_{OHL} \quad (1.4)$$

Furthermore the metallic enclosure is reliable protection from external magnetic fields and internal faults. [HK08] The GIL external magnetic fields are only 5% of the levels for conventional cable at ground level. [Koc12] This occurs because, for the low enclosure resistance, the current induced in the enclosure have the opposite direction and the same amplitude of the currents through the conductors. [DL15] In so doing there is a compensation of the magnetic field. GIL have an high level of personal safety. The GIL power rating is like an Overhead line. The high power transmission capability of the GIL,(up to 300 MVA per system at 550kV rated voltage) allows it to go directly underground in series with an overhead line without power reduction. GIL have an high reliability, no internal switching or breaking capability is needed. For this reason the GIL can be seen as a passive high-voltage gas-insulated system with no active moving parts. [Koc12]



Figure 1.14: Overhead Line-bushing connection [Koc12]

1.2.3 OverHead line connection

To connect the GIL to the overhead line, gas to air brushings are needed. To protect the GIL from transient over voltages of the overhead line from lighting strikes surge arresters are connected parallel to the bushing. Bushing and surge arresters can be located underneath the overhead line, as shown in picture 1.14 . [Koc12] Picture 1.15 shows a view of the terminal tower and a gantry in a GIS, this kind of configuration will be use in the experimental part.

1.2.4 Economic Aspects

In matter of economic aspects the first-place investment cost is high for the product and its installation. The operation cost is low. The main part of the installation cost is due to the aluminium pipes for enclosure and conductor. The second largest cost share comes from the laying and installation process. The picture 1.16 shows the split of cost share of GIL. The smallest part of the cost is in engineering, planning, calculation, project management and all kind of studies needed before. [Koc12]

1.3 Composed Lines

High voltage overhead lines in Distribution Power Systems are most commonly. On the other hand nowadays some problems about this kind of lines have been



Figure 1.15: Terminal Tower and Gantry, picture by David Neale on Flickr

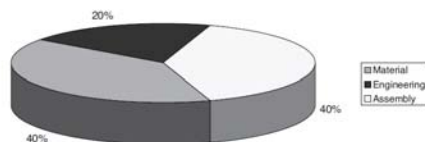


Figure 1.16: Costs of GIL [Koc12]

appeared, for example the impact on environment. For this reason some studies are taking place. In particular is shown the study by Cigrè [C3.15], about the externalities of Overhead High Voltage Power Lines. This study could be helpful in order to do a correct evaluation of the Cost Benefit Analysis. In fact generally environmental impact of transmission project should be avoided or mitigated. Any residual effects should be evaluated. Anyway some non-evaluated residual effects remain. A correct analysis is necessary in order to evaluate costs, benefits and alternative solutions. Anyway it is important to note that the elements in the environment usually not have a market price. Hence one must use various methods to construct a substitute to a market value. The main residual environmental effects are considered to be related to: landscape, biodiversity and the natural environment, proximity effect as far of fem and noise. The aim of the Cigrè study is to provide a state of the art of existing methodologies applied to power lines, and hence give a guidelines to assess the environmental externalities of High Voltage Overhead Line according to the current knowledges. The underground cables can provide some advantages: improved aesthetics, fewer outages during normal weather, far fwe momentary interruptions. On the other hand there are some potential disadvantages which need to be considered, for example costs, longer duration interruption, reduced life expectancy, higher maintenance and operating costs. For these reasons the new trend is to build a mixed lines, (or composed lines, or hybrid systems) composed by an Overhead line and underground cable. In particular in this work the electrical behaviour of a composed line by OHL and GIL is investigated. In

fact the electrical transient on a Gas Insulated Transmission Line involve in a Very Fast Transient which could be dangerous for the transmission system.

Chapter 2

Transient Analysis

2.1 Introduction

When any sudden change occurs in a circuit, there is generally a redistribution of energy to meet the new conditions. It is very important to realize that this redistribution of energy cannot take place instantaneously for two reasons. The first one is that to change the magnetic energy requires a change of current. But change of current in an inductor is opposed by an emf of magnitude LdI/dt . An instantaneous change of current would therefore require an infinite voltage to bring it about. Another way of stating this is that the magnetic flux linkage of a circuit cannot suddenly change. The second reason is that to change the electric energy requires a change in voltage. For an instantaneous change of voltage in capacitors an infinite current must flow. Usually transient phenomena in power systems are caused by switching operations, faults, and many other disturbance. The transient analysis is very helpful in order to solve important problems caused by these phenomena, for example the coordination of power apparatus and some protective devices. Transient phenomena in power systems involve a frequency range from DC to several MHz, for example it is around the 10kHz for the switching operations, and around the 400kHz for the lighting. The principle of superposition is very powerful to solving problems, and it is just as valid for the transient state as it is for the steady state. In the other hand this method can be applied only in linear circuits. Unfortunately in utility there are some components that are non linear, below will be show how can study the transient with non-linear conditions using the principle of superposition.

2.1.1 Transient Analysis with non linear conditions

The study of transient network with non linear element and switching element would be not easy. Time domain methods represent the current trend of modeling for electromagnetic transient analysis. But unfortunately it is difficult to take into account the frequency dependence, because it introduces complicated convolution procedures. On the other hand, when using frequency domain tech-

nique to analyze electromagnetic transients, the frequency dependence of electrical parameters can be taken into account very easily. It is necessary to use the superposition principle, in so doing the discontinuities, for example switching maneuvers, are treated as initial conditions problem, and the non linear elements are reduced to series of sequential discontinuities.

Ideal Switch model

An open switch can be represented by a voltage source, $V_{(sw)}$, which has the same value of the difference potential between its terminals. This is the initial condition, means the condition existing before the switch closure. In the same way a close switch is accomplished by the series connection of voltage source, $V_{(sw2)}$, equal magnitude but in the opposite sense to $V_{(sw)}$. So the total response of electrical network is obtained by the superimposing the response due to $V_{(sw)}$ to the response due to $V_{(sw2)}$. On the other hand a close switch can be represented by a current source, $I_{(sw)}$, equal to the current flowing across its terminals. A open switch is accomplished by connecting in parallel a current source $I_{(sw2)}$, which has the same magnitude but opposite sense to $I_{(sw)}$. The total response of electrical network is obtained by the superposing the response due to $I_{(sw)}$ to the response due to $I_{(sw2)}$. In order to consider the real switch is it necessary take into account also the respective resistances.

Non linear elements

In order to include the non-linear elements in the transient analysis in frequency domain, is it necessary to approximate the non-linear characteristic in piece-wise linear forms, as shown in picture 2.1. In so doing the simulation procedure is reduced to a sequence of switching operations. Each segment represent the Thevenin equivalent that the network sees toward the non linear element. The voltage between the node j and k is defined as $V_{(jk)} = V_i R_i I$.

$$V_{(xn)} = \frac{R_{(n-1)}V_n - V_{(n-1)}R_n}{R_{(n-1)} - R_n} R_{(xn)} = \frac{R_n R_n}{R_{(n-1)} - R_n}$$

When switch n is open, it can be closed only after switch n-1 has been closed. When switch n is closed, it cannot be opened if switch n+1 is still closed.

2.2 Transmission Lines Transient Analysis

The equipment's costs are more in transient than in steady-state conditions. For this reason it is important to predict accurately the behavior of the system, because, specially for the High Voltage Power Systems, any tolerance on equipment specifications may present a considerable increase of costs whit no guarantee of optimum operation. For the study of the transmission lines it isn't possible to use the approach of lumped circuit analysis, because the approximations are too great. In fact in this kind of study it's very important abandoning

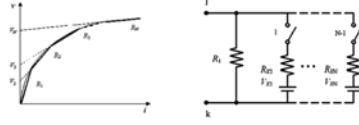


Figure 2.1: Approximation of non-linear characteristic

certain cherished notions about the behavior of circuits, for example the idea that the current is the same in all the points of the line, and that the voltage cannot be discontinuous. . If we represent the OHL or the cable by a PI-Section, when the switch at the sending end of the network close the disturbance at one end of the PI-Section network is immediately noticeable at the other end of the network, But it is not what happens in a real case, it takes a certain time before the current and voltage waves reach the end of the line. [dS01]

2.2.1 Theory of Travelling Wave

A transient phenomena in transmission lines, for example fault conditions or energization lines or fulmination conditions, generate waves which travel along the line. The transient parameters in transmission lines depends on the space, as in steady-state, but also on the time. In this case the time-dependence is really important because it is not known from the start. Transient phenomena is described through an unidirectional component and eventually periodical components. That involve an imbalance between the phases, for this reason it is necessary considerate the homopolar parameters, it means parameters associated to a current flowing to the ground.

For overhead lines

$$C_0 = \frac{24,14}{\log\left(\frac{4h}{d}\right)} \quad (2.1)$$

$$l_0 = 0,46 \log \frac{4h}{d} \quad (2.2)$$

For cable lines

$$C_0 = \frac{2\pi\epsilon_0\epsilon_r}{\ln\left(\frac{d_s}{d_c}\right)} \quad (2.3)$$

$$l_0 = \frac{\mu_0}{2\pi} \ln\left(\frac{d_s}{d_c}\right) \quad (2.4)$$

Where d_s is the diameter of the sheath, and d_c is the diameter of the core.

For the GIL cables

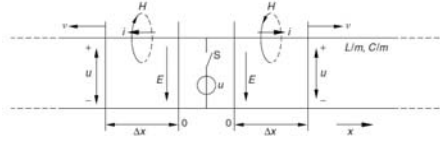


Figure 2.2: Electric and magnetic field around a line segment Δx of a transmission line

$$C_0 = \frac{2\pi\epsilon_0\epsilon_r}{\ln\left(\frac{d_i}{d_c}\right)} \quad (2.5)$$

$$l_0 = \frac{\mu_0}{2\pi} \ln\left(\frac{d_i}{d_c}\right) \quad (2.6)$$

Where d_i is the diameter of the outer housing, and d_c is the diameter of the core. This is the only case where the homopolar components are the same of the exercise components, because each cable is decoupled. [RB10]

It is also necessary to define the wave impedance as

$$Z_0 = \sqrt{\frac{l_0}{C_0}}$$

The circuit in picture 2.2 shows a line length Δx , considering a distributed parameters two-wire transmission line, v_1 and i_1 are the voltage and the current at the sending end, and v_2 and i_2 are the voltage and the current at the receiving end. [dS01]

$$v_1 = v(x, t)$$

$$i_1 = i(x, t)$$

$$v_2 = v_1 + \Delta V$$

$$i_2 = i_1 + \Delta I$$

$$v_2 - v_1 = \Delta V = l_0 \Delta x \left(-\frac{\delta i_1}{\delta t}\right) \quad (2.7)$$

$$i_2 - i_1 = \Delta I = C_0 \Delta x \left(-\frac{\delta v_1}{\delta t}\right) \quad (2.8)$$

$$\frac{\Delta V}{\Delta x} = -l_0 \frac{\delta i_1}{\delta t} \quad (2.9)$$

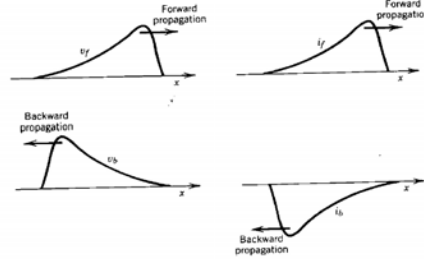


Figure 2.3: Voltage and Current Wave

$$\frac{\Delta I}{\Delta x} = -C_0 \left(\frac{\delta v_2}{\delta t} \right) = C_0 \left(-\frac{\delta(v_1 + \Delta V)}{\delta t} \right) = -C_0 \left(\frac{\delta v_1}{\delta t} + \frac{\Delta V}{\delta t} \right) \quad (2.10)$$

Neglecting the differential of second order the equation became

$$\frac{\Delta I}{\Delta x} = -C_0 \frac{\delta v_1}{\delta t} \quad (2.11)$$

$$\begin{cases} \frac{\Delta V}{\Delta x} = -l_0 \frac{\delta i_1}{\delta t} \\ \frac{\Delta I}{\Delta x} = -C_0 \frac{\delta v_1}{\delta t} \end{cases}$$

These equations relate the time-dependence with the space-dependence. The solution of this system is shown below

$$V(x, t) = V_d(x - \alpha t) + V_s(x + \alpha t) \quad (2.12)$$

$$I(x, t) = \frac{V_d(x - \alpha t)}{Z_0} + \frac{V_s(x + \alpha t)}{-Z_0} \quad (2.13)$$

In this case $\alpha = \frac{1}{\sqrt{l_0 C_0}}$ has a speed dimension. [RB10] On Overhead Transmission line the electromagnetic waves propagate close to the speed of light, but in an underground cable the velocity is considerable lower. The equations 2.12 and 2.13 show that there are two components, which one depending on $(x - \alpha t)$ and the other one depending on $(x + \alpha t)$, as shown in picture 2.3 and 2.4. These components identify two traveling waves, one forward and the other one backward. The value of these function depends on the limit condition: how the line is excited, or how the line is closed. [RB10]

For this work it is of particular interesting to investigate the travelling wave considering to have two different lines, with two wave impedance, connected at point M. As shown in picture 2.5. On the line 1, with wave impedances Z_1 , a voltage wave v_i is traveling forward. The value of this voltage wave is V_1 . If, at the time of the impact in M, the voltage on the right of M is the same

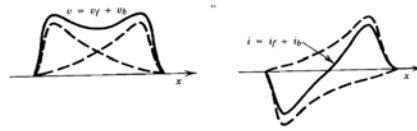


Figure 2.4: Superposition of Waves

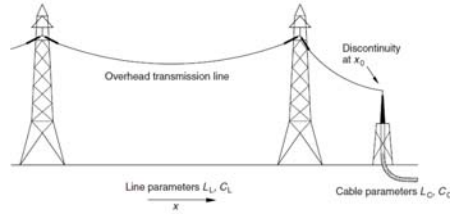


Figure 2.5: Overhead Transmission line terminated by a underground cable

value V_1 , it will be $\frac{v_i}{Z_1} \neq \frac{v_i}{Z_2}$ but for the electrical rules it is not possible to have a discontinuity between two circuits in series. For this reason it is important to understand that, at the time of the impact in M, a new step of voltage is created, with value V_r , in order to have $v_i + v_r = v_2$. v_r is the reflected and v_2 is the transmitted voltage wave. In the same way for the current is $i_i + i_r = i_2$ [RB10]

at the end it is possible to define two important coefficient: l is the reflection coefficient, and τ is the transmission coefficient. [RB10]

$$\begin{cases} l = \frac{Z_2 - Z_1}{Z_2 + Z_1} \\ \tau = \frac{2Z_2}{Z_2 + Z_1} \end{cases}$$

$$\begin{cases} v_r = lv_i \\ v_2 = \tau v_i \end{cases}$$

$$1 + l = \tau \quad (2.14)$$

It is possible to define analogous equations for the current [RB10]

$$\begin{cases} i_r = -li_i \\ i_2 = \tau \frac{Z_1}{Z_2} i_i \end{cases}$$

The speed of the reflected wave is defined as $\alpha_r = \frac{1}{\sqrt{L_1 C_1}}$ The speed of the transmitted wave is defined as $\alpha_t = \frac{1}{\sqrt{L_2 C_2}}$ [RB10]. If the voltage travelling wave encounters an OHL followed by a cable or a GIL (OC junction), the

reflection coefficient is negative. If the voltage travelling wave encounters a cable followed by an OHL the reflection coefficient is positive. For the line network discontinuity encountered by backward travelling waves, it can be noted that the reflection coefficient is always negative, because the source impedance is less than transmission lines surge impedances, in both cases of weak and strong network. In case of ideal network the reflection coefficient is $l = -1$ and $\tau = 2$. [MGI10]

Effect of Line Termination

The wave traveling behavior depends on the type of line, in particular on how the line is closed at the end.

- $R_2 = 0$ short circuit

$$\begin{cases} l = -1 \\ \tau = 0 \end{cases}$$

$$\begin{cases} v_r = -v_i \\ v_2 = 0 \end{cases}$$

- $R_2 = Z_1$

$$\begin{cases} l = 0 \\ \tau = 1 \end{cases}$$

$$\begin{cases} v_r = 0 \\ v_2 = v_i \end{cases}$$

- $R_2 = \infty$ open circuit

$$\begin{cases} l = 1 \\ \tau = 2 \end{cases}$$

$$\begin{cases} v_r = v_i \\ v_2 = 2v_i \end{cases}$$

If the extremity of the line is an inductance or a capacitance, the reflection coefficient is variable during the time. for example in case of inductance, the reflection coefficient change first $l = -1$ as a short circuit, and then become $l = +1$ as an open circuit. The opposite occurs in case of capacitance.

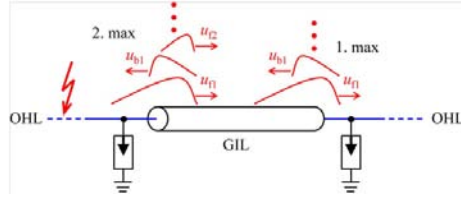


Figure 2.6: Hybrid transmission line: OHL and GIL with external surge arresters [GW15]

Attenuation and Distortion of the Travelling Wave

[dS01]

When the voltage and the current travel along a transmission line with losses, the amplitude of the wave is exponentially decreased. It means that in this case it is necessary to take into account the series resistance of the conductor, the skin effect for the high frequency, the ground resistance, the corona losses. The attenuation is small for a line with a low resistance and/or a large characteristic impedance, as shown the formulas 2.15 2.16

$$i(x, t) = i(x_0, t_0)e^{-(Rx)/(2Z)} \quad (2.15)$$

$$v(x, t) = v(x_0, t_0)e^{-(Rx)/(2Z)} \quad (2.16)$$

2.2.2 Travelling Wave in Hybrid System

In order to better understand the results obtained in the experimental part of this work, it is necessary to understand the theory of the travelling wave apply to the hybrid system. Considering the system shown in picture 2.6 composed by an Overhead Line and a GIL, the GIL is protected by a Surge Arrester at both ends and is subjected to lightning overvoltages. The voltage at the specific location x at the specific time t results from the superposition of forward u_{f1} and backward-travelling waves u_{b1} . The picture 2.6 shows the overvoltage buildup within a hybrid transmission line protected with external SA. The lightning stroke on the left system side results in a first forward travelling wave u_{f1} , which is reflected at the right end of the GIL as a first backward-travelling wave u_{b1} . This wave is again reflected at the left end of the GIL as u_{f2} and so on. The superposition of u_{f1} and u_{b1} result in a first maximum, and the superposition of u_{f1} and u_{b1} and u_{f2} result in a second maximum. In most cases the first maximum determines the global maximum in GIL and is dominant for insulation coordination purposes. [GW15]

Maximum Cable Voltage

[THUB05]

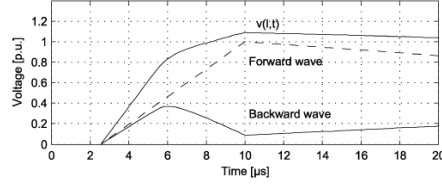


Figure 2.7: Example of voltage at cable end [THUB05]

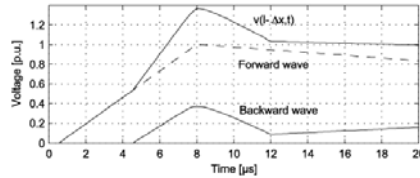


Figure 2.8: Example of voltage at the position where the maximum voltage occurs simultaneously [THUB05]

It is supposed that the length of the two part of OHL is infinite. It is reasonable to suppose that the maximum value of the overvoltage occurs at the end of the cable, because it is identify as the sum of the peak of the incoming wave (forward) and the peak of the reflected wave (backward). But this is not true, because for $x = l$ (it means at the end of the cable) the peak of the u_{f1} and u_{b1} doesn't occur at the same time. The picture 2.7 , is the experimental result from the work [THUB05] and it shows that, considering the impedance of the cable $Z_c = 30[Ohm]$ and the impedance of the OHL $Z_L = 450[Ohm]$, the peak of u_{f1} occurs at $10\mu s$ and the peak of u_{b1} occurs at $6\mu s$. But at some distance from the end of the cable the two maxima appear simultaneously. This distance could be evaluated by the formula 2.17, where v is the cable propagation velocity, and Δt is the time difference between the two maxima at the end of the cable. The picture 2.8 shows the experimental result from the work [THUB05], at the position where the maximum voltage occurs, $l - \Delta x$.

$$\Delta x = v \frac{\Delta t}{2} \quad (2.17)$$

It is important to show the trend of the reflected voltage wave as a function of the incoming voltage. It should be noted that the reflected wave is reduced if the incoming wave increases above the value that corresponds to the maximum reflected wave. The picture 2.9 show this trend, and the trend of the arrester voltage as function of the incoming voltage.

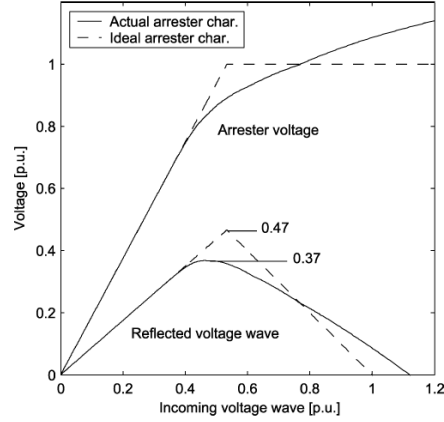


Figure 2.9: Reflected voltage wave and arrester voltage as a function of incoming voltage wave [THUB05]

Power frequency Voltage

The picture 2.10 , (experimental result from work [THUB05]) shows that the value of the reflected wave is strongly influenced by the power frequency voltage. The maximum value of the reflected wave decreases when v_0 increase, considering v_0 the instantaneous value of the power frequency voltage. It means that the arrester voltage at the remote end will be $v_0 + v(l, t)$.

Cable length

The picture 2.11 shows the trend of the incoming and reflected wave, as function of time, at the remote cable end, considering $l = 9km$. it is possible to see how the peaks don't occur at the same time, and that the peak of the incoming wave is higher than the peak of the reflected wave. Changing the length, for example just $500m$ cable length, the shape of the incoming wave change significantly, as shown in picture 2.12 and the peak is higher. It occurs because the reflected wave at the remote end becomes reflected again when it meets the exposed end. In this case the maximum value of voltage occurs close to the exposed end. And finally the pictures 2.13 show the voltage wave at the remote end and at the $x = l - \Delta x$ it means where the maximum voltage occurs, for $l = 9km$ and for $l = 50m$. The maximum at $x = l - \Delta x$ is higher than the maximum at the remote and, and for short cable the peak is higher than for long cable.

2.3 Capacitive Load Switching

Considering the circuit in picture 2.14, supposing that the CB open in $t = t'$, due the capacitance at the end of the line a capacitive current is still flowing in

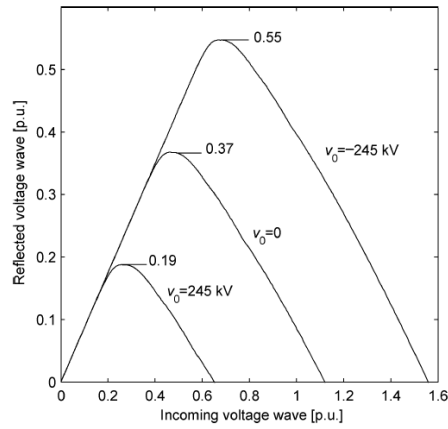


Figure 2.10: Reflected wave as function of incoming wave for different values of instantaneous value v_0 of power frequency voltage [THUB05]

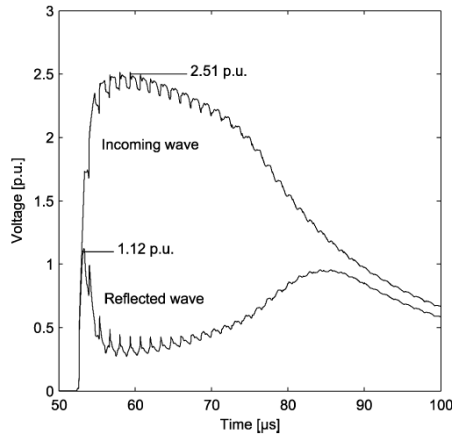


Figure 2.11: Reflected and incident voltage wave at the remote end of the cable $l = 9\text{ km}$ [THUB05]

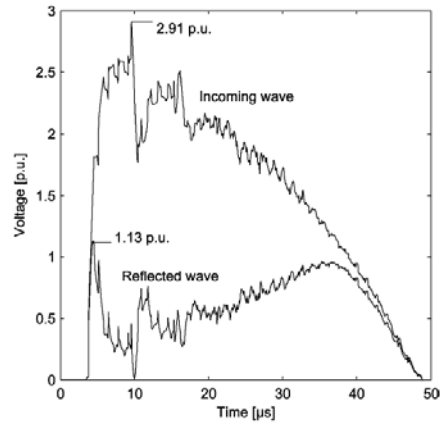


Figure 2.12: Reflected and incident voltage wave at the remote end of the cable $l = 500m$ [THUB05]

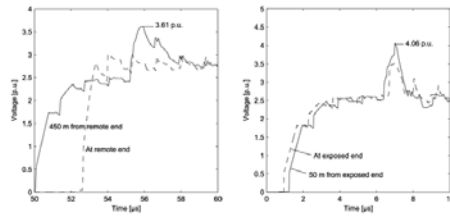


Figure 2.13: Voltage waves at the remote and and at $x = l - \Delta x$ considering $l = 9km$ at the left and $l = 500m$ at the right [THUB05]

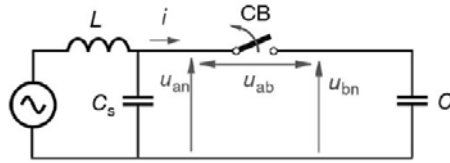


Figure 2.14: Circuit Capacitive Load Switching [DR15]

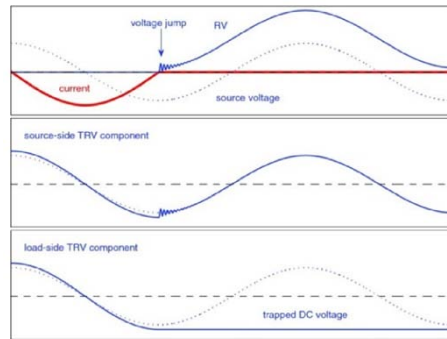


Figure 2.15: Voltage Trend during the Capacitive Load Switching [DR15]

the system after $t = t'$. [DR15] This situation could be for example the opening operation on the OHL, due the stray capacitance of the OHL, and it will be investigated in the experimental part. Picture 2.15 shows the results expected from the theory. The upper picture shows the voltage trend between the CB contacts: for $t < t'$ the CB is closed, and the voltage across the contacts is equal to 0. For $t > t'$ the CB is opened, there is a voltage jump across the contacts, and the voltage start to oscillate at the same frequency of the source voltage. The picture in the middle shows the voltage trend at the source side, it shows the L-G voltage. The voltage oscillate as the source voltage, as expected, but in $t = t'$ the voltage is influenced due the voltage jump. The bottom picture shows the voltage trend at the load side, for $t < t'$ the voltage oscillate as the voltage source, when $t > t'$ the voltage has a constant value due the trapped in the capacitance at the end of the line.

2.4 Very Fast Transient Overvoltage on Gas Insulated Systems

The coaxial conductors in Gas Insulated Substations, compared to the Air Substations, present an higher specific capacitance to heart. For this reason the capacitive currents of off-loaded bus are larger than in open air substations. On the other hand the conductors in GIS present a lower characteristic surge

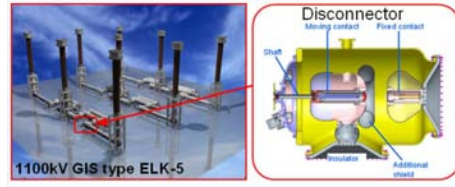


Figure 2.16: 3D simplified representation of the 1100kV GIS type ELK-5 and details of its disconnector

impedance and inductance. [ZH15] For certain switching conditions where GIS disconnectors are operated following circuit breaker operation it is possible to generate Very Fast Transient Overvoltage, VFTO, which acts as travelling waves and propagate within and external to the GIS. For the presence of the point of discontinuity on the GIS structure, there are many reflections of the travelling wave. The result is a network of high frequency over voltages appearing within the GIS. [AT15] This occurs because the disconnector contacts in GIS are moving slowly. The circuit breakers are designed to make and break continuous and fault currents. Typical contact operating times and velocities are Break time $50ms$ with contact velocity $9m/s$. Closing time: $90ms$ with contact velocity $3m/s$. In matter of disconnectors on GIS, they are designed to make and break capacitive current, as told before, and for this reason they are much slower in operations. Typical values are operating time of $5s$ with an operating velocity of between 50 to $300mm/s$. [AT15] For this reason during disconnect switch operation number of restrikes occurs. Picture 2.16 shows a 3D simplified representation of the 1100kV GIS type ELK-5, and the details of its disconnector.

The picture shows the fixed contact and the moving contact. After the contact separation, the fixed contact and the attached busduct become a floating potential body, and the moving contact and the attached busduct follow the electric potential of the network, because the moving contact is attached to the network, as picture 2.17 and 2.18 show. After the separation of the contacts, the potential difference between the contacts exceed the dielectric strength, producing an electric breakdown between the contacts at certain moment of time, as shown in picture 2.18, where U_{diff} represents the potential difference between the contacts. Numerous strikes and restrikes occur because the disconnector contacts in GIS are moving slowly, as told before. Picture 2.19 shows a very simplify 3D model of GIS. [JSR11]

Every strike causes high-frequency currents tending to equalize the potential between the contacts. The basic frequency is on the order of $100kHz$ up to several MHz , and peak value up to few kA . When the current is interrupted, because the spark is extinguished, the voltage source side and loading side will oscillate independently, again. As soon as the voltage between the contacts exceeds the dielectric strength of the gas the restrike will occur. The over voltages due to the disconnector switching can be considered as a travelling wave propa-

2.4. VERY FAST TRANSIENT OVERVOLTAGE ON GAS INSULATED SYSTEMS 47

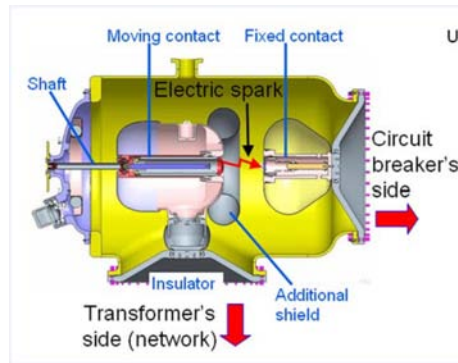


Figure 2.17: Disconnector operations

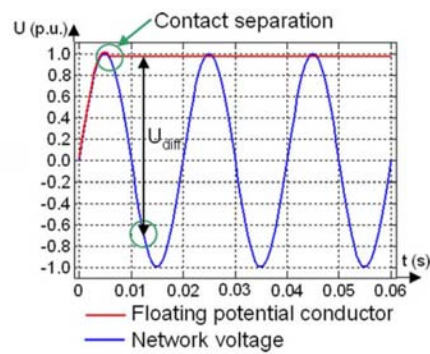


Figure 2.18: Voltage Difference Between the Contacts

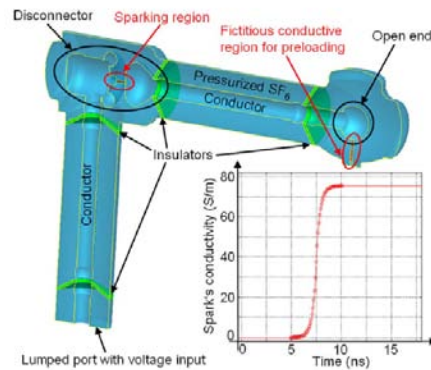


Figure 2.19: 3D simulation model of the 1100kV GIS type ELK-5

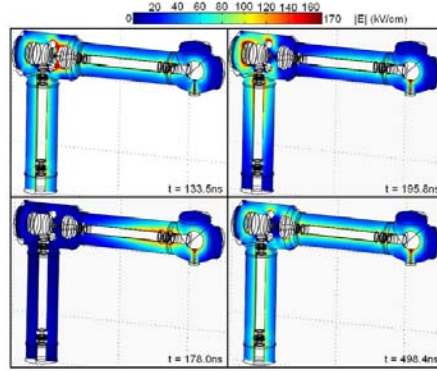


Figure 2.20: Results of the 3D time-domain full-Maxwell simulations of the 1100kV GIS type ELK-5

gating along particular elements of the substation. It depends on the substation configuration, the insulation co-ordination. Depends on the voltage level. In order to study correctly the VFT it is important represent the system accurately. It is one of the most decisive task in modern engineering approach. [ZH15] Picture 2.20 shows the result of the study of VFT. The first frame (top left) shows the electric field at the moment of time just before the electric spark. As one can see the most intensive electric field is established between the disconnector's contacts. The next two frames (top-right and bottom-left) represent the travelling electromagnetic wave, at two different moments of time after the spark ignition.

The last frame shows the steady-state after the VFT are partially dissipated. Misuraments un 420kV GIS disconnector by [DPW96] show that the VFT is characterized by a step front having a rise time between 2 and 20ns , followed by a mono-frequency oscillation of some MHz. The rise time of the voltage depends on the field strength of the gap, as shown in the formula

$$t_{rise} = 13,3 \frac{k_T}{(\epsilon/\rho_0)ph} \quad (2.18)$$

Where k_T is the Toepler spark constant, $50[kV/ns * cm]$ h is the field utilization factor p is the gas pressure And ϵ/ρ_0 is the filed strength which for the SF_6 is $860[kV/cm]$.

The overvoltage caused by VFT could be dangerous for some components, for example for the spacers, bushings, and expecially transformers in case of internal resonance. The VFT may interfere with the secondary equipement, or similar effects may occur at the transision of the OHL causing transient enclosure voltage (TEV). The TEV may interfere with secondary equipment by raising the housing potential of such equipment and by emitting free radiations. [DPW96]. For these reasons, as told before, it is possible divide the VFT into internal and external VFT. Picture 2.21 shows explicitly this classification.

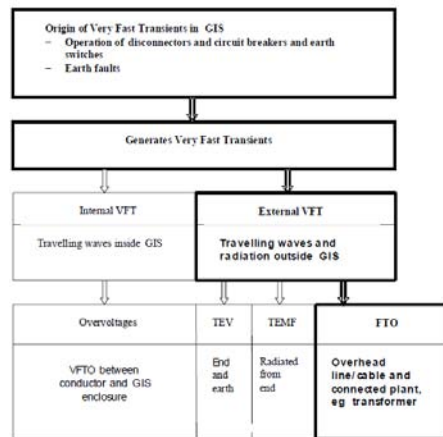


Figure 2.21: Very Fast Transient Classification

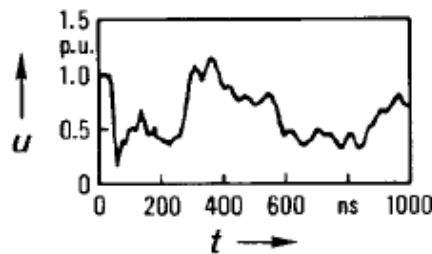


Figure 2.22: Steep Voltage Transient

Internal VFT involves travelling waves inside the GIS, and as a consequence over voltages between conductor and GIL enclosure. External VFT involves travelling wave and radiation outside the GIS. [AT15].

2.4.1 Internal VFT

[JM89]

The picture 2.22 and 2.23 show the typical waveform of the VFT on GIS, with a steep voltage impulse having, as told before, a rise time between 2 to 7[ns], and a monofrequent oscillation of some MHz and some kHz. Approximately 100s after the beginning of the flashover the arc in disconnector is extinguished. The magnitude of peak voltage depends of some factor, on the configuration of the line, the type of switch and the trapped charge. This value is typically between 1.5 to 2.4pu. Therefore the value never reach the BIL of the substation.

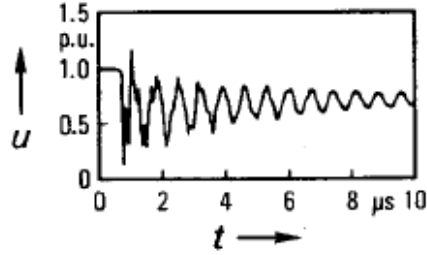


Figure 2.23: Oscillation of the GIS with some MHz

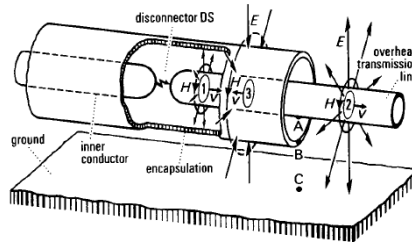


Figure 2.24: Propagation of travelling waves caused by a disconnector operation

2.4.2 External VFT

[JM89]

The picture 2.24 show how the internally generated VFT propagates as a travelling wave through the bus (1), and reaches the bushing where a part causes the transient rise of the enclosure voltage (3) and a part propagates along the OHL and may stress the adjacent equipment.

Picture 2.25 represent a simplify equivalent circuit to study the behavior of the travelling wave outside the enclosure. This is the Transient Enclosure Voltage TEV. The OHL is directly connected with the GIS, and it is represented by L_F and C_F . The bus duct is represented by $L - C$ elements as well. Z_k is the impedance of the enclosure and Z_i of the SF_6 -bus. When the travelling wave reaches the end of the bus-duct, where normally the bushing is located, an electromagnetic field occurs outside the busduct causing the transient rise of the enclosure voltage.

In order to evaluate the worst case peak U_k , it is possible to use the circuit shown in picture 2.26.

$$-U_0 = \frac{Z_k}{Z_k + Z_i + Z_f} \quad (2.19)$$

for example, considering a 420kV GIS connected to an OHL, considering

$$Z_k = (60 - 20) \text{ Ohm}$$

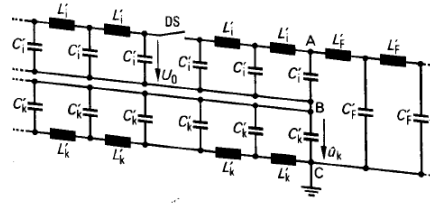


Figure 2.25: Equivalent Circuit

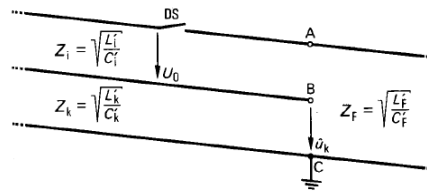


Figure 2.26: Equivalent Circuit

$$Z_i = 60\text{Ohm}$$

$$Z_f = 270\text{Ohm}$$

$$U_0 = \frac{\sqrt{2}}{\sqrt{3}} U_m \tag{2.20}$$

The U_k is in the range of some 10kV

$$U_k = -(50 - 17)\text{kV} \tag{2.21}$$

$$\frac{U_k}{U_0} = (10 - 30)\% \tag{2.22}$$

It depends on the value of Z_k , which should be as low as possible.

2.4.3 Representation of the GIL components

Since the VFT follows the same travelling wave theory as that of lightning sources in transmission lines, it is possible to represent GIS as an equivalent transmission line of series of transmission lines and lumped capacitor elements. For example pictures 2.27 2.28 2.29 [DPW96] show some electrical equivalent circuits which are commonly adopted to represent the main component of typical GIS. Other solutions are sometimes adopted, for example for elbows and spherical shields

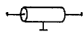

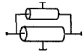
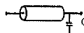
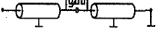
Component	Equivalent circuit	Notes
Bus duct		Loss-free distributed parameter transmission lines
Spacer		($C > 20$ pF)
Elbow		
Spherical shield		($C < 40$ pF)
Surge arrester		

Figure 2.27: Equivalent circuits for GIS components for representation of VFT (1)

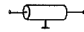
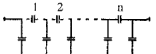
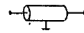
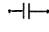

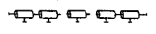
Closed switch		
Open switch		(n = number of breaking chambers)
Closed disconnector		
Open disconnector		
Disconnector during sparking		$r = r(1)$; $R < 10 \Omega$ $C > 10$ pF
Bushing (capacitive type)		n = number of equivalent shields (5 + 8) simulated

Figure 2.28: Equivalent circuits for GIS components for representation of VFT (2)

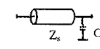

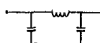

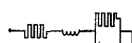
Bushing (gas filled)		$C > 10 \text{ pF}$ $Z_c \approx 250 \ \Omega$
Power transformer (termination)		parameters evaluated from the frequency response of the transformer
Current transformer		sometime negligible
Capacitive voltage transformer		
Earth connection		

Figure 2.29: Equivalent circuits for GIS components for representation of VFT (3)

and for bushings, it depends on the accuracy to be reached and the frequency interest.

The quality of the simulation depends on the quality of the model of each individual GIS component. Due to the geometrical structure of the GIS and the enclosure material the internal losses can be normally be neglected and only the dielectric losses in some components need to be taken into account. According to their internal design all part of the GIS will be represented thoroughly by line sections with the corresponding source impedance and travelling wave time, and by lumped capacitance as explained before. The value of each GIS section can be calculated from the standard formula of capacitance and inductance. [AT15].

$$C = \frac{2\pi\epsilon}{\ln(\frac{b}{a})} [pF/m] \tag{2.23}$$

$$L = \frac{\mu}{2\pi} \ln(b/a) 10^6 [\mu H/m] \tag{2.24}$$

Where C is the capacitance of the GIS busbar. L is the inductance of the GIS busbar, b is the inside diameter of the GIS enclosure, a is the outside diameter of the GIS busbar, ϵ is the absolute permittivity of $SF_6 = 8,8510^{-12}$ Mi is the absolute permeability of copper conductor $4\pi 10^{-7}$. The lumped capacitance values applicable to the insulators, busbars, line bushings and other can be determined from the formula 2.23 using the manufacturer's drawings and technical component data.

The study by [RH12] aim to modify these models in order to make them applicable to the higher frequencies.

- Bus duct

Is a single phase coaxial structure. To present this is used the distributed transmission line model, lossless, with the wave impedance around $z_c =$

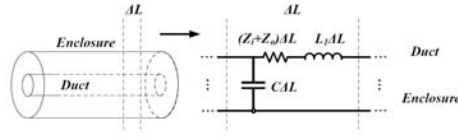


Figure 2.30: The equivalent circuit model of bus duct

60–100[Ohm] Picture 2.30 shows the structure. It is possible evaluate the inner impedance 2.25 and the outer impedance 2.26

$$Z_i = \frac{\rho m}{2\pi r_1} \coth(mr_3) - \frac{\rho}{2\pi r_1(r_1 + r_2)} [\text{Ohm}/m] \quad (2.25)$$

$$Z_o = \frac{\rho m}{2\pi r_2} \coth(mr_3) - \frac{\rho}{2\pi r_2(r_1 + r_2)} [\text{Ohm}/m] \quad (2.26)$$

$$r_3 = r_2 - r_1$$

$$m = \sqrt[2]{i2\pi f \mu / \rho}$$

Where f is the VFTO higher frequency, usually assumed as 100MHz. μ is the conductor permeability, $4\pi 10^{-7} [H/m]$ and ρ is the tabular conductor resistivity. These formulas apply only to $(r_2 - r_1)/(r_2 + r_1) < 1/8$. The capacitance and mutual inductance between duct and enclosure are evaluated by the formulas

$$L_1 = \frac{\mu_0}{2\pi} \ln \frac{R_1}{r_2} [H/m] \quad (2.27)$$

$$C = \frac{2\pi\epsilon}{\ln(R_1/r_2)} [F/m] \quad (2.28)$$

In so doing the equivalent circuit model of bus duct as distributed transmission lines is shown in picture 2.30

- disconnector

The disconnector has three states during its operations, disconnected, action state and closed state. These states are shown in picture 2.31. C_2 is the capacitance between the moving contact and the enclosure. C_1 is the capacitance between the static contact and the enclosure. C_0 is the fracture capacitance between the moving contact and the static contact. The propagation of electromagnetic wave is expressed by transmission line. During the closed state the moving and static contact are connected together. During the action state, the arc model is taken into account considering a time-varying resistance

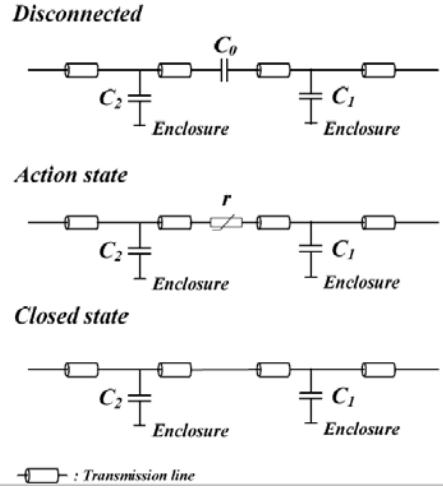


Figure 2.31: The equivalent circuit model of disconnector

for $0 < t < t_1$

$$r(t) = 0,5 + 2Ze^{-t/\tau} \quad (2.29)$$

for $t > t_1$

$$r(t) = 0,5 \quad (2.30)$$

Where Z is the wave impedance of the disconnector. t_1 is the break down delay time, typically in $10ns$. [RH12] There are many different arc models in literature, in the experimental part the most common arc model will be investigated.

- Basin insulator

The basin insulator support the duct and split SF_6 gas chambers, as shown in picture 2.32 . Analyzing the electric field distribution of a bus duct , as shown picture 2.33, with a basin-insulator, it is possible observe that the electric field distribution is altered. There is an area where the propagation of electromagnetic waves is delay. This area is equivalent to a lumped capacitance and an equal-length transmission line, as shown picture 2.34 . Picture 2.35 shows other main GIS component.

2.5 Electro Magnetic Transient Program

2.5.1 The History of the Transient Analysis in Power System

In 1854 Lord Kelvin made the first work related to a power system transient. He investigated the wave propagation characteristic on the planned Trans-Atlantic

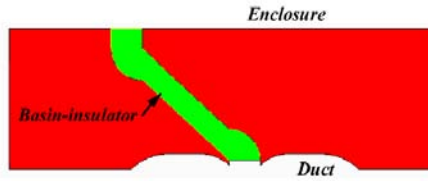


Figure 2.32: The basin-insulator diagram

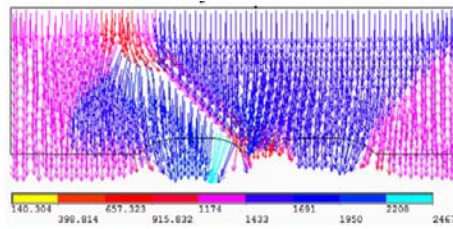


Figure 2.33: The electric field distribution of basin-insulator

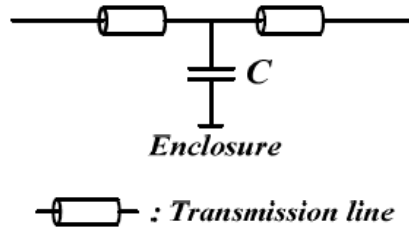


Figure 2.34: The equivalent circuit model of basin-insulator

Component	Equivalent circuit (single-phase)	notes
Overhead line		Lossy transmission line
Power transformer	 Simplified model 	C_c : coil-ground capacitance C_b : bushing-ground capacitance L : lead wire inductance R : lead wire and coils resistance
Bushing		SF ₆ gas filled
Capacitive voltage transformer		
Surge arrester		

Figure 2.35: The equivalent circuit models of other main GIS components

telecommunication cable. Between 1926 and 1928 a lot of study about the lightning began. In the 1950 a digital computer became available, and the tedious theoretical analytical formulas calculations were replaced with computer simulations. The theory of the travelling wave became one of the most powerful approach to solving transient, due the distributed nature of the transmission line. Later the graphical method to calculate the electrical transient was intruded by Allievi, Schnyder, Bergeron and Angus. At a later stage numerical Fourier transform were implemented on a digital computer, and then also the Laplace transform was applied to transient calculation.[AV] Many software have been developed to solve electromagnetic transients. First they used two different techniques: Bewley's lattice diagram and Bergeron's method, in order to solve small network with linear and non-linear lumped-parameter, as well as distributed-parameter elements. H.W.Dommel made an extension to multi-mode networks, matching the Bergeron's method and the trapezoidal rule. This solution method was the origin of the well known Electro Magnetic Transients Program (EMTP). The trapezoidal rule is used to convert the differential equations of the network components into algebraic equations. It is necessary to know also the initial condition. Some rules to be considerate in order to organize an appropriate simulation. It is necessary take in to account the frequency range of the transient. It should be better minimize the part of the system to be represented, in order to increase the accuracy and minimize the probability of wrong modeling. Moreover implement an adequate representation of losses. [Ame14] The Electromagnetic Transient Program EMTP is able to evaluate the line parameters from the geometry of the line. A series impedance and a shunt admittance are essential to study the transient, and it is possible evaluate them by the routine on EMTP, as it will be show in the experimental part of this work. The internal impedance of a cylindrical conductor is evaluate using the Schelkunoff formulae. The earth-return impedance of an overhead/underground isolated conductor was developed by Pollaczek in 1926 and Carson. The routine on EMTP evaluates automatically this matrix. In the experimental part, in order to evaluate the accuracy of the OHL model builded, the matrix obtained by EMTP will be compare with the results obtained using the analytical formulas. This will be done only considering a frequency $f=50\text{Hz}$, because the aim, as explained before, will be prove the accuracy of the line model on EMTP. In fact the Pollaczek and Carson's formulas neglected displacement currents. For this reason this formulas cannot be applied to a high frequency region. For this reason, in order to make a correct study of the transient phenomena, it is necessary take into account the range frequency of interest.

2.5.2 The Classification of frequency ranges

The frequency of interests is increasing year by year corresponding to the advancement in measuring equipment: for example 1GHz sampling of recent oscilloscope, while some 10 MHz ten years ago. The length is inversely proportional to the frequency, and therefore it becomes necessary to deal with a transient on a 1-m conductor, of which the natural resonant frequency is in the order

Group	Frequency Range	Shape Designation	Representation mainly for
I	0.1 Hz - 3 kHz	Low frequency oscillations	Temporary Overvoltages
II	50-60 Hz - 3 kHz	Slow front surges	Switching Overvoltages
III	10 kHz - 3 MHz	Fast front surges	Lighting Overvoltages
IV	100 kHz - 50 MHz	very fast front surges	Restrike Overvoltages

Table 2.1: Classification of frequency ranges [UR11]

Origin and Frequency Ranges of Transients in Power Systems	
Origin	Frequency Range
Ferroresonance	0.1Hz to 1kHz
Load rejection	0.1Hz to 3kHz
Fault clearing	50Hz to 3kHz
Line switching	50Hz to 20kHz
Transient recovery voltages	50Hz to 100kHz
Lightning overvoltages	10kHz to 3MHz
Disconnecter switching in GIS	100kHz to 50MHz

Figure 2.36:

of 100MHz. For this reason the Pollaczek's and Carson's impedances adopted in any circuit-theory based simulation tool may not be applied. It is necessary to know the frequency range and then to choose the correct model on EMTP. Each range of frequencies usually corresponds to some particular transient phenomenon. One of the most accepted classification is proposed by IEC and CIGRE [UR11]. Frequency ranges are classified into four groups, as shown in table 2.1. This task can be alleviated by looking into widely accepted classification tables, in picture 2.36.

2.5.3 The Time Step

During the Study of Transient by the digital computer programs the selection of the time step Δt is of importance. Defined the highest expected frequency by the 2.1, the Δt is given by 2.31

$$\Delta t = \frac{1}{10 * f_{max}} \quad (2.31)$$

For this reason it is reasonable to use a time step about $1\mu s$ for the group *I* and *II*, and a time step about $1ns$ for the group *III* and *IV* as we have done in the experimental part.

2.5.4 The accuracy

The accuracy of the results obtained depends on the accuracy of representation of the system components and on the accuracy of the input data. [UR11] For

example the most efficient and accurate transmission line models are distributed parameters based on the travelling time τ and the characteristic impedance Z_c of the line. It is possible to obtain this parameters (either frequency dependent or constant) by the geometrical and physical information, as told before, by using a line/cable constants program on EMTP. Whereas lumped parameter models (pi-circuits) are computationally more expensive, because a large number of cascaded short-sections are needed to approximate the distributed nature of the physical line. [btSTTFotIMoSTWG]

2.5.5 The statistical analysis

In some instances the results are highly sensitive to the value of certain parameter. For example, the maximum overvoltage for a line energization depends on the exact point on the wave at which the switch contacts close. For this reason a statistical analysis in order to obtain an overvoltage probability distribution is useful. It typically consists of 100 or more separate simulations. Circuit breaker can close at any angle on the power frequency wave. The set of circuit breaker closing times can be represented as a uniform distribution from 0 to 360 degree with reference to the power frequency. In case of three phase (pole) circuit breaker it is necessary to take into account the pole span delay between the closing instants of the three poles. To do that the pole span can be modeled with an additional statistical parameter, typically from Gaussian distribution. [btSTTFotIMoSTWG] More details about this analysis will be explained in the experimental chapters.

2.5.6 The aim of the EMTP

The results from the switching transient study are useful for: [btSTTFotIMoSTWG]

- Insulation co-ordination to determine overvoltages stresses on equipment
- Determining the arrester characteristics
- Determining the transient recovery voltage across the circuit breakers
- Determining the effectiveness of transient mitigating devices

gensymb

Chapter 3

Components Design

3.1 Overhead Line Design

The tower L-6 400kV ,double circuit tower shown in picture 3.1, has been considered. L-6 , L-2 and L-12 towers, are the most widely in use for high voltage onshore transmission in England and Wales. The L-2 is the typical transmission tower from the 1950s, carried steel-reinforced aluminium conductors in pairs from each insulator. When quadruple conductors were introduced in the 1960s, larger and more substantial towers were needed and the L-6 designs were then introduced. [SH08]

The Overhead Line has been built by EMTP, choosing $100[Ohmm]$ as soil resistivity. Adding on EMTP the geometrical characteristics the software evaluates directly the electrical components of the line. Tower geometry shown in picture 3.2 and in table 3.1 has been considered.

Picture 3.3 and 3.4 show the input data on EMTP. On the Model TAB is necessary to select the System Type: Overhead Line Model, Number of conductors (7 in this case), and the presence of subconductor. For the transient simulation is recommended to select the option "Real transf. matrix" . In this case the option "Auto bundling" has been selected in order to add the geometrical data of the sub-conductor. The proper option has been selected in order to take into account the skin effect. In matter of Conductor Geometry it is necessary to add the R_{in} , it means the inner radius of conductor in $[m]$, and R_{out} , the outer radius of conductor in $[m]$. It is necessary to add the $Resis$, it means the conductor resistance in $[Ohm/unitlength]$, this is a DC resistance in case of Skin Effect option ON, and AC resistance @ Freq. Init. if the option Skin Effect is OFF. For this work the phase conductors Zebra (UK Code)

SAG_{ew}	10.55 [m]
SAG_{ph}	7.5 [m]

Table 3.1: Tower Geometry

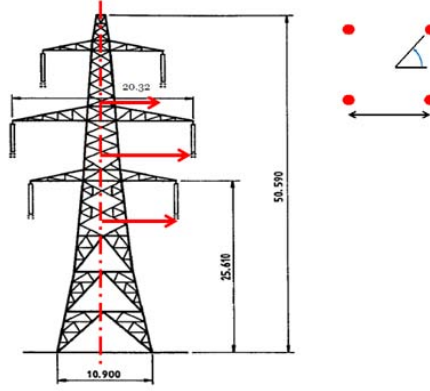


Figure 3.1: L-6 Tower 400 kV

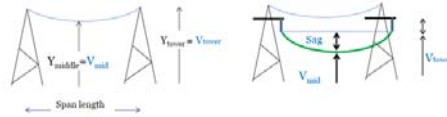


Figure 3.2: Tower Geometry

ACSR has been chosen. ACSR means Aluminium Conductor Galvanized Steel Reinforced. The number of sub-conductors is 4, with a distance of $40[cm]$. To evaluate if the model built on EMTP is correct it is necessary evaluate the electrical components of the OHL by the analytical formulas to compare it with the components evaluated by EMTP routine.

Considering the data for the resistance at $20\ C$ shown in table 3.2, using the equations 3.1 and 3.2 to evaluate the sub-conductor resistance at temperature of $50\ C$, as suggested in the work [LB11]. .

$$R_{T-DC} = R_{20-DC}[1 + \alpha(T - 20)] \quad (3.1)$$

$$R_{50} = R_{20}[1 + 4(50 - 20)] = 0.07548[Ohm/km] \quad (3.2)$$

In the case of bundles, as in our case, with n subconductor, it is possible to know the equivalent resistance of one subconductor as suggested in [Kie02] by the formula 3.3

$r_{subconductor}$	$0.0674 [Ohm / km]$
$r_{shieldwires}$	$0.1654 [Ohm / km]$

Table 3.2: Resistance at 20

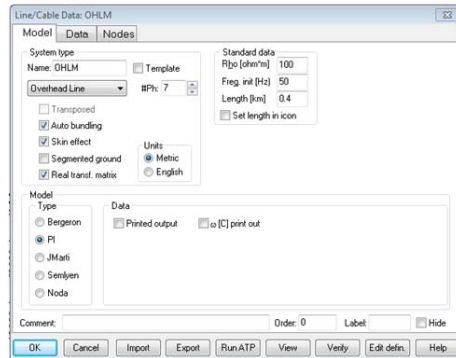


Figure 3.3: ElectroMagnetic Transient Program

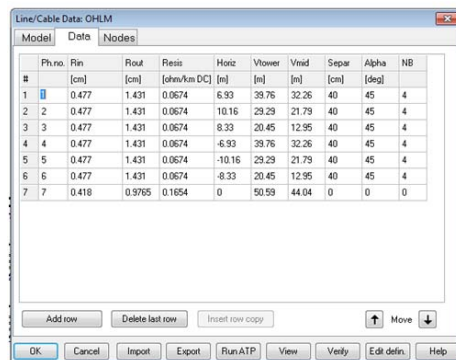


Figure 3.4: ElectroMagnetic Transient Program

$r_{subconductor}$	0.07548 [Ohm/ km]
c	10.4107 [nF/km]
l	1.076 [mH/km]

Table 3.3: Electrical Components

$$r_{conductor} = R_{50}/4 = 0.01887[Ohm/km] \quad (3.3)$$

In order to evaluate the capacitance it is necessary to use the equation 3.4 , where D_m is the Geometric Mean Distance GMD, defined by the formula 3.5, and φ is the equivalent diameter, defined by 3.6. [LB11]

$$c = \frac{24.14}{\log\left(\frac{2D_m}{\varphi_{eq}}\right)} \quad (3.4)$$

$$D_m = \sqrt[3]{D_{12} + D_{13} + D_{23}} \quad (3.5)$$

$$\varphi = 2R \sqrt[n]{\frac{nr}{R}} \quad (3.6)$$

In order to evaluate the inductance it is necessary to use the formula 3.7, assuming $k' = 0.0408$, as suggested in [LB11], this parameter depends on the material of the conductor. The results obtained by the analytical formula are show in table 3.3

$$l = \frac{k'}{n} + 0.46 \log \frac{2D_m}{\varphi} [mH/km] \quad (3.7)$$

In order to compare the results obtained by EMTP and the analytical formulas, it is necessary evaluate the zero sequence impedance of overhead line conductors. The impedance involves in the self-impedances and the mutual impedances of ground return circuits. The basic equations to evaluate the zero-impedance were determined by Pollaczek and Carson, ah shown the formulas 3.8 and 3.9 suggested by [RB10] and the picture 3.5.[LB11] D_e is the distance between conductors and the barycentre of the current which flows through the ground. f is the power frequency, and ρ_T is the electrical resistivity of the soil.[RB10] [LB11]

$$Z_{i,i} = r_i + \pi^2 10^{-4} + j4\pi 10^{-4} f \ln\left(\frac{2D_e}{d'_i}\right) [Ohm/km] \quad (3.8)$$

$$Z_{i,j} = \pi^2 10^{-4} + j4\pi 10^{-4} f \ln\left(\frac{D_e}{d_{i,j}}\right) [Ohm/km] \quad (3.9)$$

$$\rho_t = 100 [Ohmm]$$

$$f = 50 [Hz]$$

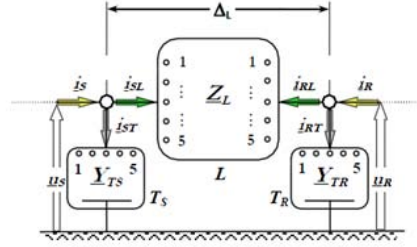


Figure 3.5: Overhead Line Model [LB11]

$r_{conductor}$	0.01887 [Ohm/ km]
R	0.2888 [m]
d'_i	0.1705 [m]
D_e	930.55 [m]
d_{sub}	0.2862 [m]
k''	0.04086
f	50 [Hz]
ρ_T	100 [Ohm m]

Table 3.4: Data Evaluated

$$D_e = 685 \sqrt{2 \frac{\rho_t}{f}} = 930.55 [m]$$

n is the subconductor's number. K'' is a corrective factor, which depends on the specific conductor. r is the resistance per unit length of conductor, which has been evaluated before. R is the radius of the circumference where the subconductors are disposed, in the case of $n = 4$. d'_i is defined by 3.10. [LB11]

$$d'_i = 2GMR = 2 \sqrt[n]{nk'' \frac{d_{sub}}{2} R^{n-1}} \quad (3.10)$$

The data evaluated are shown in table 3.4

For the geometry of the L-6 the distances between the conductors are shown in table 3.5

Due to the formulas 3.8 and 3.9 the self-impedance and the mutual impedances are evaluated. Below a comparison between the results by EMTP and analytical formula are shown in table 3.6. Obviously $Z_{ij} = Z_{ji}$

3.2 GIL Model

The typical data for 400kV GIL are shown in table 3.7, as suggested in the work [LB11]

Conductors	Distance [m]
1-2 and 4-5	9.02
2-3 and 5-6	10.95
1-3 and 4-6	19.36
4-1	16.66
5-2	20.32
6-3	13.86
1-5 and 4-2	20.49
3-4 and 6-1	24.61
2-6 and 5-3	21.62

Table 3.5: Distance Between the conductors

	Analytical formula	EMTP
$Z_{12} \text{ and } Z_{45}$	0.049+j0.2913	0.0472+j0.2936
$Z_{23} \text{ and } Z_{56}$	0.049+j0.2814	0.0463+j0.286
$Z_{13} \text{ and } Z_{46}$	0.049+j0.2433	0.0466+j0.2462
Z_{41}	0.049+j0.2527	0.0476+j0.2546
Z_{52}	0.049+j0.2402	0.0467+j0.2431
Z_{63}	0.049+j0.2643	0.0458+j0.268
$Z_{15} \text{ and } Z_{42}$	0.049+j0.2397	0.0471+j0.2421
$Z_{34} \text{ and } Z_{61}$	0.049+j0.2282	0.0466+j0.2312
$Z_{26} \text{ and } Z_{53}$	0.049+j0.2363	0.0462+j0.2446

Table 3.6: Comparison of the Electrical Parameters of the Overhead Line evaluated by the analytical formulas and by the software

S_{ph}	5341 [mm ²]
S_{enc}	16022 [mm ²]
R_{outph}	0.009 [m]
R_{inph}	0.008 [m]
SF_6/N_2	20/80 [%]
prex	7 [bar]
r_{ph60}	6.286 [mOhm/km]
r_{enc50}	2.33 [mOhm/km]

Table 3.7: GIL 400 kV

r_{ph20}	5.419 [m Ohm /km]
r_{en20}	2.08 [m Ohm /km]
r_{tot}	8.616 [m Ohm /km]
r_{tot20}	7.5 [m Ohm /km]

Table 3.8: GIL Electrical Parameters evaluated

ρ_{ph}	$2.89*10^{-8}$ [Ohm/m]
ρ_{en}	$3.33*10^{-8}$ [Ohm/m]

Table 3.9: GIL Electrical Parameters evaluated

The resistance has been calculated by the formulas 3.11 3.12 3.13 3.14 , considering the resistance of the enclosure and the resistance of the phase. The results are shown in table 3.11

$$r_{tot} = r_{ph} + r_{en}[Ohm/km] \quad (3.11)$$

$$r_{\theta} = r_{20}[1 + 4 * 10^{-3}(\theta - 20)] \quad (3.12)$$

$$r_{ph20C} = \frac{r_{ph60C}}{1 + 4 * 10^{-3}(60 - 20)} \quad (3.13)$$

$$r_{en20C} = \frac{r_{en50C}}{1 + 4 * 10^{-3}(50 - 20)} \quad (3.14)$$

In order to design the GIL line on EMTP it is necessary to know the resistivity of the conductor and the resistivity of the enclosure. It is possible evaluate this in the following way by the formulas 3.16 and 3.17. [LB11] The results are shown in table 3.9

$$r_{20C} = \frac{\rho_{20C}}{S} = 2.08[mOhm/km] \quad (3.15)$$

$$\rho_{ph} = r_{ph20C}S_{ph} \quad (3.16)$$

$$\rho_{en} = r_{en20C}S_{en} \quad (3.17)$$

It is possible to evaluate the inductance as the sum of l_a , which represent the phase internal inductance, l_b , which represent the magnetic field between phase and enclosure, and l_c , which represent the enclosure internal inductance, using the formulas 3.18 3.19 3.20, and the capacitance by the formula 3.21 according with [LB11].

$$l_a = \frac{\mu_0}{2\pi} \left[\frac{R_1^4}{(R_2^2 - R_1^2)^2} \ln(R_2/R_1) + \frac{(R_2^2 - 3R_1^2)}{4(R_2^2 - R_1^2)} \right] [H/m] \quad (3.18)$$

r	8.616 [mOhm/km]
l_a	0.0074 [mH/km]
l_b	0.20433 [mH/km]
l_c	0.0026 [mH/km]
l_{tot}	0.21433 [mH/km]
prex	7 [bar]
c_{ph60}	0.0545 [mFi/km]
g	neglected

Table 3.10: GIL Electrical Parameters

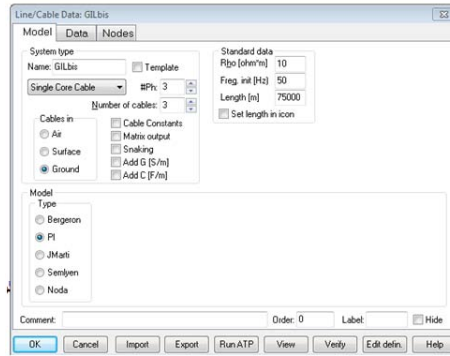


Figure 3.6: GIL Design on EMTP

$$l_b = \frac{\mu_0}{2\pi} \ln(R_3/R_2)[H/m] \quad (3.19)$$

$$l_c = \frac{\mu_0}{2\pi} \left[\frac{R_4^4}{(R_4^2 - R_3^2)^2} \ln(R_4/R_3) + \frac{(R_3^2 - 3R_4^2)}{4(R_4^2 - R_3^2)} \right] [H/m] \quad (3.20)$$

$$c = \frac{2\pi\epsilon_0}{\ln(R_3/R_2)} [F/m] \quad (3.21)$$

Considering $\epsilon_0 = 8.8542 \times 10^{-12} [F/m]$. According to the analytical formulas, the results are shown in the table 3.10

The Characteristic Impedance has been evaluated by the formula 3.22 considering $\epsilon_r = 1$. [LB11]

$$Z = \frac{138}{\sqrt{\epsilon_r}} \log(R_3/R_2) = 61.23 [Ohm] \quad (3.22)$$

On EMTP it is possible to represent the GIL line as three cable single core.

Using the routine ‘‘cable constant’’ on EMTP the program valuate automatically the line constant. The results obtained by the analytical formula and the results obtained by EMTP routine are almost the same, as shown in the table

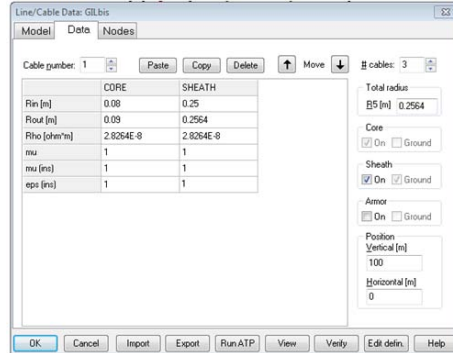


Figure 3.7: GIL Design on EMTP

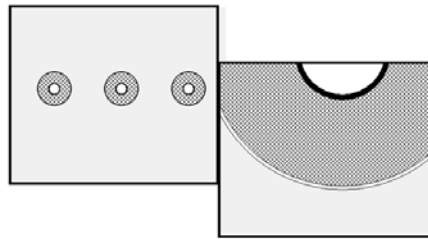


Figure 3.8: GIL Design on EMTP

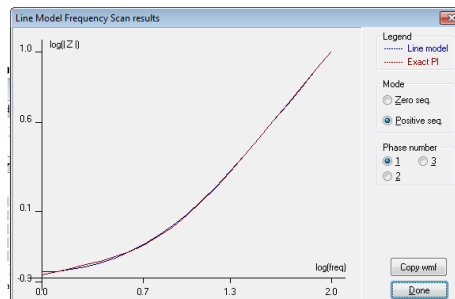


Figure 3.9: Line Model Frequency Scan Results

	Analytical Formula	EMTP
r [Ohm/m]	$8.62 \cdot 10^{-6}$	$8.30 \cdot 10^{-6}$
l_{tot} [H/m]	$2.14 \cdot 10^{-7}$	$2.13 \cdot 10^{-7}$
c [F/m]	$5.45 \cdot 10^{-11}$	$5.68 \cdot 10^{-11}$
g	neglected	neglected

Table 3.11: GIL Electrical Parameters

	P_{cc} [MVA]	jX [Ohm]	L [mH]
Weak Network	4000	40	127.3
Strong Network	30000	5.3	16.98

Table 3.12: Network

3.11. It means that this is a good model for the GIL line. The GIL elements are connected in solid bonding, it means that the enclosures are connected in series without transposition, and are ground connected at the sending and the receiving end. For this reason the automatically ground connection on EMTP for the routine is a good approximation for the solid bonding connection.

3.3 Source Design

In matter of the source design it is possible to use a Thevenin equivalent circuit, in so doing it is necessary introduce a fem Ug in series with an impedance. This impedance is the sub-transient short circuit three phases impedance, $Z_{cc''_f}$. Typical data about two extreme cases of weak and strong line, for the 400kV line are shown in table 3.12 and picture 3.10, by the work [MGI10]. In fact the short circuit power, according with the standard data for the Italian network in normal operation, is in the range (4000 – 30000)MVA. For simplicity it is reasonable consider the impedance only inductive.

The tables 3.13 3.14 show the value of voltage, rms and peak value, considering L-L voltage and L-G voltage, for 400[kV] system. It is useful to well know this value in order to do the next analysis.

gensymb

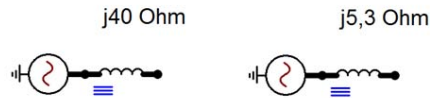


Figure 3.10: Source Design

Nominal System Voltage [kV] (rms)	400
Maximum System Voltage [kV] (rms)	420
Minimum System Voltage [kV] (rms)	380
Nominal System Voltage [kV] (peak value)	$400\sqrt{2} = 565.68$
Nominal System Voltage [kV] (peak value)	$420\sqrt{2} = 593.96$
Nominal System Voltage [kV] (peak value)	$380\sqrt{2} = 310.26$

Table 3.13: Value of the Voltage L-L

Nominal System Voltage [kV] (peak value)	$565/\sqrt{3} = 326.59$
Maximum System Voltage [kV] (peak value)	$593.96/\sqrt{3} = 342.92$
Minimum System Voltage [kV] (peak value)	$537.4/\sqrt{2} = 310.26$

Table 3.14: Value of the Voltage G-L

Chapter 4

Internal Overvoltages

4.1 Introduction

To better understand the Transient in Power Systems it is important to explain the classification of the overvoltages. In fact the overvoltages are divided in two main family: External and Internal Overvoltages. For example the first one can be caused by lighting, which included direct spark or induced or back-flashover. The second one includes transient overvoltages, for example the closing/reclosing of a line and the interruption of capacitive/inductive currents, the transient overvoltages requiring a frequency $f = 10kHz$, or temporary overvoltages, for example the load rejection, the Ferranti Effect, the ground faults, the temporary overvoltages requiring a frequency $f = 1kHz$, or steady state overvoltages for example contact with circuits of higher voltages, or resonance phenomena, etc. Some of these overvoltages are investigated in this work. [AH04] The table 4.1 shows the limit value of the overvoltages in different cases of study.

4.2 Temporary Overvoltages: The Ferranti Effect

The most frequent causes of temporary overvoltages are Ferranti Effect and ground faults. Most of these overvoltages are in the range between 1.2 and 1.5pu , but in severe conditions they may reach 2pu . The highest TOV (Tem-

Nominal Voltage	400[kV]
Maximum Voltage	420[kV]
Lightning Impulse Voltage	1425[kV]
Switching Impulse Test	1050[kV]

Table 4.1: Limit Value of the Overvoltage [AH04]

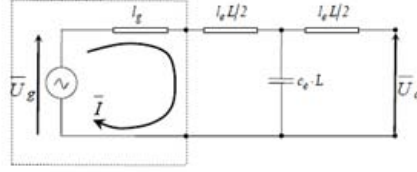


Figure 4.1: Equivalent Circuit [LB11]

porary OverVoltages) occurs in case of long line connected with a weak network. Temporary overvoltages due the Ferranti Effect and load rejection are limited by shunt reactor, but on the other hand, because the shunt reactors remain connected to the system under normal conditions, could be a problem of reactive power consumption. [AH04]. In this work the Ferranti Effect has been investigated. In order to evaluate correctly the Ferranti Effect during the no-load energization, different case studies will be investigated. As well known the Ferranti Effect depends on different factors: for example the value of the voltage at the receiving end, U_a , is bigger if the line length increase, or if the frequency increase. In the same way the value of U_a is bigger if the product $L_{line}[H/km] * C_{line}[F/km]$ increase. It is possible see it by the formula 4.1 [LB11]. It is important to note that this analytical formula is an approximation of the real conditions, because this considers the equivalent circuit shown in picture 4.1. [LB11]

$$\frac{\Delta U}{U_a} = \frac{U_a - U_g}{U_a} = 1 - \frac{U_g}{U_a} = \frac{\omega^2 l_e c_e L^2}{2} \quad (4.1)$$

As explained in Chapter 2 the GIL capacitance is four times lower than the cable capacitance and it is four times higher than the OHL capacitance [LB11], for this reason the Ferranti Effect on GIL is much lower than the ferranti effect on cable, and is slightly higher than the case of Overhead Line. As explained before about the source design, we consider three extreme cases of weak and strong line, for 400kV, respectively $L_g = 127,3[mH]$ and $L_g = 16,98[mH]$, and in ideal network. Two different scenarios are shown in picture 4.2 4.3, considering 100[km] and 300[km] line length. For this analysis a $f = 50[Hz]$, because there are not switching operations, and PI model has been considered. The overvoltage at the receiving end is higher in presence of weak network, because the L of the network increase the global inductance of the line, as shown in pictures. The Ferranti Effect increase if the line length increase, in fact for Gas Insulated Transmission Line the overvoltage value is 1.08[pu] in case of weak network $l = 100[km]$ and reaches 1.33[pu] in case of weak network $l = 300[km]$ length. Considering the Overhead Line the overvoltage value is 1.04[pu] for $l = 100[km]$ and 1.2[pu] for $l = 300[km]$ in case of weak network. By the analytical formula 4.1. The Ferranti Effect expected is $\Delta U_{OHL}/\Delta U_{GIL} = 0.9216$, considering an ideal network with infinite power (it means $X'' = 0$). The experimental results show, for both cases $l = 100[km]$ and $l = 300[km]$,

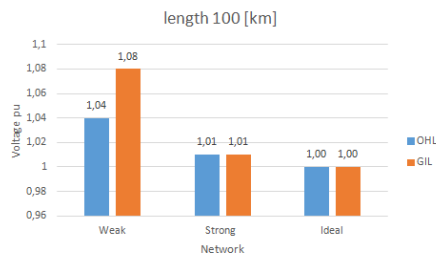


Figure 4.2: Ferranti Effect in case of 100 km line length (considering the phase A)

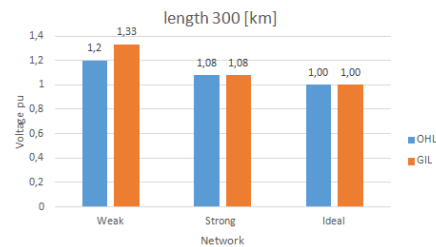


Figure 4.3: Ferranti Effect in case of 300 km line length (considering the phase A)

that the ratio is $\Delta U_{OHL}/\Delta U_{GIL} = 1$ in case of ideal network on EMTP, the same results are obtained considering a strong network. In case of weak network the ratio is $\Delta U_{OHL}/\Delta U_{GIL} = 0.96$ for $l = 100[km]$ and $\Delta U_{OHL}/\Delta U_{GIL} = 0.90$ for $l = 300[km]$. These results are in agreement with the approximated analytical formula.

Composed Line

In this work will be investigated a mixed line configuration, composed by an Overhead line and GIL. Considering to represent the terminal tower and a gantry as shown in the model in picture 4.41, with a bushing to connect the OHL with a GIL line modeled as a lumped capacitance $C = 500pF$, as one suggested in literature for $400kV$ and as explained in the Chapter2. Considering the case of weak network, because is the more severe condition, the Ferranti Effect is investigated changing the OHL and GIL line length, as follow:

- Overhead Line: 90 km
- Overhead line and GIL have the same length: OHL 45 km and GIL 45 km
- Overhead line is longer than GIL: OHL 60 km and GIL 30 km



Figure 4.4: Model of the Composed Line on EMTP: Source-OHL- terminal tower and a gantry-GIL-open end

- GIL is longer than Overhead line: OHL 30 km and GIL 60 km
- GIL: 90 km

The total length of the composed line is 90km . Considering PI model to make the simulation on EMTP. It is important to note that the peak values are been considered. In so doing all the values shown in the graphics and in the tables represent the maximum values of the peak voltage G-L.

The graphics 4.5 shows the results, considering the phase A. In this case it was important to investigate the behaviour of the other phases, as shown in picture 4.6 and 4.7, the results don't change. It is important to observe how, at the end of the composed line, the value of the overvoltage doesn't change significantly with the changing of the length of the Overhead Line and the Gas Insulated Line. It occurs because the line length is not been changed significantly, $30 - 45 - 60\text{km}$. Considering the first case, $l_{OHL} = 90[\text{km}]$, the overvoltage reaches $1.038[\text{pu}]$, it means the rms value of the L-L voltage is $415.189[\text{kV}]$, less than the limit value $420[\text{kV}]$. Considering the same length for the OHL and the GIL ($45[\text{km}]$ and $45[\text{km}]$), the overvoltage reaches $425.188[\text{kV}]$, it means that exceed the limit value. Because the GIL length influence the Ferranti Effect at the end of the line, the third case considers the $l_{OHL} = 60[\text{km}]$ and $l_{GIL} = 30[\text{km}]$. In so doing the rms of the voltage L-L is $422.788[\text{kV}]$, the situation is better. Changing the length, for example $l_{OHL} = 30[\text{km}]$ and $l_{GIL} = 60[\text{km}]$, the overvoltages reaches $427.388[\text{kV}]$, more than the limit value. The more severe situation occurs in case of $l_{GIL} = 90[\text{km}]$, as expected, and the value of the voltage is $428.388[\text{kV}]$. Picture 4.8 shows the Ferranti Effect at the end of the mixed line, in case of $l_{OHL} = 45[\text{km}]$ and $l_{GIL} = 45[\text{km}]$. Considering a long transmission line, for example $300[\text{km}]$ line length instead $90[\text{km}]$ ($240[\text{km}]$ for the OHL and $60[\text{km}]$ for the GIL), the overvoltage at the receiving end increases, it reaches $1.25[\text{pu}]$, in case of weak network. This value is very high, but it's a severe condition, in fact on the other hand, considering a strong network $300[\text{km}]$ line length the overvoltage reach $1.09[\text{pu}]$ at the receiving end. The value in case of strong network is lower, as expected.

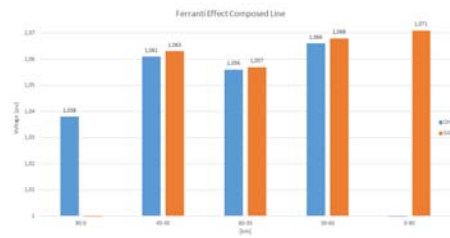


Figure 4.5: Ferranti Effect in case of Weak Network in a Composed Line, phase A

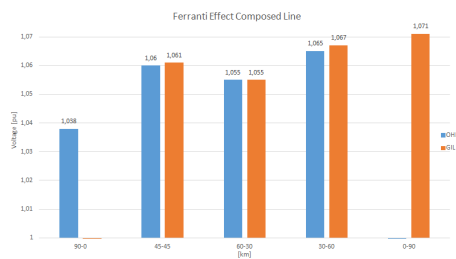


Figure 4.6: Ferranti Effect in case of Weak Network in a Composed Line, phase B

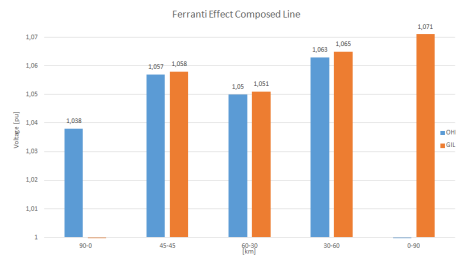


Figure 4.7: Ferranti Effect in case of Weak Network in a Composed Line, phase C

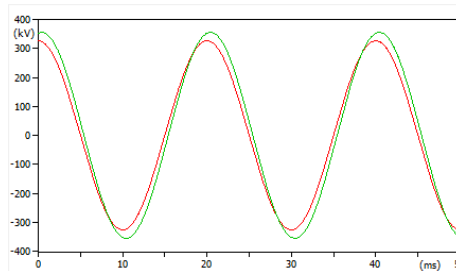


Figure 4.8: Ferranti Effect: Voltage at the source side (red) and at the receiving end (green)

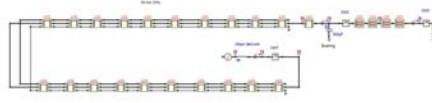


Figure 4.9: Composed Line Model on EMTP considering the energization of the first circuit in the L-6 tower

4.3 Transient Overvoltages: No-Load Energization

4.3.1 No-Load Energization of Overhead Line

Switching of capacitive currents includes capacitor banks, unloaded overhead lines and cable. The transient occurs when the circuit breaker operates from open to close. A surge is applied to the transmission line when the breaker is closed and travels to the end of the line. As well known, the reflection of the surge from the end of the transmission line is a complex function decided by surge impedance, line length, an eventually trapped charge, system impedance and closing time of the circuit breaker, earth resistivity. [YF13] The recovery voltage may reach $1.5pu$ across the contact of the circuit breaker. Half a cycle later, when the voltage at the source side is maximum, a voltage of $2.5pu$ is then established across the circuit breaker contacts. Many techniques have been developed to reduce the peak value, for example switching resistors, controlled synchronised of circuit breakers, shunt reactor and drainage of trapped charge before reclosing. [AH04]. Considering the limit condition observed about the weak network, the no-load energization has been investigated in order to better understand the behavior of this configuration. PI model and a sample time $1[\mu s]$ has been considered. Considering SW1 close in $t = 20[ms]$, during the peak of the voltage source, and SW2 and SW3 are opened. The parameters have been calculated for $f = 10[kHz]$ as suggested in literature. The line length is $30[km]$ represented by 20 minor section, because PI model works better with short sections. The model of the line on EMTP is shown in picture 4.9. It is possible to note that in this case, because the L-6 tower is a double circuit, the second circuit is opened, in order to consider a more realistic situation where during the energization of the line first the first circuit has been energized and then the second one. The same analysis has been done considering the circuit in picture 4.10, and the results don't change significantly. The picture 4.11 shows the trend of the voltage downstream the SW1 in comparison with the voltage source.

The picture 4.13 shows the voltage trend upstream the Switch. The picture 4.14 shows the comparison between the trend of voltage at the sending end (red) and the voltage at the receiving end (green). After $300[ms]$ the transient is finished.

Because the SW1 close in $t = 20[ms]$, during the peak of the voltage in



Figure 4.10: Composed Line Model on EMTP considering the energization of both circuits at the same time

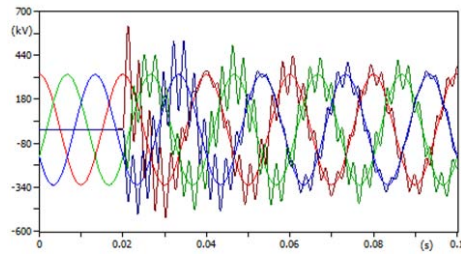


Figure 4.11: Voltage trend downstream the Switch compared with the voltage trend of the source

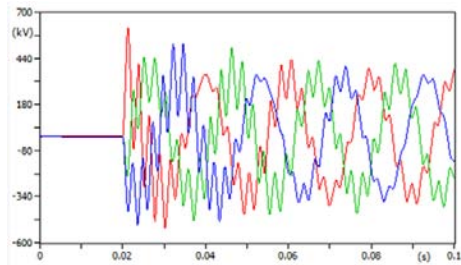


Figure 4.12: Voltage trend downstream the Switch

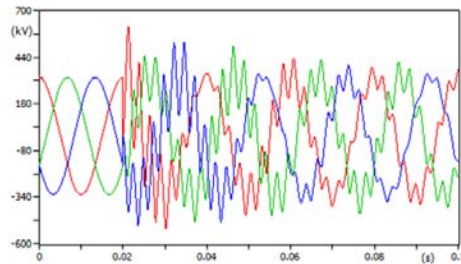


Figure 4.13: Voltage trend upstream the Switch

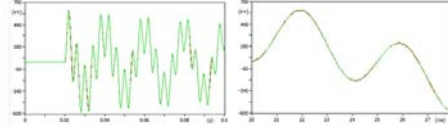


Figure 4.14: Trend of the Voltage at the Sending End (red) and at the Receiving End (green)

	Upstream the OHL	Downstream the OHL
Voltage [pu]	1.84	1.85
Voltage [kV]	600,960	604,721

Table 4.2: Overvoltages Phase A

the phase A, the maximum value of voltage occurs in the phase A, the results are shown in table 4.2. For the transient due the energization of the line the maximum value of the overvoltage is $1.84[pu]$ at the sending end, it means upstream the OHL. The Ferranti effect at the end of the OHL is not too much pronounced, just $0.01[pu]$ because the length of the line is only $30[km]$, as shown by the previous results.

Statistical Analysis

Another factor which influence the peak value of voltage is the pole-span delay between phases. It is possible do a Statistical Analysis, it means that, chosen the mean closing time of the master switch, it is possible to choose the pole-span delay of the slave switches. The closing time of each switch is randomly changing as a Gaussian or uniform distribution. In order to complete the analysis the necessary data are: the mean closing time, the standard deviation and the number of switching operations. The result is the probability distribution function of the switching of the peak value at each node. This distribution is characterized by its 2% value, is deviation and its truncation value. The $U_2\%$ is the overvoltage having the 2% probability of being exceeded. The international standard IEC 60071-2 give, on a quality level, the range of 2% overvoltage value, in pu $\sqrt[3]{2} \frac{U_s}{\sqrt[3]{3}}$, which may be expected between phase and hearth. The picture 4.15 should be used as an indication of whether or not the overvoltage for a given situation (depends on a lot of factor as shown in picture) can be high enough to cause a problem.

We have choosen that the master switch is closed when the instantaneous value of the phase to ground voltage is equal to zero. The average delay for the slave switches in phase B and C is set 120 and 60 electrical degrees, it means $Tb = 0.0066$ and $Tc = 0.0033sec$ respectively. The deviation standard is $2ms$. Considering 1000 simulations and sample time $1[\mu s]$. These data are suggested in literature [LP09]. The total time of simulation $0.1sec$. For this kind of analysis it is necessary to use a J.Marti model: the initial frequency is $0.001[Hz]$

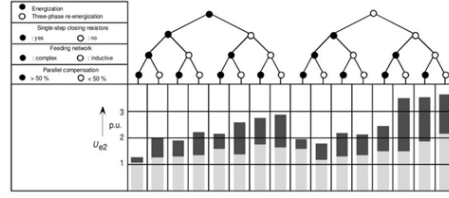


Figure 4.15: Value of $U_{2\%}$ by international standard IEC 60071-2

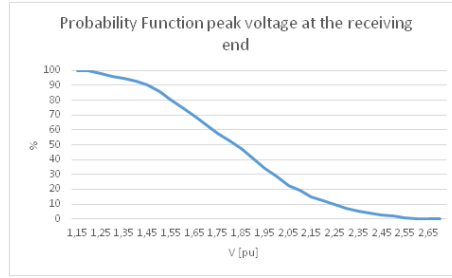


Figure 4.16: Probability Function in case of OHL 30km no-load energization

and the Matrix calculation is $50000[Hz]$. In this case the circuit has been changed because the simulation was overlap. Because J Marti model has been used it was possible reduce the number of the minor sections from 20 to 4 , as suggested in literature using J. Marti Model. Picture 4.16 shows the probability function Downstream the Overhead line for the phase A. The $U_{2\%}$ evaluated by the probability function at point 98% is less than $1.25[pu]$, this value perfectly agrees with the standard IEC 60071-2. The range of overvoltages suggested in literature is between $1,5[pu]$ to $2,5[pu]$, as told before, the Probability Function shows how the probability to have $V = 2,5[pu]$ is less than 2%.

4.3.2 No-Load Energization of the GIS

As explained before, the model on EMTP considers that between the OHL and the GIL there is a Gas Insulated Switchgear. The model of the GIS is simplified model, because it consider the presence of a terminal tower and a gantry, the bushing, and the presence of a Circuit Breaker or a Disconnecter as an ideal switch. Although this is an approximation for the model it is useful in this study. PI model has been considered. In this case, as told in the Chapter 2 about the Very Fast Transient on GIL, it is characterized by a step front having a rise time of some $[ns]$, followed by oscillations from $100[kHz]$ to $50[MHz]$. These transients have a magnitude in the reange between 1.5 and $2.0[pu]$ of thevoltage peak value L-G , but it can reach values as high as $2.5[pu]$. [MB14] To evaluate correctly the VFT on GIL it is necessary choose a sample time of $1[ns]$. The disconnecter DS close in $2[ns]$, and it is represented as an

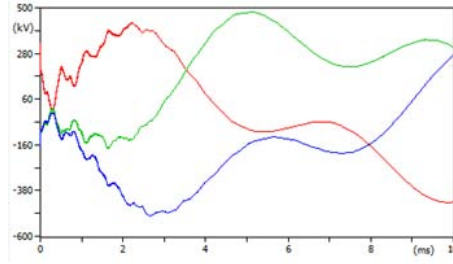


Figure 4.17: Voltage Trend at the Bushing side, phase A (red), phase B (green) and phase C (blue)

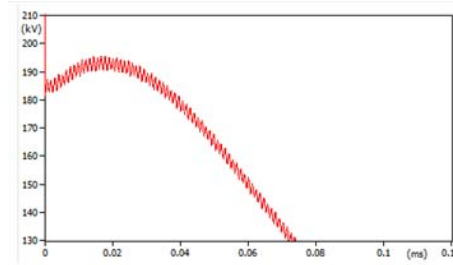


Figure 4.18: Zoom of picture 4.17: Voltage Trend at the Bushing side phase A - high frequency components -

ideal switch. The generated transient depends on the GIS configuration and on the superposition of the surges reflected and refracted on line discontinuities like junction or bushings. In fact, as a consequence of multiple reflections and refractions a very high frequency oscillations occur. In this case, in order to have a more realistic model, the elbows are introduced as a lumped capacitance of value $6\mu F$, as one suggested in literature. The parameters have been calculated for $f = 100[kHz]$. Pictures 4.17 and 4.18 show the voltage trend at the bushing side.

The picture 4.19 shows the rise time. The length of the connected GIS segments and lines therefore controls the frequency of the transients, but not the rise time. The rise time depends on the type of the disconnector, for example depends on the velocity of the contacts. In this case the rise time is about $1[ns]$, instead $(2 - 7)[ns]$ as suggested in literature. This probably occurs because an ideal switch has been used, it is a very important simplification. In the analysis about the opening operation a more complex model of the disconnector will be introduced.

It is also important to investigate the VFT downstream the DS. The pictures 4.20, 4.21 and 4.22 show the results. At the receiving end of the GIL, as shown the picture 4.23, there are not oscillating components of some MHz as at the sending end.

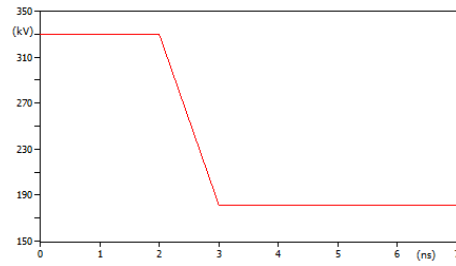


Figure 4.19: Rise Time at the bushing side - 1[ns]

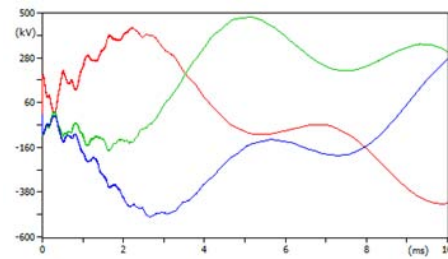


Figure 4.20: Voltage Trend Downstream the Disconnecter: phase A (red), phase B (green) and phase C (blue)

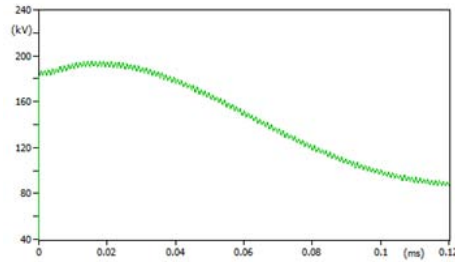


Figure 4.21: Zoom of picture 4.20 : Voltage Trend Downstream the Disconnecter phase A - high frequency components -

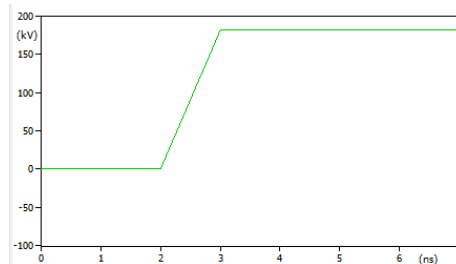


Figure 4.22: Rise Time Downstream the Disconnecter - 1[ns] -

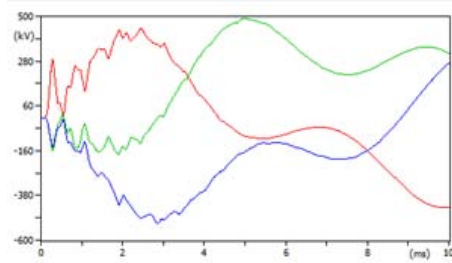


Figure 4.23: Voltage Trend at the Receiving End: phase A (red), phase B (green) and phase C (blue)

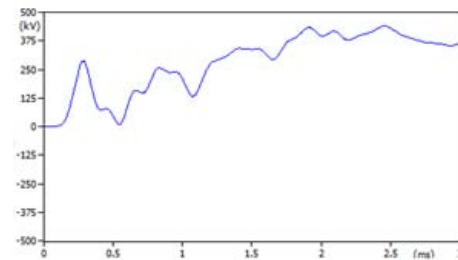


Figure 4.24: Zoom of picture fig:receivingend1: Voltage Trend at the Receiving End phase A - no high frequency components -

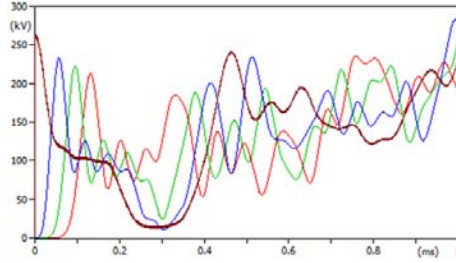


Figure 4.25: Voltage trend at $l = 0[km]$ (brown), $l = 10[km]$ (blue), $l = 20[km]$ (green), $l = 30[km]$ (red).

Picture 4.32 shows the comparison between the trend of the voltage at the receiving end (blue) and at the source side (red) and sending end downstream the DS (green). The parameters has been calculated for $f = 100[kHz]$. The oscillations in high frequency are damped along the GIL. To better understand this situation a new model has been considered, with 12 minor sections instead 4 as the previous case, $5[km]$ each. The picture 4.25 shows the voltage trend at $l = 0[km]$ (brown), $l = 10[km]$ (blue), $l = 20[km]$ (green), $l = 30[km]$ (red). It is possible to note how, after $10[km]$ from the sending end of the GIL the high frequency components are damped. Unfortunately the high frequency components occur in the OHL. Picture 4.26 shows the voltage trend at the end of the OHL (it means before the terminal tower), and picture 4.27 shows the zoom of picture 4.26. Fortunately these high frequency components after $10[km]$ from the end of the OHL are damped, as shown in picture 4.28. In matter of the peak values the value of the voltage at the receiving end of the GIL is higher than at the sending end of the GIL, as expected. The table 4.3 shows the value of the peak voltage calculated by EMTP routine on the file.lis. It is possible to note that the highest value occurs for the phase A, and, agree with the theory, occurs at the end of the line. The Switching Operation in the GIS involves a Very Fast Transient OverCurrent (VFTC). Picture 4.29 shows the current trend at the bushing side, the value of the current exceed $20[kA]$ and an high frequency components occur. Picture 4.30 shows the trend of the current downstream the Disconnecter. After $20[km]$ the high frequency components are damped, as shown in picture 4.31.

Statistical Analysis

It is necessary to do a statistical analysis for the reasons explained before. J. Marti Model has been considered: the literature [Eln14] suggest to use as frequency to evaluate the matrix $20000[Hz]$ in case of cable. The Line model on EMTP is shown in picture 4.33. Statistical switches of Gaussian-type are chosen to represent the DS. The SWA is the master, and the remaining two are slave. The same value of the previous analysis are chosen. The results are shown in picture 4.34.

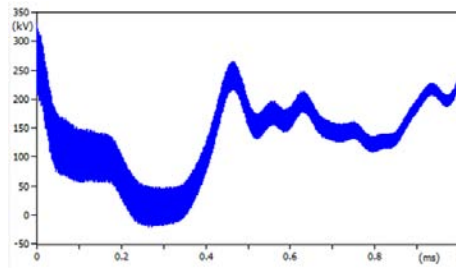


Figure 4.26: Voltage trend at the end of the OHL

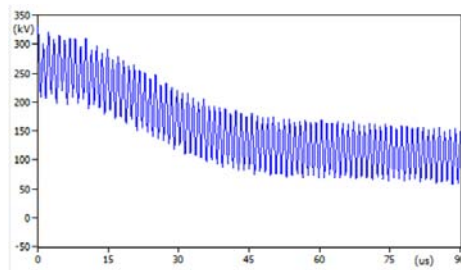


Figure 4.27: Zoom of the picture 4.26: Voltage trend at the end of the OHL

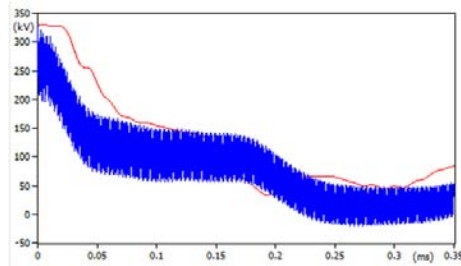
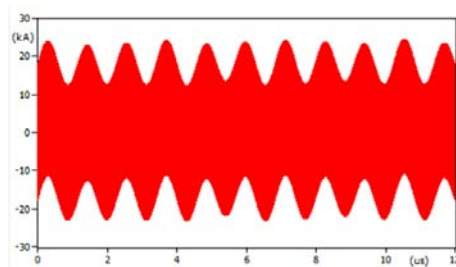
Figure 4.28: Voltage trend at the end of OHL $l = 30[km]$ (blue) and at $l = 20[km]$ (red)

Figure 4.29: Current at the bushing side

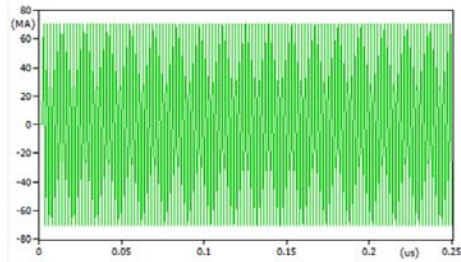


Figure 4.30: Current downstream the DS

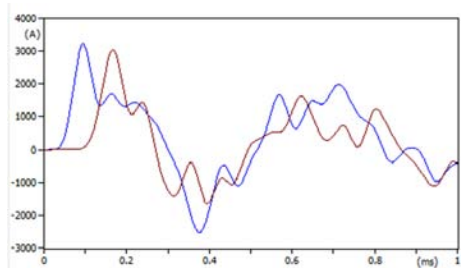
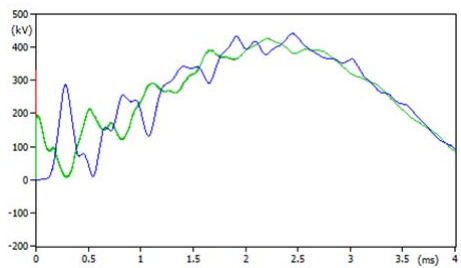
Figure 4.31: Current at $l = 20[km]$ (blue) and $l = 40[km]$ (brown) along the GIL

Figure 4.32: Comparison between the trend of the voltage at the receiving end (blue) and at the source side (red) and sending end downstream the DS (green))

	Bushing	Downstream the DS	Receiving End
VFTO [pu] [1.3	1.3	1.4

Table 4.3: Overvoltages During the GIL Energization

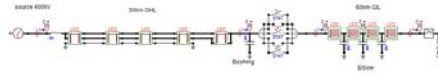


Figure 4.33: Model Line on EMTP in case of Statistical Analysis During GIL Energization

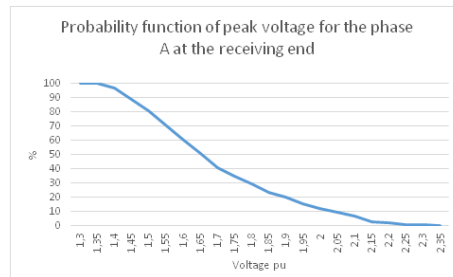


Figure 4.34: Probability Function

Trapped Charge

Two forms of trapped charge can exist: DC and oscillating. A trapped charge on a line with no other equipment attached to the line exists as a DC trapped charge, and the charge can persist for some minutes before dissipating. Because on our model we don't have transformer or shunt-reactor, in order to build a more realistic model, the literature propose to add a grounded capacitance carrying with an initial voltage, as shown in picture 4.36. The value of the capacitance is the equivalent capacitance of no-load line to the enclosure of GIS, in this particular case the capacitance evaluated is $3.4\mu F$. This methods ignores that the distribution of residual charge is non-uniform and varies with time, as explained in [MB14]. The picture 4.35 shows the line model on EMTP. Considering $1[pu]$ trapped charge, supposing that the SW close in $t = 2[ns]$. The picture 4.36 shows the trend of the voltage at the sending end (left) and at the receiving end (right). The parameters has been calculated using PI model, $f = 100[kHz]$, sample time $1[ns]$. Picture 4.36 and table 4.4 show the result.

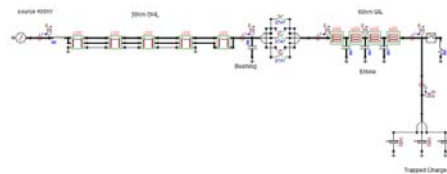


Figure 4.35: Line Model on EMP with Trapped Charge

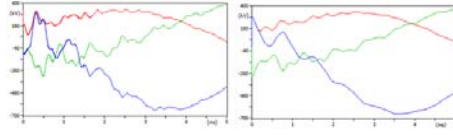


Figure 4.36: Voltage Trend at the sending end (left) and at the receiving end (right) with Trapped Charge

	Bushing	Downstream the DS	Receiving End
VFTO [pu] [1.45	1.45	1.38

Table 4.4: Overvoltages During the GIL Energization with a trapped charge by a grounded capacitance

Making the same considerations made before for the statistical analysis in case of energization of overhead line, a statistical analysis has been done. Pictures 4.37 4.38 4.39 show the results.

It is important to note to models the trapped charge as a grounded-capacitance could be an important approximation. In fact it is important to choose the correct value of the capacitance, and it should be not easy. It is possible to see how the Probability Function Downstream the DS, picture 4.38 , evaluated by the statistical analysis, is not accurate. The work [MA15] model the trapped charge using the specific function on EMTP, with three current generators which, at the start of the simulation, evaluate the initial conditions of the network and load the network with a choosed value of trapped charge in [pu]. This model is more accurate because it is not necessary to choose the correct value of capacitance, the EMTP evaluate automatically this value. Picture 4.40 shows the model on EMTP, and the picture 4.41 shows the values choosen for the AC-SOURCE to model the trapped charge. The statistical analysis has been done as in the previous case. The results show in picutres 4.42 4.43 4.44 are in agreement with the results obtained modeling the trapped charge as a capacitance, but in this case are more accurate.

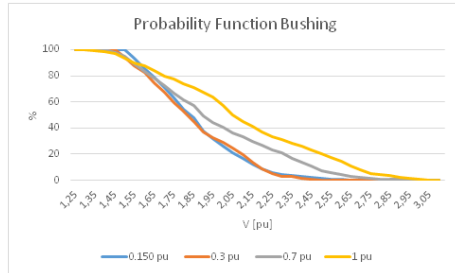


Figure 4.37: Probability Function at the Bushing

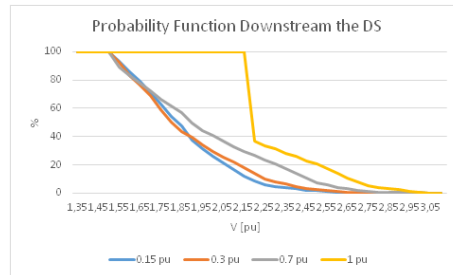


Figure 4.38: Probability Function Downstream the DS

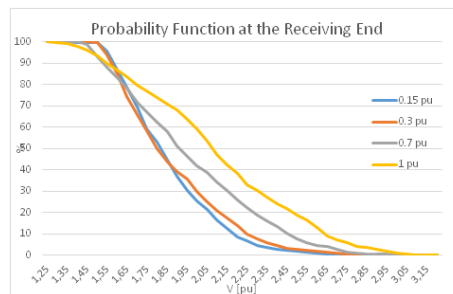


Figure 4.39: Probability Function at the Receiving End

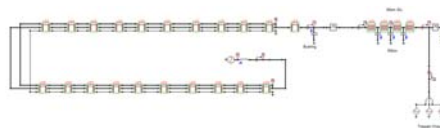


Figure 4.40: More Accurate Model on EMTP For the Trapped Charge as suggested by [MA15]

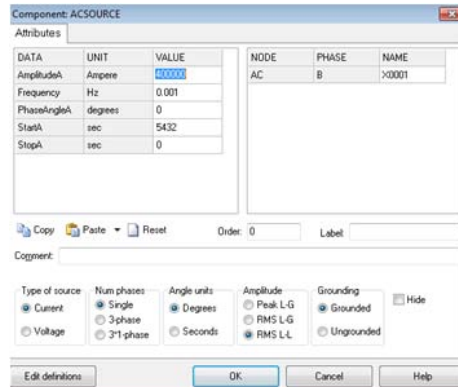


Figure 4.41: AC-Source to model the trapped charge on EMTP, as suggested by [MA15]

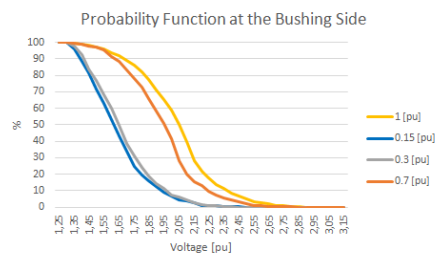


Figure 4.42: Probability Function at the bushing Side considering AC-Source to model the trapped charge

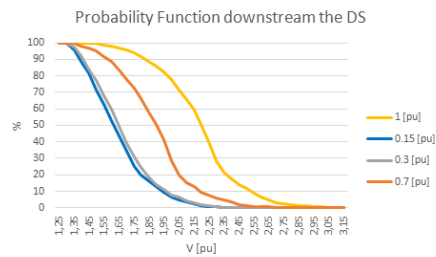


Figure 4.43: Probability Function Downstream the DS considering AC-Source to model the trapped charge

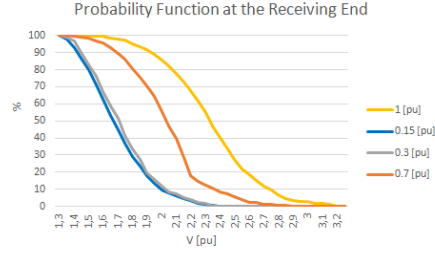


Figure 4.44: Probability Function at the Receiving End of the GIL considering AC-Source to model the trapped charge

4.4 Opening Operations

4.4.1 Opening Operations on OHL

In this scenario the load is already switched off by a Switch at the remote end of the line. Supposing to have a fault, for example a fault to ground, on the OHL, as shown in picture 4.45 and the Switch open in $t = 20[ms]$, this is the most severe condition because the Switch open during the peak of the voltage at the phase A. As explained in the Chapter 2, due to the stray capacitance of the OHL and GIL, a capacitive current is still flowing in the system. Because we are considering an high voltage system ($400[kV]$) and a GIL is attached, the current is in the range of several hundreds of ampere, in this specific case of $l_{OHL} = 30[km]$ and $l_{GIL} = 60[km]$ the value of current is around $350[A]$. The pictures 4.46 shows the voltage trend across the contacts of the Circuit Breaker. This result is in agreement with the theory explained in the Chapter 2, for $t < 20[ms]$ the voltage is equal to 0, when $t > 20[ms]$ the voltage, after the voltage jump, start to oscillate at the frequency of the source. Picture 4.47 shows the trend of the current across the contacts of the CB. Also in this case the result is in agreement with the theory explained in Chapter 2, for $t > 20[ms]$ the current is equal to 0. The picture 4.48 shows Voltage Trend at the source side (red) and downstream the Switch (green). As expected from the theory the voltage at the source side is influenced by the voltage jump, picture 4.49 shows the zoom of the voltage jump. The Voltage downstream the CB become at the floating potential. The same occurs for the voltage at the bushing side as shown in picture 4.50. Picture 4.51 shows the voltage trend at the source side (red), downstream the switch (green) and at the bushing side (blue). Picture 4.52 shows the voltage trend at the source side, 3-phases, compared with the voltage trend downstream the Switch.

Picture 4.53 and 4.54 shows the voltage trend along the GIL, at $l = 30[km]$ (green) and $l = 60[km]$ (blue) and at the bushing side. As told before the current is in the range of several hundreds of Ampere. Picture 4.55 shows the trend of the current at the bushing side (blue) and downstream the CB (green). At the open end of the GIL the current is in the range of some $[mA]$.

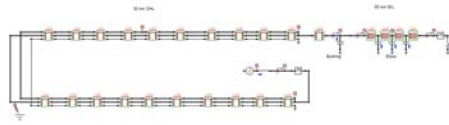


Figure 4.45: Circuit on EMTP for the Opening Operations on the OHL

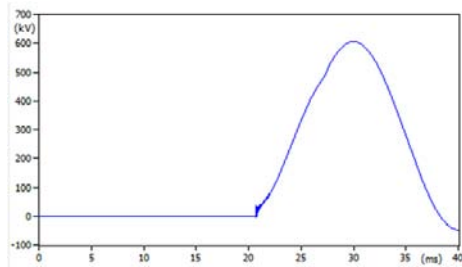


Figure 4.46: Voltage Trend Across the contacts of the CB

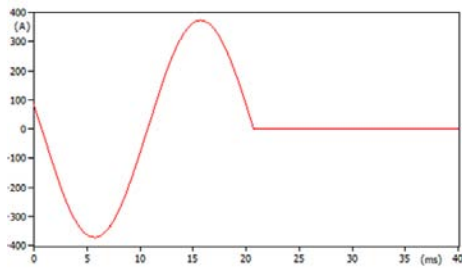


Figure 4.47: Current Across the contacts of the CB

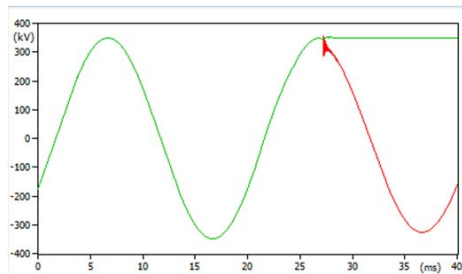


Figure 4.48: Voltage Trend at the source side (red) and downstream the Switch (green)

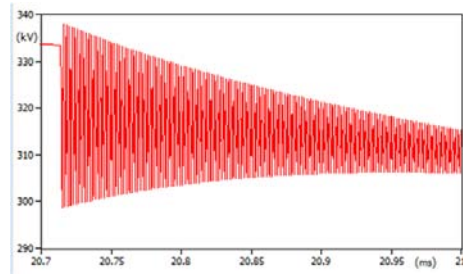


Figure 4.49: Zoom of the voltage jump at the source side

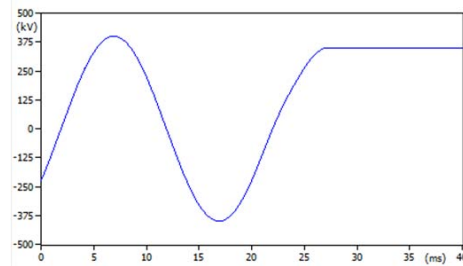


Figure 4.50: Voltage Trend at the Bushing

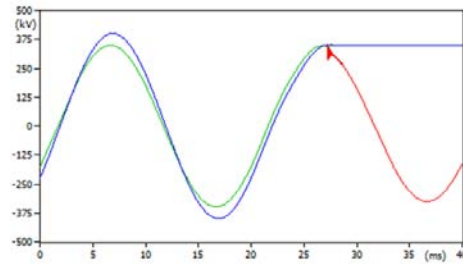


Figure 4.51: Voltage Trend at the source side (red), downstream the switch (green) and at the bushing side (blue)

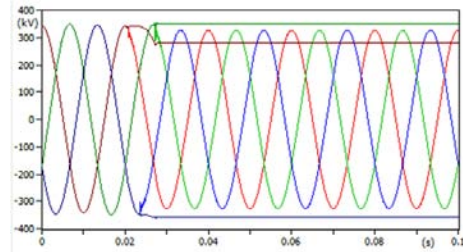


Figure 4.52: Voltage trend at the source side, 3-phases, compared with the voltage trend downstream the Switch

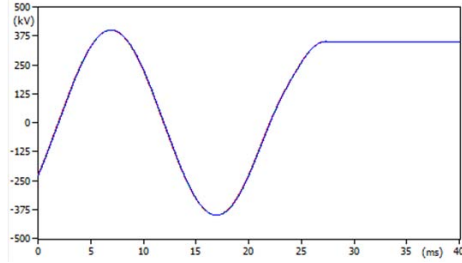


Figure 4.53: Voltage trend at the busching side (red), at $l = 30\text{ km}$ (green) and $l = 60\text{ km}$ (blue)

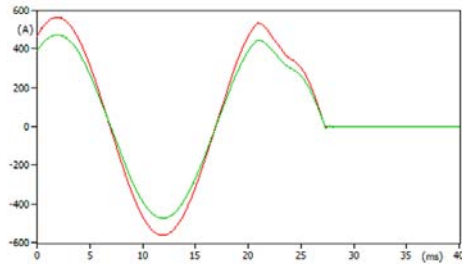


Figure 4.54: Voltage trend at the busching side (red) and at $l = 30\text{ km}$ (green)

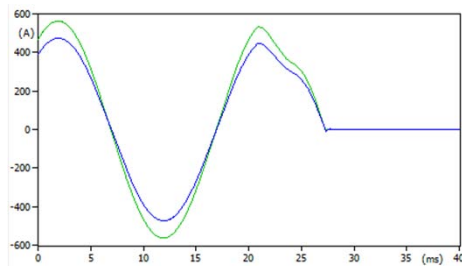


Figure 4.55: Trend of the current at the bushing side (blue) and downstream the CB (green)

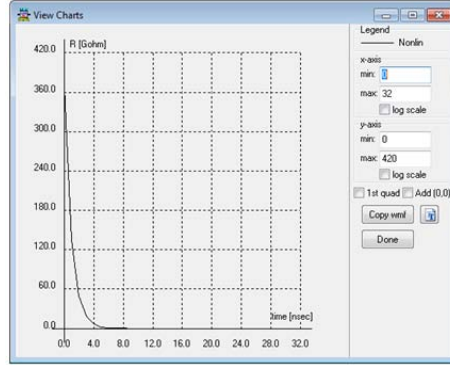


Figure 4.56: Non-Linear Resistance on EMTP

4.4.2 Opening Operations on GIL

As explained in the Chapter 2, during opening operations in Gas Insulated Switchgear a conducting spark channel is established with a time lag of a few ns after a breakdown channel has connected to the electrodes. During this time the spark resistance changes from a very large to a very small value. In order to build a correct model of the spark between the contacts during opening operations a more complex model is introduced. [VVKN01] The arc resistance is modelled by the exponential formula

$$R = R_a + R_0 e^{-t/\tau}$$

Where R_a is taken as 0.5Ω , and it represent the residual spark resistance. R_0 is taken as $10^{12}\Omega$ and τ is $1ns$. [VVKN01] This resistance varies from very high value [$M\Omega$] to a low value 0.5Ω in $30ns$. After $30ns$ the $r(t)$ can be neglected because its value is less than 0.09Ω . The picture 4.56 shows the arc resistance model build using a non linear resistance $R(t)$ on EMTP.

The model of the composed line during the spark built on EMTP is shown in the pictures 4.59 and 4.60, considering, as the previous analysis $l_{OHL} = 30[km]$ and $l_{GIL} = 60[km]$. As explained in the chapter 2, when the Disconnecter open and the spark is extinguished the voltage at the source side oscillate at the frequency of the network, and the voltage at the load side oscillate independently at the floating potential. This is a single spark approach, where the only one breakdown selected from the entire VFT process is taken into account, whereas, as explained in the chapter 2, for the slow –moving contacts numerous discharges occur during operation. Considering the Weak Network, and considering $f = 500[kHz]$ for the opening operations, picture 4.57 shows the voltage trend of the source (blue), at the bushing side (red) and at the load side (green). Picture 4.58 shows the zoom of the picture 4.57, it is possible to note how the high value of the inductance of short circuit, because we are considering a weak network, involve in a distortion on the voltage wave at the bushing side. The results are

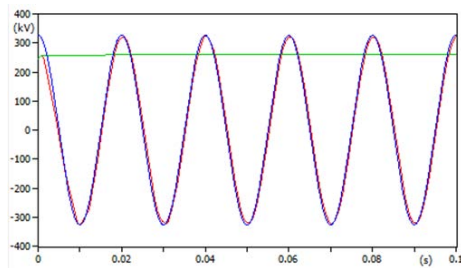


Figure 4.57: Voltage trend of the source (blue), at the bushing side (red) and at the load side (green)

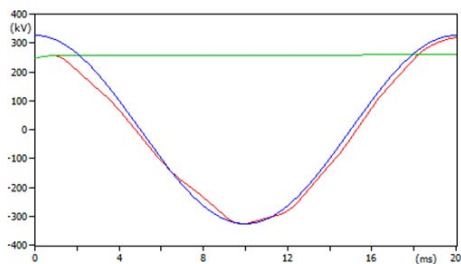


Figure 4.58: Zoom of picture 4.57

in agreement with the theory, because the voltage at the source side oscillate as a voltage source, and the voltage at the load side is a floating potential. The same analysis has been done in case of strong network.

The table below shows the results obtained by EMTP routine. The picture 4.57 shows the trend of the voltage at the bushing (red), Downstream the disconnector (green) and downstream the GIL (blue).

Considering that the DS open in $t = 1[ns]$, when the phase B is the maximum value (negative). For this reason the maximum value of overvoltage occurs at the phase B, as expected. The results in table 4.5 show the overvoltage considering a weak network. It is possible to not how the maximum value of voltage occurs downstream the CB, as expected. The table 4.6 show the results considering a strong network.

In matter of trapped charge in this case was not possible to do an accurate

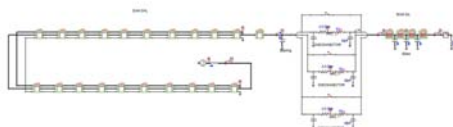


Figure 4.59: Line Model on EMTP

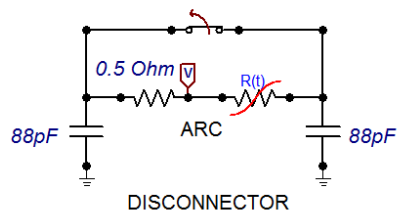


Figure 4.60: Arc Model on EMTP

	VFTO [pu]
Downstream the CB	1.12
Bushing Side	1.107
Source Side	1.07

Table 4.5: Overvoltages During the GIL Opening Operations in case of weak network

	VFTO [pu]
Downstream the CB	1.06
Bushing Side	1.04
Source Side	1.008

Table 4.6: Overvoltages During the GIL Opening Operations in case of strong network

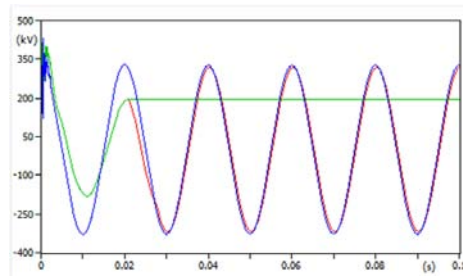


Figure 4.61: Voltage Trend at the Source Side (blue), at the bushing side (red) and downstream the CB (green), considering $t_{opening} = 20[ms]$

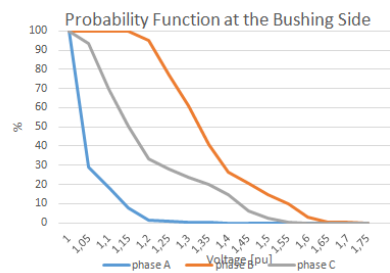


Figure 4.62: Probability Function at the Bushing side

analysis. In fact was not possible to use the AC-Source to model the trapped charge, because the EMTF was not able, with this kind of system, to evaluate the initial conditions. Modeling the Trapped Charge as a grounded capacitance the system works, but it was possible to note an influent peak values of voltage due the DC trapped charge, as shown in picture 4.61. The file.lis was influenced by these peak values, for this reason was not possible to do an accurate analysis in matter of trapped charge for this scenario.

Statistical Analysis

A statistical analysis has been done, considering the same parameters explained in the previous analysis. Whithout taking into account the trapped charge, for the reasons explained before, in this case was necessary to do the analysis considering the three separate phases of the GIL. The pictures 4.62 4.63 4.64 show the results. It is possible to see how the more severe condition occurs for the phase B, for the same reasons explained before. Anyway the overvoltages don't reach high value, the probability to reach $1.7[pu]$ is very low.

gensymb

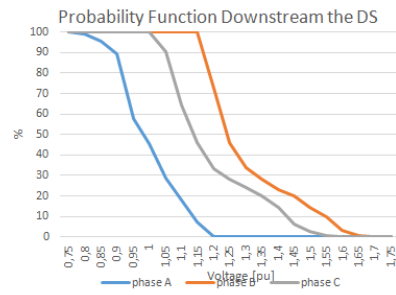


Figure 4.63: Probability Function Downstream the DS

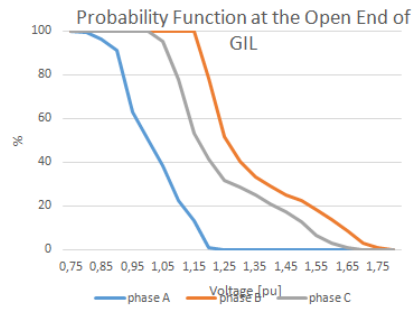


Figure 4.64: Probability Function at the Open End of the GIL

Chapter 5

External Overvoltages: Lightning

5.1 Introduction

It is possible to consider the lightning channel as an impedance Z_f evaluated as the ratio between the impedance of a metallic conductor of 500Ohm and a propagation speed of $(0.1 - 0.3)$ times the speed of light, as shown in formula 5.1 [AB11]

$$Z_f = \frac{500}{(0.1 - 0.3)} = 5000 - 1650[\text{Ohm}] \quad (5.1)$$

Considering the lightning strikes as a system with resistance R_p , and potential between cloud and ground V_f , the current associated with the strike will be 5.2 [AB11]

$$I_f = \frac{V_f}{(R_p + Z_f)} = \frac{V_f}{Z_f} \quad (5.2)$$

It is important to note that the current is independent from the systems which the lightning strikes. For this reason it is possible to imagine that this current is imposed from an equivalent current generator. [AB11] The lightning current has a particular shape, usually it has a front duration between $0.5 - 5\mu s$, and the time between 30% and 90% value of peak-1 at the wave front is between $20 - 60\mu s$. [AB11] The picture ?? and ?? show the typical lightning current and its parameters. This current can reach 200kA. [Coo10]

Several expressions have been proposed for such waveform, the most widely used is so-called Heidler model, which will be implemented on EMTP. It is given by 5.3, where I_p is the peak current, η is the correction factor of the peak current, n is the current steepness factor, as shown in picture 5.3, and $k = t/\tau_1$ where τ_1 and τ_2 are time constant determining rise and decay time, respectively. The

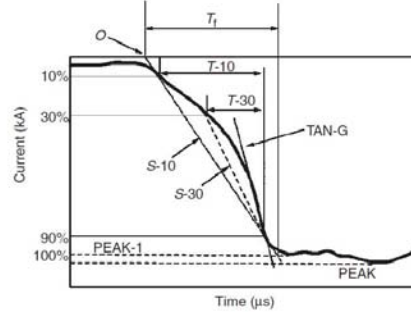


Figure 5.1: Lightning Current [Coo10]

PEAK-1 (kA)	Maximum amplitude of the first peak
PEAK (kA)	The highest current peak
T_f (μ s)	Front duration
$T-10$ (μ s)	Time between the 10% and 90% values of PEAK-1 at the wave front
$T-30$ (μ s)	Time between the 30% and 90% values of PEAK-1 at the wave front
T_r (μ s)	Stroke duration; time from the virtual zero time to the half-peak value at the wave tail
TAN-10 ($\text{kA } \mu\text{s}^{-1}$)	Rate of rise at the 10% point of PEAK-1
TAN-G ($\text{kA } \mu\text{s}^{-1}$)	Maximum rate of rise
S-10 ($\text{kA } \mu\text{s}^{-1}$)	Average rate of rise between the 10% and 90% values of PEAK-1
S-30 ($\text{kA } \mu\text{s}^{-1}$)	Average rate of rise between the 30% and 90% values of PEAK-1

Figure 5.2: Characterist Parameters of Lightning Current [Coo10]

picture 5.3 shows the Heidler model for different values of n , choosing $1, 2[\mu\text{s}]$ as rise time and $50[\mu\text{s}]$ as decay time. [MCA05]

$$i(t) = \frac{I_p}{\eta} \frac{k^n}{1 + k^n} e^{-t/\tau_2} \quad (5.3)$$

The study considers two different cases: the direct stroke on tower for the shielding failure, and the stroke on tower peak. For the first case, because the reflection factor at the OHL-GIL junction is negative for travelling waves moving from the OHL to GIL (because $Z_{GIL} < Z_{OHL}$), the insulation failure has not been considered, because the voltage buildup over the OHL insulators is low. [GW15] The second case is the most common real case. In fact adding the shield wires the probability of direct stroke on the tower is only 5%. [AB11] In this case the voltage between the insulators is higher than in case of shielding failure, due to the mutual capacitances and inductances between the conductors and the shielding wire. [AB11] In this case R_t , the ground resistance of the tower, is very important. If the value of R_t increase the value of the overvoltages increase, and a failure of the insulators can occur. But also the reflections can be dangerous because very high value of voltage could occur. [AB11] As suggested in literature [fM09] the ground resistance of the struck tower is assumed variable, and it is possible to evaluate it by the formula 5.4, where R_g is the resistance at tower foot at low current and low frequency. I is the current flowing along the resistance; I_g is the limiting current initiating soil ionization, evaluated by

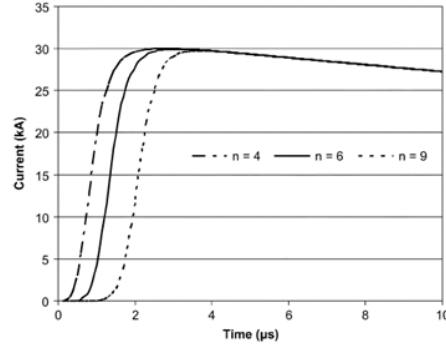


Figure 5.3: $I(t)$ for different steepness factor

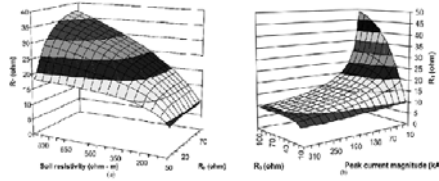


Figure 5.4: Variation of R_t as a function of I, E_0, ρ

the formula 5.5.

$$R_t = \frac{R_g}{\sqrt{1 + I/I_g}} [Ohm] \tag{5.4}$$

$$I_g = \frac{1}{2\pi} \frac{E_0 t}{R_g^2} \tag{5.5}$$

where E_0 is the soil critical value, assumed $350kV/m$ and p , is the soil resistivity. [MCA05]

It is important to note that due to the presence of GIL connected with an OHL, the value of overvoltage will be lower, as explained in theory of the reflection waves. The GIL, and the cable in general, is self-protected if its length is higher than the “self-protection length”. [AB11] It means the minimum length for which the overvoltages do not exceed the maximum acceptable value. In the case of $400kV$ GIL this value is $1425[kV]$. It occurs because the time which the propagation wave spend to travel along the GIL is higher than the impulse incident. [AB11] As explained in the Chapter 2, for the theory about the travelling waves, if we are considering a no-load line, the overvoltage at the end of the line will be two times higher than the incident wave. But this happens for the theoretical case of rectangular wave. In case of current lighting the overvoltage never receive these values. [AB11]

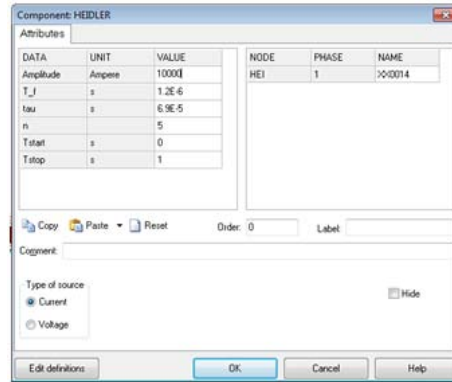


Figure 5.5: HEIDLER component on EMTP

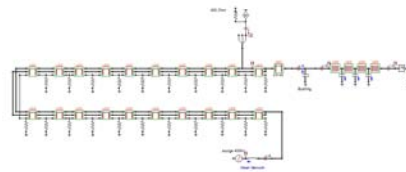


Figure 5.6: model on EMTP for shield failure

5.2 Model on EMTP

An HEIDLER component has been used to model the current lightning, as shown in picture 5.5 . The typical wave form $1.2/50\mu s$ has been considered with $I_{peak} = 10kA$. It is necessary to evaluate the R_{ground} . For R_g the literature proposes a value in a range from 7.5 to 14Ω . The value proposed by [Ame14] is 10Ω for $400kV$. For the formulas 5.4 proposed the R_{ground} evaluated for the struck tower is $9,92\Omega$, because the I_g evaluated is $55,50[kA]$ and the I measured is $893,56[A]$. The lightning path impedance chosen is $400[\Omega]$ as suggested in [Ame14].

5.3 Shielding Failure

For this analysis PI model is considered, because in this case J. Marti model involved problems during the simulation. The parameters have been calculated considering $f = 500kHz$. For this analysis it has been considered that the stroke occurs during the maximum value of the voltage at the source side, which is the worst case.

The system considered is shown in picture 5.6. The OHL length is $8[km]$. The GIL length is $3[km]$.

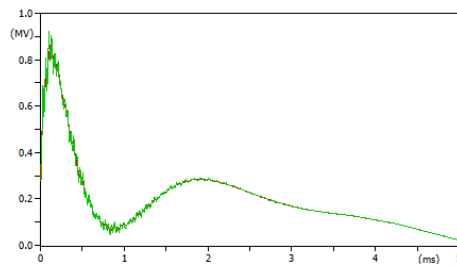


Figure 5.7: Trend of the voltage at the sending end of the GIL (red), at the receiving end (green) in case of Shielding Failure

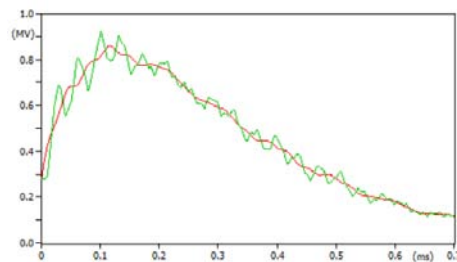


Figure 5.8: Zoom of the picture 5.7

Considering that the SW at the receiving end is opened, using a sample time $1[ns]$, the pictures 5.7 5.8 show the trend of the voltage at the sending end of the GIL (red) and the receiving end of the GIL (green). The higher stress occurs at the receiving end. The picture 5.9 shows the trend of the lightning voltage. Picture 5.10 shows the trend of the voltage at the sending end of the GIL (red), at the receiving end (green) and lightning voltage (blue). And picture 5.11 shows the lightning current.

The graphic 5.12 and the table 5.1 show how the Maximum Value of Voltage increase when the GIL length decrease.

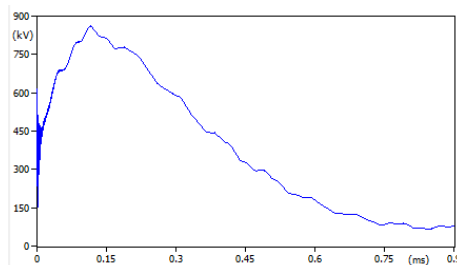


Figure 5.9: Lightning Voltage in case of Shielding Failure

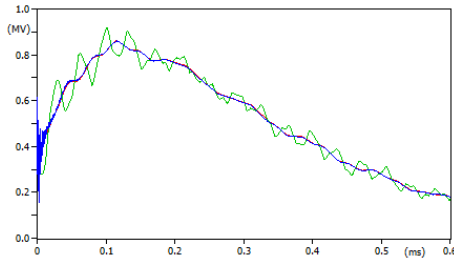


Figure 5.10: Trend of the Voltage at the sending end of the GIL (red), at the receiving end (green) and lightning voltage (blue) in case of Shielding Failure

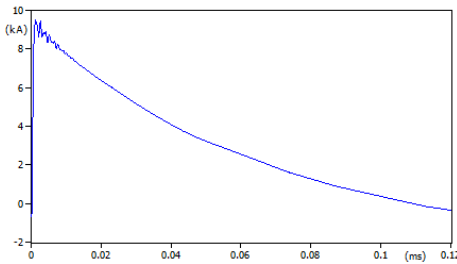


Figure 5.11: Lightning Current

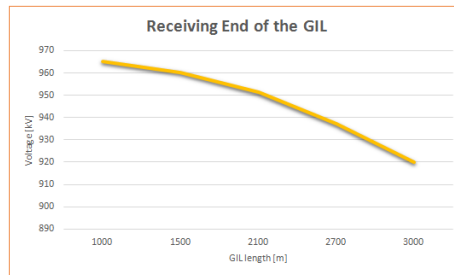


Figure 5.12: Value of Voltage as a function of GIL length

length [m]	Sending End [kV]	Receiving End [kV]
3000	860,943	920,096
2700	866,089	937,29
2100	888,97	951,36
1500	906,75	960,34
1000	922,12	965,28

Table 5.1: Maximum Value of Voltage as a function of GIL length

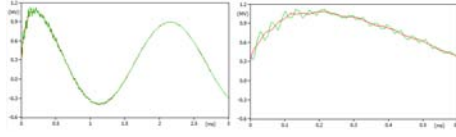


Figure 5.13: trend of the voltage at the sending end of the GIL (red) and the receiving end of the GIL (green) without taking into account the lightning-path impedance in case of Shielding Failure

The value of voltage is less than 1425 kV. On the other hand, without taking into account the lightning-path impedance, as done in the work [AB11] the values of overvoltage are higher. In fact considering 3[km] GIL length the value of voltage at the receiving end is 1090, 15[kV]. The picture 5.13 shows the trend of the voltage at the sending end of the GIL (red) and the receiving end of the GIL (green) without taking into account the lightning-path impedance.

5.4 Stroke on Tower Peak

The system considered is shown in picture 5.14. The I_{peak} for the lightning current is 200[kA], for the classical case 0.6/350[μs], as suggested in literature. The literature suggest to evaluate the parameters considering 400[kHz] frequency. Since, as explained before, in this particular case the reflections could be dangerous, it is necessary to simulate the behaviour of the insulators. To do that the insulator is represented by a simple switch controlled by voltage.[AB11] The value chosen for the limit voltage is 1300[kV], as done in the work [AB11]. It is necessary to add a capacitance in parallel. Typical capacitance values for suspension insulators are 80pF/unit.[AB11] For this reason in our case it reasonable to suppose a capacitance about 3.63[pF]. Considering this model means consider the worst case, because the voltage across the switch became higher than 1300[kV] in a short time, whereas in a real case the wave cross the insulator when it is slightly attenuated, for this reason in a real case the overvoltages expected are lower. [AB11] The picture 5.15 shows the trend of the voltage at the sending end of the GIL (red) and at the receiving end of the GIL (green). The maximum value of voltage at the receiving end is 1285, 96[kV], lower than the limit value, considering the GIL length 3[km].

5.5 Accurate Tower Model by Akiro Ametani

[Ame14]

To build a more accurate model it is necessary take into account the model circuit of the tower. In fact in principle the surge impedance is varying along the tower [UR11]. The work [Ame14] suggest, for 400kV system, to represent the transmission tower by a distributed-parameter lines. The work by A. Ametani suggest, for 400kV system, a tower height $h = 79.5[m]$. The tower top is

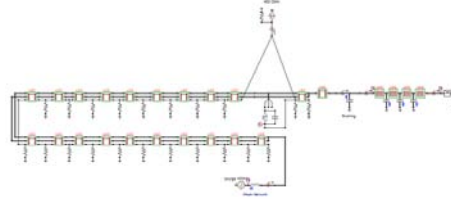


Figure 5.14: Model on EMTP in case of Stroke on Tower Peak

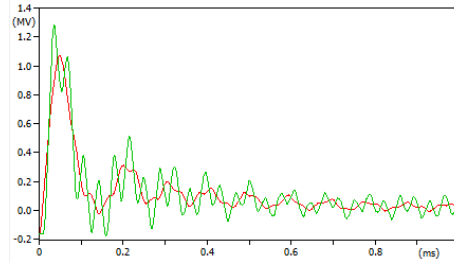


Figure 5.15: trend of the voltage at the sending end of the GIL (red) and at the receiving end of the GIL (green) in case of Stroke on Tower Peak

represent as a $Z - line$ without losses with $Z = 220[Ohm]$ and four section respectively $7.5[m]$, $14.5[m]$ and $14.5[m]$, whereas the tower bottom is represent as a $Z - line$, without losses, with $Z = 150[Ohm]$ and length $43[m]$. The propagation velocity of a travelling wave along a tower is taken to be the light velocity in free space, $300m/\mu s$. In this model the travelling wave attenuation and distortion are represent as an RL parallel circuit, as illustrated in picture 5.16. Where R and L are defined as follow. $\alpha = 0.89$ is the traveling time along tower.

$$R_i = \Delta R_i * x_i$$

$$L_i = 2\tau R_i$$

$$\Delta R_1 = \Delta R_2 = \Delta R_3 = 2Z_{ti} \frac{\ln(1/\alpha)}{h - x_4}$$

$$\Delta R_4 = 2Z_{t4} \ln(1/\alpha)/h$$

$$T = h/c_0$$

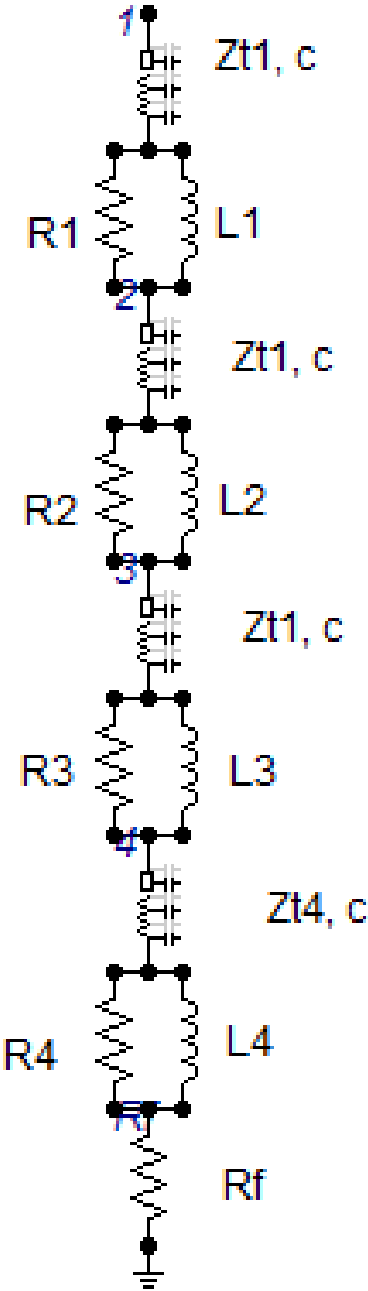


Figure 5.16: Tower Model Recommended in Japan [Ame14]

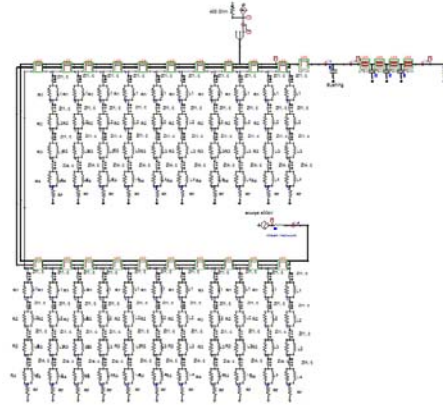


Figure 5.17: Model on EMTP

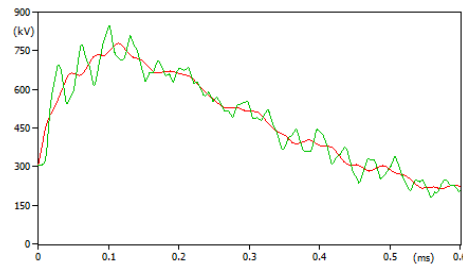


Figure 5.18: Trend of the voltage at the sending end of the GIL, accurate tower model, Shielding Failure

5.5.1 Shielding Failure

The model on EMTP to study the shielding failure is shown in picture 5.17 . The same analysis has been done. The pictures 5.18 and 5.19 show the trend of the voltage at the sending end of the GIL (red) and at the receiving end (green) and the lightning voltage (blue) for GIL length 3000[m] . It is possible to note in table 5.2 how this result agrees with the result of the previous analysis, in fact the tower model doesn't have important influence in the study of the shielding failure.

5.5.2 Stroke on Tower Peak

The same analysis with the same model has been done for the case of stroke on tower peak. In this case the model results much more accurate than the first one, because in this analysis the tower model is very important, as told before. The model considered is shown in picture 5.20. The picture 5.21 shows

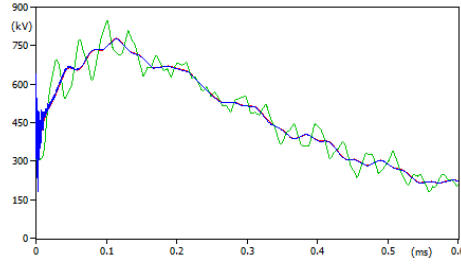


Figure 5.19: Trend of the voltage at the receiving end of the GIL, accurate tower model, Shielding Failure

length [m]	Accurate Model [kV]	Simplify Model [kV]
3000	948,24	922,53
2700	967,43	937,29
2100	980,26	951,36
1500	989,34	960,34
1000	994,37	965,28

Table 5.2: Comparison between the results obtained by the simplify tower model and the accurate tower model in case of shielding failure

the trend voltage at the sending end (red) and at the receiving end (green). It is possible to note how the behaviour of the transient change significantly, the values of the overvoltage are very high $1966,27[kV]$, more than the limit value $1425kV$ for $3[km]$ GIL length. And also the wave shape is changed significantly.

It is possible to affirm that the first simplify model is not accurate for this analysis, for this reason it is necessary to use the second one. Anyway, in so doing, the value of the overvoltage is too high, it happens because the model of the insulator is not accurate for the reason explained before. As well known it is possible to simulate the behaviour of the insulator as a function V-t. For the first instants the insulator is able to sustain a high value of voltage, this value decrease with the time. On the [LP09] the rule that the insulators play in such a back-flashover study is simulated using a MODELS flash, which controls a TACS/MODELS controlled switch. Using these models available on the library, we have chosen the parameters suggested in literature [LP09] for $400kV$ system. On the flash model is implemented the insulator characteristic V-t, as follows

$$U_{ins} = U_{inf} + (U_0 - U_{inf})e^{t/\tau}$$

The model flash receive as input the voltage across the insulator, and the output is close command for the switch. At $t = 0$ the $U_{ins} = U_{inf}$, the switch is opened. U is the voltage between the switch, if this voltage is higher than U_{init} the simulation goes on, and the time is incremented. When U became higher than U_{ins} the switch closes. It represent a good approximation of the real case,

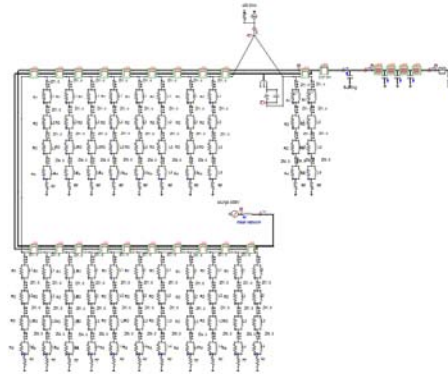


Figure 5.20: Accurate Tower Model on EMTP in case of Stroke on Tower Peak

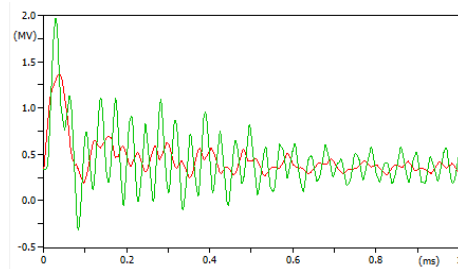


Figure 5.21: Voltage at the sending end (red) and at the receiving end (green) in case of Stroke on Tower Peak

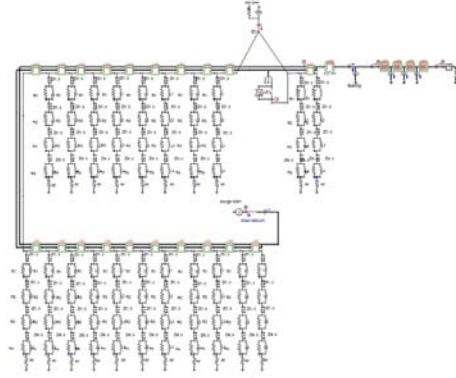


Figure 5.22: Model on EMTP using a MODELS flash and controlled switch

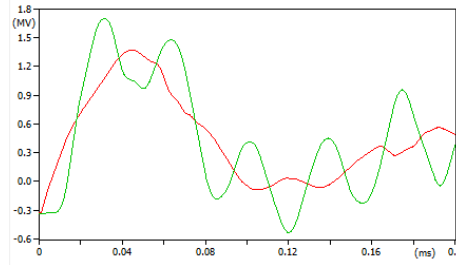


Figure 5.23: Trend of the voltage at the sending end (red) and at the receiving end (green) in case of Stroke on Tower Peak using a MODELS flash and controlled switch

because the characteristic of the insulator is constantly compared between the voltage across the insulator (it means across the switch), when the value of the voltage exceed the value of the characteristic it means that there is a flashover between the insulator and the conductor. [LP09] For this analysis it is necessary increase the limit of the file.lis from 3.0 to 6.0 . The model on EMTP is showed in picture 5.22. The picture 5.23 shows the trend of the voltage at the sending end (red) and at the receiving end (green). Using this model to simulate the behaviour of the insulator the maximum value of the voltage is $1702,73[kV]$, which exceed the maximum limit value $1425[kV]$, but is $293,54[kV]$ less than the value obtained using the simple switch to simulate the insulator. And it is possible to note how the system is less stressed. The picture 5.24 shows the trend of the voltage across the insulator (blue) and the voltage in the OHL (red).

A different kind of insulator has been choosed, with a less strength, for example $U_{inf} = 1650[kV]$, whereas in the first case was $U_{inf} = 3000[kV]$, and $U_0 = 650[kV]$, whereas in the first case was $U_{inf} = 1400[kV]$. [LP09] For this

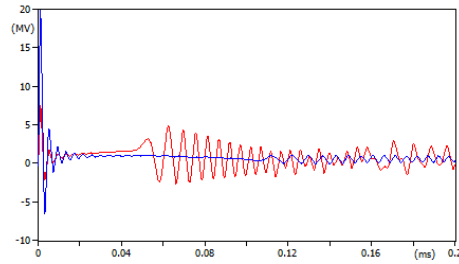


Figure 5.24: Trend of the voltage across the insulator (blue) and the voltage in the OHL (red)

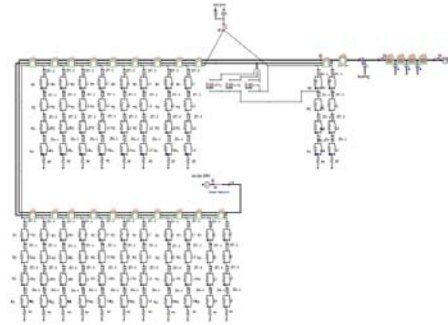


Figure 5.25: Model on EMTP 3-phase flashover,

reason it is reasonable to suppose that the flashover between one phase and the conductor became a 3-phase flashover, as suggested in literature [LP09]. The system is shown in picture 5.25. The picture 5.26 shows the trend voltage at the sending end of the GIL (red) and at the receiving end of the GIL (green). As expected this case is more severe than the other one, in fact the maximum value of voltage at the receiving end is $1798,83[kV]$. Because in our case the $L - 6$ overhead line with a double circuit is represented, the same analysis has been done considering that the flashover between the insulator and conductor occurs for the phase A in both circuits. The picture 5.27 shows the result. As expected this case is more severe than the other one, in fact the maximum value of voltage is $2207[kV]$. The same consideration has been done for the 3-phase flashover case. The picture 5.28 shows the result. In this case the maximum value of voltage is $2184,6[kV]$.

5.6 The Surge Arresters

The Surge Arresters offer a protection against the overvoltages. The metal oxide surge arresters are widely used. Both porcelain and polymer tube design surge

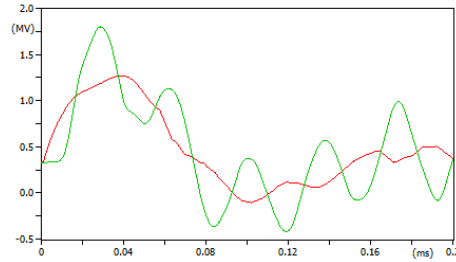


Figure 5.26: Trend voltage at the sending end of the GIL (red) and at the receiving end of the GIL (green) in case of 3-phase flashover,

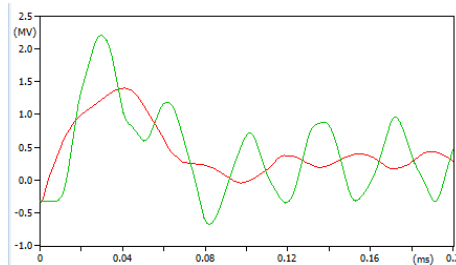


Figure 5.27: Trend voltage at the sending end of the GIL (red) and at the receiving end of the GIL (green) considering that the flashover between the insulator and conductor occurs for the phase A in both circuits

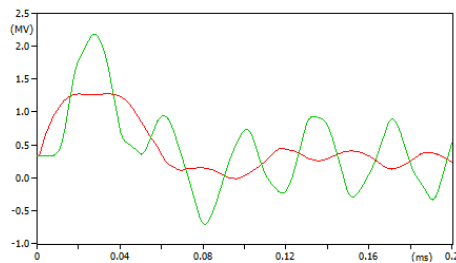


Figure 5.28: trend voltage at the sending end of the GIL (red) and at the receiving end of the GIL (green) for the 3-phase flashover case in both circuits

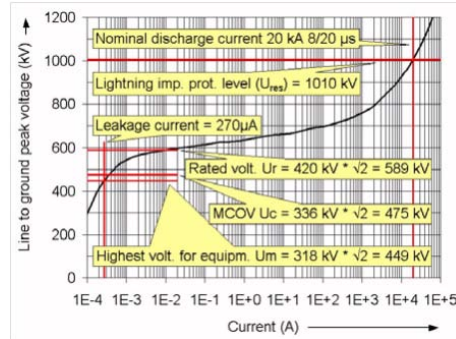


Figure 5.29: Protection Characteristic of Surge Arrester for 550kV applications [KS03]

arresters are used in these applications. Polymer tube offers some advantages compared with the porcelain arrester, for example the light weight, high mechanical resistance and safe short circuit behaviour. [KS03] The purpose is to always limit the voltage across the terminals of the equipment to be protected below its insulation withstand voltage. This is achieved by connecting elements with an extremely non-linear voltage current characteristic in parallel to the terminals of the equipment. So called metal oxide (MO) surge arresters containing ceramic bodies mainly made from zinc oxide (ZnO) and bismuth oxide are used nowadays. [KS03] The surge arresters do have to fulfil two basic requirements: the arresters must be rated to provide sufficient electric protection of the equipment installed in the system and it must remain thermally stable even under the most severe conditions. Sufficient electric protection means that the voltage across the equipment is limited below its withstand voltage including an appropriate safety margin. [KS03] For 400kV system the BIL is 1425kV, but taking into account the safety margin the limit value is $BIL/1.15 = 1239.13kV$. The picture 5.29 shows the typical rating for standard outdoor surge arresters for 550kV AC system. [KS03] It is possible to see how the characteristic is non-linear, so that if the current increase the peak voltage L-G doesn't change significantly. The most important data are shown in the picture.

In matter of thermal stability, the arrester must be rated not to exceed a specific internal temperature. The picture 5.30 shows the trend of the power loss by MO elements and the trend of the heat dissipation of surge arrester. There are two intersection, the stable operating point and the limit of thermal stability. Below the limit of thermal stability the arrester will always return to the stable operating point. However, over this limit the arrester will become thermally unstable and be destroyed. [KS03] The picture 5.31 shows the surge arrester design on high voltage overhead transmission line.

The picture 5.32 shows a hybrid system, composed by an Overhead Line and a GIL. In this type of system it is possible to have external surge arresters, it means surge arresters on the Overhead line side, and/or integrated surge

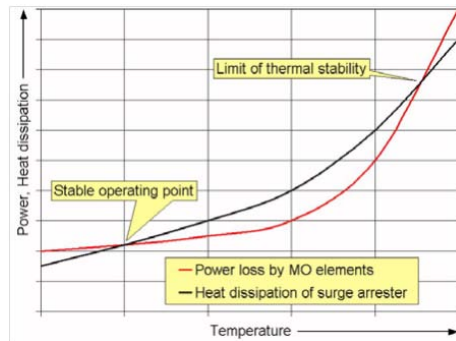


Figure 5.30: Thermal Stability Characteristic of Surge Arrester for 550kV applications [KS03]



Figure 5.31: Surge Arrester Design for Overhead Transmission Line HV [KS03]

arresters on the GIL. The first one is the conventional application, but the second one could have some advantages.

5.6.1 The model of Surge Arrester on EMTP

The work [PG99] proposes a simplified model for the MO surge arrester. The model is shown in the picture 5.33, it is composed by a resistance of $1[M\Omega]$, two inductances evaluated by the formulas 5.7 5.6 where V_n is the arrester rated voltage, V_{r_1/t_2} is the residual voltage at $10kA$ fast front current surge, $1/T_2$, and $V_{r_{8/20}}$ is the residual voltage at $10kA$ current surge with a $8/20[\mu s]$ shape.

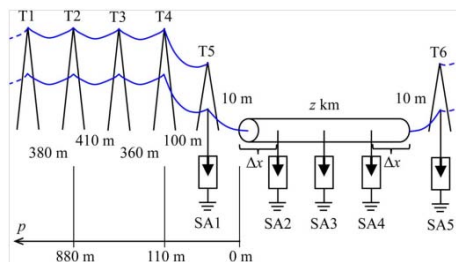


Figure 5.32: Hybrid transmission line: OHL and GIL [GW15]

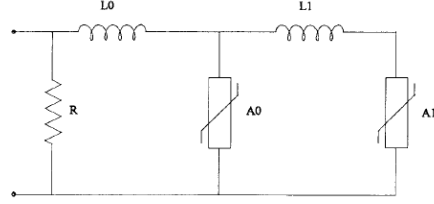


Figure 5.33: Surge Arrester simplified model by [PG99]

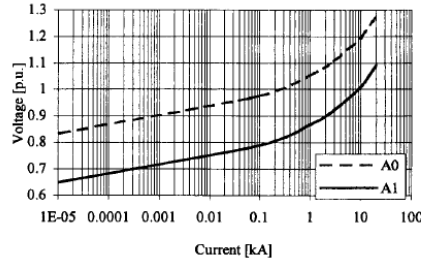


Figure 5.34: Non-linear resistances characteristic [PG99]

A_0 and A_1 is the non-linear resistance, modelled using type 92 branch cards on EMTP. In this work has been used the characteristics of the A_1 and A_0 shown in the picture 5.34 , suggested by [PG99].

$$L_1 = \frac{1}{4} \frac{V_{r1}/t_2 - V_{rs}/20}{V_{rs}/20 V_n} \quad (5.6)$$

$$L_0 = \frac{1}{12} \frac{V_{r1}/t_2 - V_{rs}/20}{V_{rs}/20 V_n} \quad (5.7)$$

The value of the characteristic are reported in the table 5.3.

The work [GW15] consider a surge arrester for $500kV$ applications. This kind of SA is suitable for $400kV$ applications. In particular this SA has a maximum continuous operating voltage of $525kV$, a rated voltage of $656kV$, and

I [kA]	$A_0[kV]$	$A_1[kV]$
$2 * 10^{-6}$	37.4	28.8
0.1	45	36.4
1	48.6	40
3	51.2	42.6
10	55.2	46.6
20	59	50.4

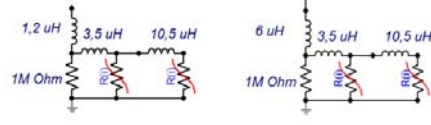


Figure 5.35: Model on EMTP: External SA (right) and Internal SA (left)

a maximum energy rating of $5.8[kJ]$. The residual voltage for $10 - kA$ current impulse is $1016[kV]$ for the $8/20$ current impulse and $1081[kV]$ for the current impulse. So that the inductances L_0 and L_1 are calculated as $3,5[\mu H]$ and $10,5[\mu H]$ respectively. This surge arrester characteristic is equal for external SA and for integrated SA, the only difference is the value of the lead wire (modelled by a lumped inductance) which connect the arrester from the earth point to the phase conductor. In case of integrated SA the value of the inductance is $0.3[\mu H/m]$ and the length is $4[m]$, in case of external SA $L = 1[\mu H/m]$ and the length is $6[m]$. Because in severe conditions the experimental values exceed the limit value of $1425[kV]$, the study has been done adding the Surge Arresters on the EMTP model. The picture 5.35 shows the integrated SA model (left) and the external SA model (right).

5.6.2 Integrated Surge Arrester

In case of hybrid system, Overhead line connected with a GIL, the conventional application of external Surge Arresters could results in high electrical stress on the insulation of GIL, it occurs because the overvoltage development is more critical than in cables. For this reason, and for the modular structure of GIL, the configuration considering the Integrates SA has been investigated.

Shielding Failure

Considering the previous case of Shileding Failure, two Internal Surge Arresters has been attached at the start and at the end of the GIL. Considering the stroke between the 18th and the 19th tower, which is the most severe case. As well known from the previous study the overvoltage value doesn't exceed the limit value, but anyway the test has been done in order to prove the efficiency of the SA. The picture 5.36 show the waveform in both cases, without integrated SA and with integrated SA. It is possible to note how in the second case the travelling waves are lessened, at the sending end of the GIL (red) and at the receiving end of the GIL (green). In fact the value of the voltage at the sending end in the first case is $758,53[kV]$, attaching the SA the voltage reaches the value of $478,07[kV]$. At the receiving end the value of the voltage is $873,87[kV]$ but attaching the SA the value is $506,58[kV]$.

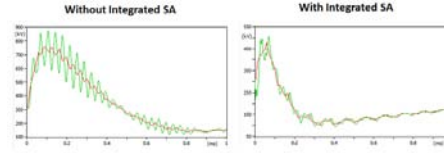


Figure 5.36: Voltage trend at the sending end of the GIL (red) and at the receiving end (green), without SA (left) and with Integrated SA (right) in case of shielding failure

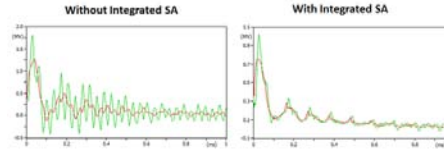


Figure 5.37: Voltage trend at the sending end of the GIL (red) and at the receiving end (green), without SA (left) and with Integrated SA (right) in case of Stroke on Tower peak

Stroke on the Tower Peak

But the most interesting case is the Stroke on Tower Peak, because the overvoltage can be exceeded the limit value. Considering $I_{peak} = 200[kA]$ the study has been done. This is the most severe case, in fact the [Ame14] suggest to consider the $I_{peak} = 150[kA]$ for $400[kV]$ applications. The picture 5.37 shows the waveform at the sending end of the GIL (red curve at the left side) without Integrated SA. The value of the voltage is $1270,37[kV]$. Attaching the Integrated SA (red curve at the right side) the value of the voltage become $762,08[kV]$. At the receiving end, without Integrated SA (green curve at the left side) the value of the overvoltage reaches $1800,44[kV]$, this value exceed the limit value, but considering the Integrated SA the value of the overvoltage become $1026,43[kV]$, which is within the safety range. Also in this case the picture shows how the travelling waves has been lessened.

5.6.3 Effect of Tower Model

These study has been done considering the footing resistance $R_f = 10[Ohm]$, as suggested by [Ame14] for $400[kV]$ applications. The correct value of R_f is one of the most important parameter during the study of the stroke on tower peak, as well known from the previous studies. The literature proposes value in the range from $10[Ohm]$ to $14[Ohm]$. As suggested by the work [PNMNCMHVL10] the effect of tower model has been investigated, considering the range $10 - 14[Ohm]$ for the foot resistance, for both cases without and with integrated SA. The pictures 5.38 and 5.39 show the trend of the voltage increasing the value of the footing resistance at the sending and at the receiving end, for $I_{peak} = 200[kA]$

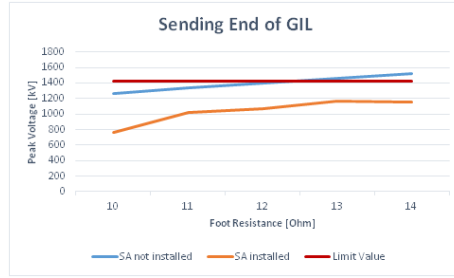


Figure 5.38: Voltage trend at the sending end of the GIL as a function of the foot resistance considering $I_{peak} = 200[kA]$

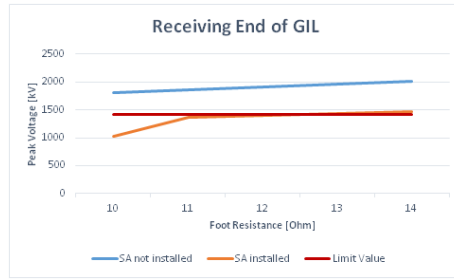


Figure 5.39: Voltage trend at the receiving end of the GIL as a function of the foot resistance considering $I_{peak} = 200[kA]$

. As expected from the theory the overvoltage increase if the R_f increase. For $R_f > 12[Ohm]$ the overvoltages reach the limit value, but attaching the internal SA the overvoltages don't exceed $1200[kV]$. Same consideration for the voltage trend at the receiving end, for $R_f > 11[Ohm]$ the overvoltages exceed the limit value, for this reason it is necessary to add the SA in order to remain within the limit.

More realistic case has been investigated, considering $I_{peak} = 150[kA]$, as shown in picture 5.40. It is possible to do similar considerations about the overvoltage trend. The limit value is exceeded just in case of $R_f > 12[Ohm]$ at the receiving end, but attaching the integrated SA the overvoltage remain on the limit.

5.6.4 Comparison with the External Surge Arrester

The external surge arresters are the conventional solution, but in hybrid system with a long overhead line and GIL this application results in high electrical stress on the insulator of GIL. For this reason in this work the Integrated (or Internal) surge arrester has been preferred to an external one. Anyway should be interesting to do a comparison between the Integrated and the External SA. The pictures 5.42 and 5.43 show the results considering $I_{peak} = 200[kA]$. The results,

R foot [Ohm]	Without SA [kV]	With SA [kV]
10	1800	1026,43
11	1852,77	1357,47
12	1904	1391,89
13	1956,7	1426,07
14	2008,34	1460,01

Table 5.4: Overvoltages at the Receiving End of the GIL considering $I_{peak} = 200[kA]$

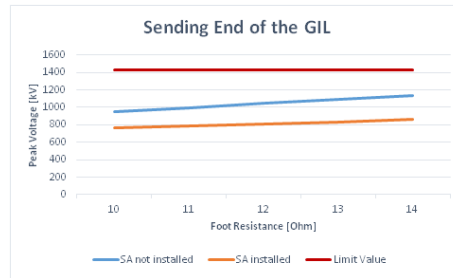


Figure 5.40: Voltage trend at the sending end of the GIL as a function of the foot resistance considering $I_{peak} = 150[kA]$

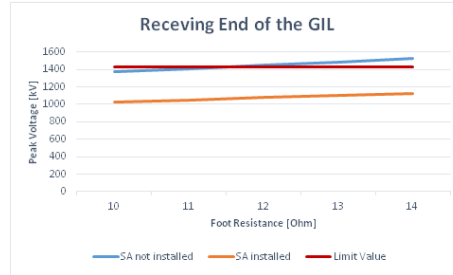


Figure 5.41: Voltage trend at the receiving end of the GIL as a function of the foot resistance considering $I_{peak} = 150[kA]$

R foot [Ohm]	Without SA [kV]	With SA [kV]
10	1369,96	1026,44
11	1408,34	1051,58
12	1446,58	1076,54
13	1484,67	1101,3
14	1522,37	1125,85

Table 5.5: Overvoltages at the Receiving End of the GIL considering $I_{peak} = 150[kA]$

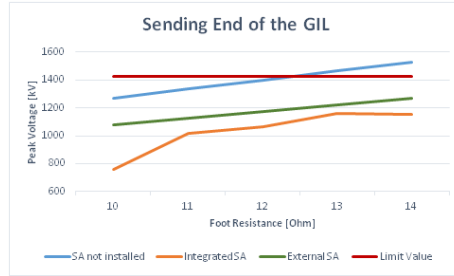


Figure 5.42: Voltage trend at the sending end of the GIL as a function of the foot resistance considering $I_{peak} = 200[kA]$

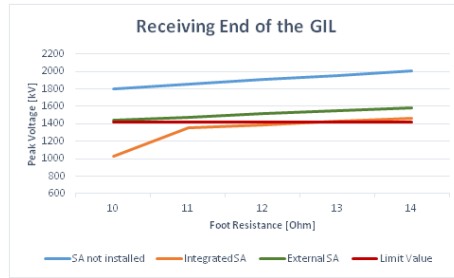


Figure 5.43: Voltage trend at the receiving end of the GIL as a function of the foot resistance considering $I_{peak} = 200[kA]$

obtained for different values of Foot Resistance, confirm that with external surge arresters the insulator of GIL is high stressed. Especially considering the Receiving End, where the highest overvoltage value occurs, for $R_f > 10[Ohm]$ the overvoltage exceed the limit value $1425kV$, it means that this solution is not applicable. The same analysis has been done considering $I_{peak} = 150[kA]$, the pictures 5.44 and 5.45 show the results. In this case both solutions are applicable, but in case of Integrated Surge Arresters the Overvoltage is around $100V$ less than the case of External Surge Arresters.

5.7 The load effect

Until now the analysis have been done considering the end of the GIL as an open end. It means that we were considering the $R_{load} = \infty$, and, as explained in the Chapter 2 about the theory of the Travelling Wave, in this case the reflection coefficient is $l = 1$ and the transmission coefficient is $\tau = 2$. It means that $v_{backward} = v_{forward}$ and $v_{transmitted} = 2v_{forward}$. This is the most severe case, and for this reason it has been investigated. Anyway should be interesting to investigate the load effect in order to better understand the behaviour of the system, as suggested in the work [JD]. To do that four different values of resistive

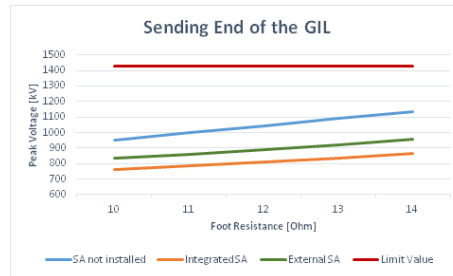


Figure 5.44: Voltage trend at the sending end of the GIL as a function of the foot resistance considering $I_{peak} = 150[kA]$

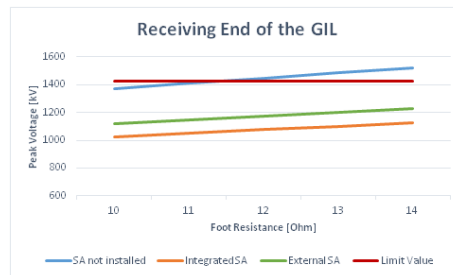


Figure 5.45: Voltage trend at the receiving end of the GIL as a function of the foot resistance considering $I_{peak} = 150[kA]$

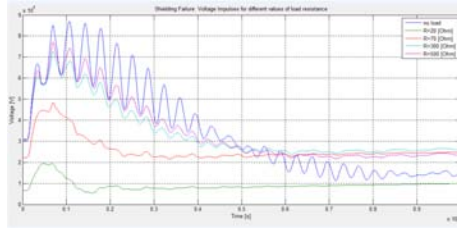


Figure 5.46: Voltage Impulses for different value of load resistance, in case of Shielding failure, $I_{peak} = 10[kA]$, without Surge Arresters, considering the Accurate Tower Model

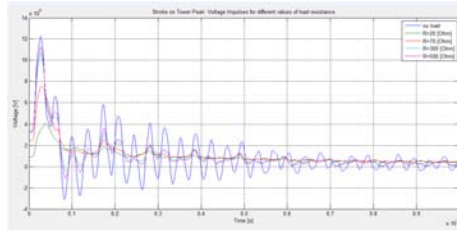


Figure 5.47: Voltage Impulses for different value of load resistance, in case of Stroke on Tower Peak, $I_{peak} = 200[kA]$, without Surge Arresters, considering the Accurate Tower Model

load have been chosen: $R = 20[Ohm]$: in this case the value of the resistance is $< Z_{GIL}$ and $< Z_{OHL}$, as well known from the theory the reflection coefficient is negative $l = -0.5$, it means that the reflected wave has been subtracted from the travelling wave, and therefore the peak value of the impulse is lower. The transmission coefficient is positive, $\tau = 0.5$. $R = 70[Ohm]$: in this case the value of the resistance is $\simeq Z_{GIL}$ it means that we are in condition of adapted line. As well known from the theory the reflection coefficient is zero, in our specific case is $l = 0.0668$, it means that we don't have a reflected wave, or it is very small. The transmission coefficient is $\tau = 1$, in our specific case $\tau = 1.07$. $R = 300[Ohm]$: in this case the value of the resistance is $\gg Z_{GIL}$ it means that we are close to the condition of $R_{load} = \infty$. In our specific case is $l = 0.66$. The transmission coefficient is $\tau = 1.66$. $R = 500[Ohm]$: as in the previous case the value of the resistance is $\gg Z_{GIL}$ it means that we are close to the condition of $R_{load} = \infty$. In our specific case is $l = 0.78$. The transmission coefficient is $\tau = 1.78$. Both cases have been investigated, Shielding Failure and Stroke on Tower Peak. The results obtained on EMTP have been implemented in Matlab. The pictures 5.46 and 5.47 show the results. As expected the case $R_{load} = \infty$ e $R_{load} = 300[Ohm]$ e $R_{load} = 500[Ohm]$ have a similar voltage trend at the end of the GIL. If R_{load} decrease the voltage wave decrease, for the reason explained before. The results confirm this behaviour.

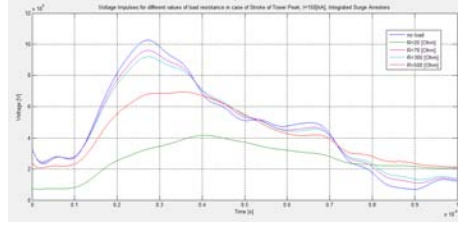


Figure 5.48: Voltage Impulses for different value of load resistance, in case of Stroke on Tower Peak, $I_{peak} = 150[kA]$, with Integrated Surge Arresters, considering the Accurate Tower Model

5.7.1 Travelling Wave along the GIL for different values of R_{load}

The work [THUB05] suggest a method in order to evaluate the contribute of the forward and backward wave to the voltage drop along the GIL. As explained in Chapter 2, the voltage at any point x along the cable can be expressed as the sum of a forward and backward propagation wave as shown by the formula 5.8 . It is possible describe the arrester current as a function of the forward wave, the voltage drop and the characteristic impedance of the GIL (or cable in general) and the OHL, as shown in the formula 5.9. In order to do this analysis it is necessary to consider the case with the presence of surge arresters, instead the previous cases shown in pictures 5.46 and 5.47, becuaseit is necessary to consider the current through the surge arrester.

$$v(x, t) = v_f(x, t) + v_b(x, t) \quad (5.8)$$

$$i_{arrester}(t) = \frac{2 * v_f(l, t)}{Z_c} - \frac{v(l, t)}{Z_c} - \frac{v(l, t)}{Z_L} \quad (5.9)$$

For the analysis just the case of Stroke on Tower Peak has been investigated, considering the more realistic case with $I_{peak} = 150[kA]$. We have considered the Akiro Ametani Tower Model, and the presence of Integrated Surge Arresters. The first step of the analysis is to measure by the probe on EMTP the voltage at the end of the GIL and the current through the SA, for different values of R_{load} . The sample time is $1[ns]$ for the reasons explained in the previous analysis, and the $T_{max} = 100[\mu s]$, because as it is possible to note from the previous analysis, the peak value occurs in the first $100[\mu s]$. Picture 5.48 shows the obtained Voltage Trend for different value of load resistance.

The second step suggested by [THUB05] is to evaluate the $v_{forward}$ by the formula 5.9, where Z_c is the impedance of GIL, evaluated in the Chapter 2, and Z_L is the R_{load} . After that it is possible to evaluate the $v_{backward}$ by the formula ???. To do that a Matlab algorithm has been implemented, and all the study cases have been investigated. Picture 5.49 shows the forward and backward travelling wave in case of $R_{load} = 20[Ohm]$. $v(l, t)$ is the voltage at the end

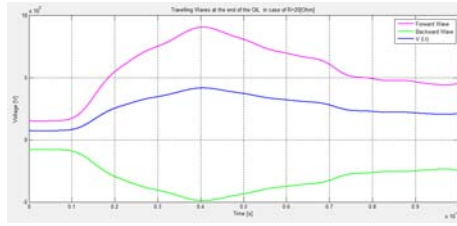


Figure 5.49: Travelling wave at the end the GIL in case of Stroke on Tower Peak considering $R_{load} = 20[Ohm]$

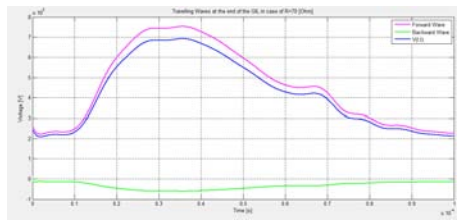


Figure 5.50: Travelling wave at the end the GIL in case of Stroke on Tower Peak considering $R_{load} = 70[Ohm]$

of the GIL $x = l$. It is possible to note how the backward travelling wave is negative, because, as explained before, the reflection coefficient is negative. For this reason the value of the $v(l, t)$, obtained as a sum of $v_f + v_b$ is low.

Picture 5.50 shows the case where $R_{load} = 70[Ohm]$. In this case we are almost in condition of adapted line, in fact the value of the backward travelling wave is very low, and the forward travelling wave is almost the same of the $v(l, t)$. This is not exactly the case of adapted line, because in the Chapter 3 the Z_{GIL} has been evaluated, but without taking into account the bushing, the elbows and other important components which have an influence on the value of the characteristic impedance. Anyway it is possible to affirm that the results are in agreement with the theory.

Picture 5.51 shows the case where $R_{load} = 300[Ohm]$. In this case the reflection coefficient is positive, and in fact $v(l, t)$, obtained as a sum of $v_f + v_b$ is higher than v_f . It is possible to do the same considerations for the picture 5.52 where $R_{load} = 500[Ohm]$.

It is possible to evaluate the $v_{backward}$ also in another way: in fact it is possible to evaluate the reflection coefficient as define in the Chapter 2. In case of $R_{load} = 20[Ohm]$ $l = -0.5$, if $R_{load} = 70[Ohm]$ $l = 0.0668$, if $R_{load} = 300[Ohm]$ $l = 0.66$ and finally $R_{load} = 500[Ohm]$ $l = 0.78$. Because $v_{backward} = l * v_{forward}$, it is possible to evaluate the backward wave by this formula, according with the theory. It is really important to note that formula is an important approximation, in fact, as explained in the Chapter 2 this formula consider that the only discontinuity is the connection point with the GIL and the load, without

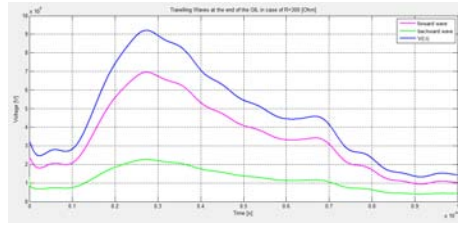


Figure 5.51: Travelling wave at the end the GIL in case of Stroke on Tower Peak considering $R_{load} = 300[Ohm]$

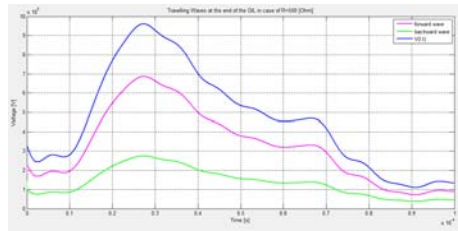


Figure 5.52: Travelling wave at the end the GIL in case of Stroke on Tower Peak considering $R_{load} = 500[Ohm]$

taking into account the discontinuity due the elbows, the Surge Arresters, the bushing. The first method is more accurate than the second one because it is based on real values of voltage and current measured directly on the system. It is possible to note how in case of $R_{load} \leq R_{GIL}$ the theoretical results are close to the experimental results. When $R_{load} \gg R_{GIL}$ the discontinuity along the GIL is more severe, because the reflection and the transmission coefficient are high, $l \simeq 1$ and $\tau \simeq 2$, for these reasons the experimental results are far from the theoretical results.

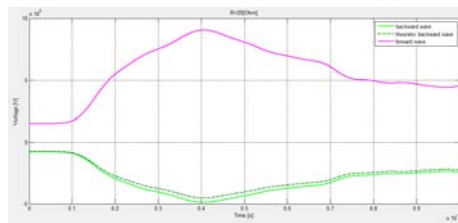


Figure 5.53: Travelling wave at the end the GIL in case of Stroke on Tower Peak considering $R_{load} = 20[Ohm]$

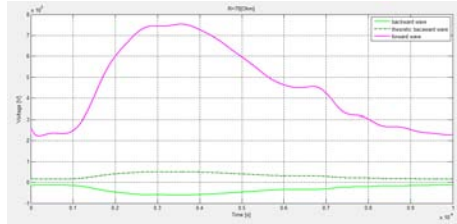


Figure 5.54: Travelling wave at the end the GIL in case of Stroke on Tower Peak considering $R_{load} = 70[Ohm]$

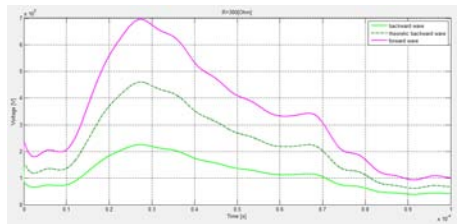


Figure 5.55: Travelling wave at the end the GIL in case of Stroke on Tower Peak considering $R_{load} = 300[Ohm]$

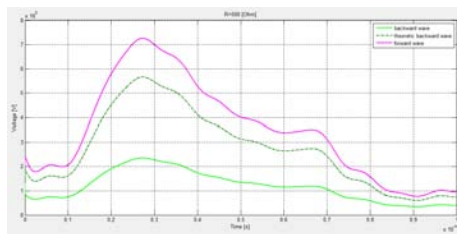


Figure 5.56: Travelling wave at the end the GIL in case of Stroke on Tower Peak considering $R_{load} = 500[Ohm]$

Chapter 6

Conclusion

In this work a 400[kV] mixed lines composed by Overhead Transmission Lines and Gas Insulated Transmission Lines (GIL) has been investigated. It represents an interesting compromise between costs, efficiency, and environment. There are several issues regarding the behaviour of the mixed lines in both steady state and transient conditions. The model of the transmission line has been built using the software EMTP: it involves a source, a overhead line, the terminal tower and the gantry, the bushings, a simplified model of a Gas Insulated Switchgear (GIS) considering the Circuit Breaker and the Disconnecter as an ideal switch, and finally the GIL. The line constants evaluated by the routine of the software have been compared with the values obtained by the analytical formulas in order to prove the validity of the model. Different scenarios has been considered, in particular Internal and External Overvoltages has been investigated. Regarding the Ferranti Effect at the open end of the line, it has been found that the overvoltage at the end of the line is higher in case of Gas Insulated Transmission Line than the case of Overhead Line, according to the theory. In matter of mixed line it has been found that the Ferranti effect increase if the line lenght increase, and the more severe case is the one related to the greater lenght of the GIL. The Ferranti Effect is higher in case of weak network. With the No-Load Energization analysis it has been found that in case of energization of the OHL the overvoltage reaches 1.93pu without high frequency components, as expected. The No-Load Energization of a GIL involves in a VFTO. The value of the overvoltage does not reach a high value, around 1.5pu. On the other hand there is the presence of high frequency oscillations which reach the OHL and may be dangerous. It has been found that after 10[km] on the OHL the high frequency components are damped. A statistical analysis has been done considering the Re-Energization of the GIL with different values of trapped charge. Increasing the value of trapped charge causes the probability to have an high overvoltages to increase. In particular the most high values of overvoltage have been observed downstream the disconnecter and at the end of the line. Opening operations in the GIS have been evaluated. To do that an accurate arc model has been build on the EMTP, considering the non-linear resistance

and the residual spark resistance. It has been found that during the opening operations there is a voltage jump across the contacts and at the source side the voltage oscillates following the source voltage, as expected, and at the load side the voltage has a constant value due the trapped charge in the capacitance at the end of the line. Regarding External Overvoltages both cases of Stroke on Tower Peak and Shielding Failure have been investigated. An accurate tower model recommended in Japan has been build on EMTP. It has a particiular influence for the analysis in case of Stroke on Tower Peak, because it has been found that considering the accurate tower model the overvoltages reached the limit value of $1425[kV]$. For this reason a model of Integrated Surge Arrester has been build on EMTP. In so doing the overvoltage was within the limit value. A comparison between Integrated and External Surge Arresters has been done, and it has been found that with the first solution the GIL was less stressed. Some analysis have been done considering different values of the ground resistance, and it has been found that increasing the R_{ground} the value of overvoltage increases. In order to better understand the behaviour of the mixed line in matter of external overvoltage, the value of the resistance load at the end of the line has been changed. Different scenarios has been considered, in particular $R_{load} < Z_{GIL}$, $R_{load} = Z_{GIL}$ and $R_{load} > Z_{GIL}$. The travelling waves along the GIL have been evaluated and the results have been compared with the theory.

Bibliography

- [AB11] relatore: Roberto Benato Alessandro Boscaro. Tesi magistrale:sovratensioni di origine atmosferica in line elettriche miste ti dipo aerea-cavo o aerea-blindata. 2011.
- [ABB09] ABB. *ABB brochure Gas Insulated Switchgear ELK-04*. ABB, 1 edition, 2009.
- [AH04] D. Warne A. Haddad. *Advances in High Voltage Engineering*. IEE PowerEnergy, 1 edition, 2004.
- [Ame14] Akihiro Ametani. International workshop on power system transient. 2014.
- [AT15] D.S. Pinches M. A. Al-Tai. Very fast transient overvoltages generated by gas insulated substations. 2015.
- [AV] Juan A.Martinez-Velasco.
- [btSTTFotIMoSTWG] Report Prepared by the Switching Transients Task Force of the IEEE Modeling and Analysis of System Transients Working Group. Modeling guidelines for switching transients.
- [C3.15] Cigrè Technical Brochure WG C3.08. Externalities of overhead high voltage power lines. 2015.
- [Coo10] Vernon Cooray. *Lighting Protection*. IET, 1 edition, 2010.
- [DL15] S. Quaia D. Lauria. Technical comparison between a gas-insulated line and a traditional three-bundled ohl for a 400 kv, 200 km connection. 2015.
- [DPW96] O. Volcker D. Povh, H. Schmitt and R. Wltzmann. Modelling and analysis guidelines for very fast transients. 1996.

- [DR15] Mirsad Kapetanovic David F. Peelo Anton Janssen Di Renè, Lou Van der Sluis. *Switching in Electrical Transmission and Distribution Systems*. Wiley, 3 edition, 2015.
- [dS01] Lou Van der Sluis. *Transients in Power Systems*. Wiley, 1 edition, 2001.
- [Eln14] Khalifa Elnaddab. Evaluation of gas insulated lines (gil) for long distance hvac power transfer. 2014.
- [fM09] Rossano Musca fabio Massaro, Giuseppe Morana. Transient behaviour of a "mixed" overhead-cable ehv line under lightning events. 2009.
- [GW15] Felix Goll and Rolf Witzmann. Lighting protection of 500-kv dc gas-insulated lines (gil) with integrated surge arresters. 2015.
- [HK08] PES Substations Committee Hermann Koch, Senior Member of IEEE. Basic information on gas insulated transmission lines (gil). 2008.
- [JD] Milan Bernat Jaroslav Dzmura, Marek Hvizdos. Over-voltage phenomena in low voltage network.
- [JM89] K. Feser W. Pfaff J. Meppelink, K. Diederich. Very fast transients in gis. 1989.
- [JSR11] Jadran Kostovic Jasmin Smajic, Walter Halaus and Uwe Riechert. 3d full-maxwell simulations of very fast transients in gis. 2011.
- [Kie02] Nolasco Kaintzyk Kiessling, Nefzger. *Overhead Power Lines*. Springer, 1 edition, 2002.
- [Koc12] Hermann Koch. *Gas-Insulated Transmission Lines*. WILEY and IEEE, 1 edition, 2012.
- [KS03] Daniel Pepper Siemens AG Berlin Kai Steinfeld, Reinhard Göhler. High voltage surge arresters for protection of series compensation and hvdc converter stations. 2003.
- [LB11] F. Guglielmi S. Dambone Sessa Luca Bellin, relatore: R. Benato. Tesi magistrale:sovratensioni di origine interna di manovra in line elettriche ibride aerea-cavo e aerea-blindata. 2011.
- [LP09] Hans Kristian Hoidalen Lászlò Prikler. *ATP DRAW Users' Manual*. ATP DRAW TM, 1 edition, 2009.

- [MA15] H. Griffiths P.Coventry M. Albano, A. Haddad. Air insulated compact substations. 2015.
- [MB14] Ghasem Nouridad Maziar Babei, Mehdi Babei. Analysis of influential factors in determining very fast transient overvoltages of gis substations. 2014.
- [MCA05] Juan A. Martinez and Ferley Castro-Aranda. Lightning performance analysis of overhead transmission lines using the emtp. 2005.
- [MGI10] Giuseppe Morana Rossano Musca Mariano G. Ippolito, Fabio Massaro. No-load energization of very long ehv mixed overhead-cables lines. 2010.
- [PG99] P. Pinceti and M. Giannettoni. A simplified model for zinc oxide surge arresters. 1999.
- [PNMNCMHVL10] Zacharias G. Datsios Pantelis N. Mikropoulos¹, Thomas E. Tsovilis and Faculty of Engineering Aristotle University of Thessaloniki Nikos C. Mavrikakis High Voltage Laboratory, School of Electrical Computer Engineering. Effects of simulation models of overhead transmission line basic components on backflashover surges impinging on gis substations. 2010.
- [RB10] A. Paolucci R. Benato. *EHV AC Undergrounding Electrical Power- Performance and Planning*. Springer, 1 edition, 2010.
- [RH12] Weijiang Chen Zelai Sun Lei Qi Weidong Zhang Zhibin Li Min Dai Rong Hu, Xiang Cui. Simulation of very fast transient overvoltage on uhv 1000kv gis test circuit. 2012.
- [SH08] Ivo Spreuwenberg and Andrew Hiorns. National grid input into uk offshore energy sea. impact on onshore electricity transmission system. 2008.
- [THUB05] Senior Member IEEE Georg Balog Thor Henriksen, Bjørn Gustavsen and IEEE Ulf Baur. Maximum lightning overvoltage along a cable protected by surge arresters. 2005.
- [UR11] J. SMAJIC A. SHOORY M. SZEWCZYK W. PIASECKI S. BUROW S. TENBOHLEN U. RIECHERT, M. BÖSCH. Mitigation of very fast transient overvoltages in gas insulated uhv substations. 2011.

- [VVKN01] Joy Thomas M. V. Vinod Kumar and M. S. Naidu. Influence of switching conditions on the vfto magnitudes in a gis. 2001.
- [YF13] Shanshan Yang and Gregory A. Franklin. Switching transient overvoltage study simulation comparison using pscad/emt dc and emtp-rv. 2013.
- [ZH15] R. Mahmutkehajif Z. Haznadar, S. CarSimamovid. More accurate modeling of gas insulated substation components in digital simulations of very fast electromagnetic transients. 2015.